REPORT DOCUMENTATION PAGE

Form Approved
OMB No. 0704-0188

1. AGENCY USE ONLY (Leave blank)	2. REPORT DATE	3. REPORT TYPE AND DATES COVERED
	February, 1996	Final Report 1/1/91-12/31/94

4. TITLE AND SUBTITLE

The Deposition of Electro-Optic Films on Semiconductors

5. FUNDING NUMBERS

1131
N00179
N66005
4B855

6. AUTHOR(S)

A. I. Kingon, O. Auciello, and Alice F. Chow

7. PERFORMING ORGANIZATION NAME(S) AND ADDRESS(ES)

North Carolina State University
Department of Materials Science and Engineering
Raleigh, NC 27695-7907

8. PERFORMING ORGANIZATION REPORT NUMBER

N00014-91-J-1307

9. SPONSORING/MONITORING AGENCY NAME(S) AND ADDRESS(ES)

10. SPONSORING/MONITORING AGENCY REPORT NUMBER

11. SUPPLEMENTARY NOTES

12a. DISTRIBUTION/AVAILABILITY STATEMENT

Approved for Public Release; Distribution Unlimited

12b. DISTRIBUTION CODE

13. ABSTRACT *(Maximum 200 words)*

Highly epitaxial, dense, and reproducible $KNbO_3$ thin films were produced using a unique ion beam deposition method and characterized using x-ray diffraction, Rutherford backscattering spectroscopy, atomic force microscopy, transmission electron microscopy, prism coupling, and optical loss measurements. Second harmonic generation (SHG) was demonstrated for these thin films where infrared light was doubled in frequency to green by phase-matching in a $KNbO_3$ thin planer waveguide. The current obstacle limiting the development of $KNbO_3$ thin film waveguides is high optical losses. In this study optical losses in these $KNbO_3$ thin films were correlated with different film microstructures to determine the dominant loss mechanisms. It has been shown that volume absorption, interface scattering, and domain boundary scattering all contribute to the high optical losses measured. The $KNbO_3$ thin films were also integrated with Si, GaAs, and Al_2O_3 substrates using an MgO buffer layer.

14. SUBJECT TERMS

$KNbO_3$, thin films, ion beam deposition, second harmonic generation, waveguides, optical losses, epitaxy

15. NUMBER OF PAGES

87

16. PRICE CODE

17. SECURITY CLASSIFICATION OF REPORT	18. SECURITY CLASSIFICATION OF THIS PAGE	19. SECURITY CLASSIFICATION OF ABSTRACT	20. LIMITATION OF ABSTRACT
UNCLAS	UNCLAS	UNCLAS	SAR

The Deposition of Electro-Optic Films on Semiconductors

ONR Contract No. N0014-91-J-1307

Final Project Report

Covering the period January 1, 1991 - December 31, 1994

Principal Investigators:

Angus I. Kingon Orlando H. Auciello Klaus J. Bachmann

North Carolina State University
Department of Materials Science and Engineering
Raleigh, NC. 27695-7907
(919) 515-2867

This contract report was prepared by A. I. Kingon, O. Auciello, and Alice F. Chow.

DISCLAIMER NOTICE

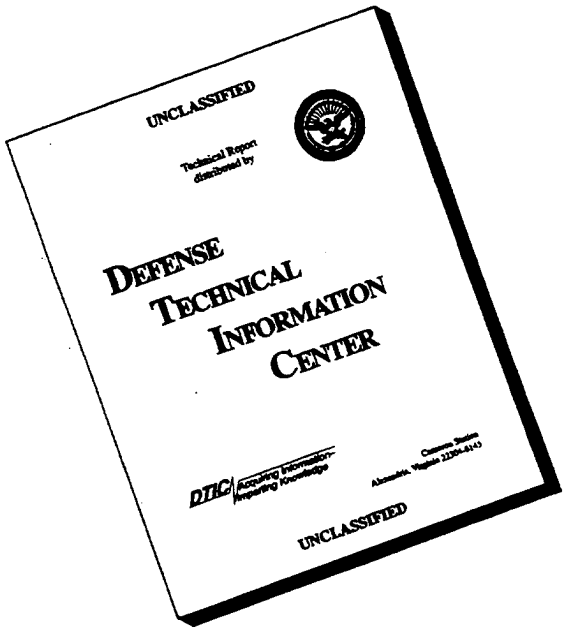

THIS DOCUMENT IS BEST QUALITY AVAILABLE. THE COPY FURNISHED TO DTIC CONTAINED A SIGNIFICANT NUMBER OF PAGES WHICH DO NOT REPRODUCE LEGIBLY.

1.0 Introduction

This is the final report of the project period (1 Jan 1991 - 31 Dec 1994) covering research undertaken under sponsorship of the Office of Naval Research. The contract builds upon an earlier one, *viz* "The Deposition of Multicomponent Films for Electrooptic Applications via a Computer Controlled Dual Ion Beam Sputterring System" (ONR N00014-88-K-0526, period July 1, 1988 to Dec 31, 1991)

The project objectives include the deposition of $KNbO_3$ thin films on silicon, sapphire, gallium arsenide, and other substrates; the design of simple electro-optic and nonlinear optic devices; and the addressing of issues of scaleup.

The achievements of our research in this project period consist of the following:

1) $KNbO_3$ thin films can be produced by a unique ion beam deposition method. These films have been characterized by x-ray diffraction, Rutherford backscattering spectrometry, atomic force microscopy, transmission electron microscopy, scanning electron microscopy, prism-coupling and an optical loss measurement. The results show that the films are highly epitaxial, dense, and reproducible with the proper substrate preparation and deposition conditions.

2) The characterization of the electrooptic properties of $KNbO_3$ thin films, initiated under the previous contract, has been completed. The measured values of electrooptic coefficients were larger than those reported in the literature.

3) Second harmonic generation (SHG) in $KNbO_3$ thin films has been demonstrated. IR light was frequency doubled into green light by phase-matching in a $KNbO_3$ thin film planar waveguide. We have collaborated with Battelle Memorial Institute for these measurements. This is the first report of SHG in a $KNbO_3$ thin film waveguide. Results are extremely promising in terms of blue/green light sources.

4) The current obstacle for the development of $KNbO_3$ waveguides are the high optical losses. Therefore, the optical losses in the $KNbO_3$ waveguides have been correlated with different film microstructures to determine the dominant loss mechanisms. Other oxide materials with simpler crystal systems, such as Ta_2O_5, $K(Ta,Nb)O_3$, and $KTaO_3$, have also been grown to aid in the loss study. It has been shown that volume absorption, interface scattering, and domain/grain boundary scattering must all be minimized.

5) We have investigated the integration of $KNbO_3$ thin films with present semiconductor technology. Studies include include the deposition and

characterization of MgO thin film buffer layers on silicon, gallium arsenide, and sapphire substrates. The results imply that the direct deposition on Si and GaAs substrates via appropriate buffer layers are limited primarily by interface roughness.

6) A collaboration with DuPont has resulted in the development of an ion-assisted deposition system and a novel MOCVD deposition system. These systems allowed us to exploit various processing advantages offered by each technique and extend our understanding of $KNbO_3$ film growth and microstructure.

In addition, two Ph.D theses were completed. The first, by Thomas M Graettinger, was undertaken largely under the auspices of the previous project, but completed under this one. A second Ph.D thesis was completed by Dr Alice F Chow.

2.0 Accomplishments - NCSU

2.1 Background

Compact, blue or green lasers can increase up to four times the present storage capacity of optical recording disks. An infrared laser beam can be converted efficiently to the green or blue by second harmonic generation using high quality nonlinear materials under the appropriate conditions. Many approaches have been examined to develop these high frequency lasers. Semiconductor diode lasers from II-VI materials have potential; however, difficulties arise from absorption losses and doping problems. Polymer materials have also been interesting because of their large nonlinearities but their processing, purification, and crystallization procedures are difficult, and the laser damage thresholds are low.

Dielectric oxides, such as KTP, KDP, $LiNbO_3$, and $BaTiO_3$, have shown success in nonlinear optics. These materials in the form of an optical waveguide can potentially generate extremely high fields due to its beam confinement. However, low conversion efficiencies, impractical for a viable device, have consistently been met. One reason for such poor efficiency is that much of this research has centered around bulk crystals where there is little beam confinement and consequently low power densities as compared with thin film waveguides. Second, although researchers have generated

blue light from $LiNbO_3$ thin films, the nonlinear properties and damage threshold of $LiNbO_3$ are not favorable.

$KNbO_3$ possesses one of the highest figures of merit for second harmonic generation, and in waveguide form, it is superior to most other oxide materials presently being used. However, the device efficiency is limited by the high optical losses. Microstructural defects and interface roughnesses are known to contribute significantly to dielectric waveguide losses. Thus, one focus of the research has emphasized both an investigation of the materials properties that affect optical losses as well as an exploration of the potential of using $KNbO_3$ thin films for second harmonic generation.

2.2 Processing of $KNbO_3$ Thin Films

$KNbO_3$ thin films have been grown on various single crystal substrates including MgO, $MgAl_2O_4$ (spinel), and $KTaO_3$ to explore a variety of film properties and optical losses. An ion-beam sputter deposition technique has been developed and optimized to produce highly epitaxial and dense $KNbO_3$ thin films. Nb and KO_2 targets are sequentially sputtered by an xenon ion source via computer control, thus allowing a layer by layer growth to be implemented. The optimal processing parameters include: growth temperature ranging from 650 to 700°C, beam voltage of 800 volts, oxygen pressure of 1 X 10^{-4} Torr, and interdiffusion layers of about 10 Å. The deposition procedure can be found in Appendix 6, as well as papers published under the auspices of the previous project.

Another critical factor for epitaxial film growth is the substrate surface quality. All substrates are at least cleaned in acetone, methanol, and deionized water prior to mounting with silver paste on the deposition holder. In addition, MgO substrates are annealed at 1150°C for 14 hours to eliminate any hydroxides that may have formed. Next, substrates are cured at 120°C to bake off solvents from the silver paste and ensure good thermal contact. With this careful substrate preparation, very low substrate surface roughness, rms (root mean square) values of 8 to 15 Å, can be achieved. A study of the annealed substrate surface showed that substrates need to be used within a few days before hydroxide growth recur.

In the pursuit of high quality thin films, various substrates were investigated to search for the smoothest surface possible. It was discovered that the MgO substrate surface characteristics differed depending on the vendor. Sapphire substrates polished by a novel technique possessed lowest surface roughness according to our experience. Optical losses have shown to decrease significantly when the substrate surface is smoother. These results are further discussed in Appendix 1, as well as the Ph.D. thesis of Alice Chow.

2.3 Characterization of $KNbO_3$ Thin Films

X-ray diffraction is systematically used to confirm a single orthorhombic film orientation for the $KNbO_3$ thin films. X-ray rocking curves and Rutherford backscattering spectroscopy channeling provide information about the grain tilt and misorientation, in turn revealing the epitaxial integrity of the films. Both measurements revealed the $KNbO_3$ films to possess highly epitaxial orientation. X-ray rocking curve FWHM values of 0.25°, 0.30°, and 0.84° were detected for films on $KTaO_3$, spinel, and MgO, respectively, while channeling displayed minimum yields of 7%, 9%, and 18%, respectively, for the niobium peak. A strong correlation between the lattice mismatch and the grain tilt can be made, as the lowest amount of grain tilt was detected for films on $KTaO_3$ where the lowest lattice mismatch occurs. The surface roughnesses of the films were measured by atomic force microscopy. Low film surface roughnesses with rms values of only 13 to 37 Å were found. These results are discussed in detail in Appendix 6.

The film refractive indices were found to be close to the bulk $KNbO_3$ refractive index values. The TE (light polarized in the film plane) film refractive indices range from 2.27 to 2.29 while for the TM (light polarized perpendicular to the film plane) mode, 2.20 to 2.23 were measured. The TE and TM bulk refractive indices for our film orientation are 2.274 and 2.222, respectively. The closeness of these film values to the bulk suggests that these films are of good crystalline quality and density. (Film density is an problem mentioned by researchers reporting on other process methods.)

The optical losses were analyzed by a optical fiber method. An optical fiber scans the scattering light as seen from the film waveguide surface and the intensity is digitized to a nanovoltmeter. For dielectric optical waveguides, the dominant loss mechanism is

scattering losses. Thus, the optical fiber method for loss measurement is appropriate under the assumption that the total optical losses of the films are comprised basically of the scattering losses measured. Guided light streaks of > 8mm were found for $KNbO_3$ films of ~950 to 1200 Å, while thicker films exhibited shorter streaks of only 2 to 3 mm. The optical losses were calculated to be around 30 dB/cm for the thinner films while > 50 dB/cm losses were measured for the thicker films. Since, the microstructure and surface roughness of the films did not change with thickness, the likely explanation for the disparity in losses is discussed in the following section.

Two types of scattering losses exist: surface and volume scattering. Surface scattering is attributed to the inhomogeneous boundaries at the substrate/film and film/air interfaces. Any roughness of these interfaces allows the electromagnetic field to scattering incoherently. However, surface scattering should decrease as the film thickness increases due to a reduced number of reflections. This effect is the opposite of the trend that we observe. On the other hand, the volume scattering phenomenon would yield the behavior we observe. Volume scattering is comprised of microstructural defects including grain boundaries and impurities. If indeed the film-material properties are not changing with thickness, then the actual film losses should not be changing either. However, as the thickness of the films decreases, more of the field is propagating in the low loss single crystal substrate. Therefore, the total losses measured for the waveguide decrease as the film thickness decreases. There are two possible factors for the high volume losses. First, 90° twin domains form upon transforming from the tetragonal to the orthorhombic orientation. Light attenuation occurs as these domain boundaries are traversed. Second, although the amount of grain misorientation has been found to be small, nevertheless these low angle grain boundaries can contribute to the scattering losses in a similar fashion as the twin domains. Appendix 7 contains additional information regarding $KNbO_3$ optical loss theory.

It should also be noted that as the losses are strongly thickness dependent, it is important to characterize the thickness dependence of the losses, as described above. This approach is not normally adopted by researchers in the field of crystalline oxide films. The problem is that it is easy to produce anomalously low losses simply by having relatively little of the light confined within the film. (See Appendices 1 and 7)

2.4 Ta_2O_5, $K(Ta,Nb)O_3$, and $KTaO_3$ Thin Films

Ta_2O_5, $K(Ta,Nb)O_3$, and $KTaO_3$ thin films have been grown by ion beam sputtering on MgO and Al_2O_3 substrates to isolate various loss mechanisms. These samples were subjected to post-deposition annealing treatments and various oxygen pressure conditions. Their optical properties would reflect the loss mechanisms that are characteristic of the different crystal structures.

Amorphous Ta_2O_5 films were deposited by ion beam sputtering of a tantalum metal target in an oxygen environment. The amorphous nature of the films suggests that interface and surface roughnesses alone contribute to losses. Therefore, the optical properties of these films would reveal the lowest losses achievable for our deposition apparatus. Initial films suffered from oxygen deficiency and thus, displayed no light streaks and higher than bulk refractive indices. However, with post-deposition annealing in oxygen or with increased oxygen flow during deposition, long light streaks and near bulk refractive indices were observed, indicative of high optical quality films. Elastic resonant scattering experiments which can analyze oxygen content confirmed the oxygen deficiency. Under optimum conditions, the lowest loss streak measured in the Ta_2O_5 films was less than 5 dB/cm. These results emphasize the importance of oxygen stoichiometry in reducing the optical losses. It is deduced that the oxygen vacancies act as volume scattering or absorption centers.

Tetragonal $K(Ta,Nb)O_3$ films are interesting because of their high nonlinearity and the absence of twin domains when grown in the unique direction. These films were grown by sequential sputtering of Ta and Nb metal targets and one KO_2 target. Film composition was easily controlled by adjusting the target sputtering times. The optical losses were consistent with the $KNbO_3$ film results, which might suggest that the same dominant loss mechanism is present in both sets of films. Conventional XRD analysis cannot confirm whether the direction of growth is the a-axis or c-axis in the $K(Ta,Nb)O_3$ films. Therefore, it is highly possible that these films contain both types of domains and twin domain scattering is evident.

Cubic $KTaO_3$ films were deposited by ion beam sputtering of a Ta metal target and two KO_2 targets. At first, these films showed no light streaks and low refractive indices. However, upon annealing in oxygen, the losses decreased, which again suggest the importance of adequate oxygenation. In this case, the post-deposition annealing times

and temperatures were critical, since film roughening can occur and increase the losses tremendously. It was discovered that the lowest losses were obtained when annealed at a compromise temperature of 650°C for 2 hours in O_2. Details of these results are discussed in Appendix 1.

3.0 Second Harmonic Generation - Battelle/NCSU Collaboration

A Nd:YLF laser source with wavelength of 1.053 um was used as the fundamental beam for SHG measurements in the $KNbO_3$ thin film planar waveguides. Under mode-locked operation, 80 psec, 100 MHz pulses were first directed transversely through the sample. Thereafter, a harmonic beam splitter transmits the fundamental beam to a beam block while the second harmonic is reflected through a tilted 532 nm bandpass filter onto a ground-glass screen. Strong green light was observed for $KNbO_3$ films with thicknesses varying from 4600 to 6500 Å. Next, light was coupled into a $KNbO_3$ film on an MgO substrate with a varying thickness from 2200 to 2800 Å via a 90° rutile prism in a waveguiding mode. This assures that phase-matching will occur at some point on the film. A 3 to 4 mm green light streak can be seen when coupling in the TM_0 mode. calculations confirm that the TM_0 mode (at 1.053 um) is phase-matching with the TE_1 mode (at 5265 Å) by modal dispersion at a film thickness of about 2300 Å. This is the first demonstration of SHG by a $KNbO_3$ thin film in a waveguide configuration. Furthermore, we expect these films will similarly demonstrate SHG of blue light with the appropriate laser source. More details of the SHG experiments can be found in Appendix 2.

4.0 Buffer Layers on Silicon, Gallium Arsenide, and Sapphire

Preferrentially oriented [100] magnesium oxide buffer layers have been grown on sapphire (1102), silicon (100), and gallium arsenide (100) as documented by XRD and TEM electron diffraction patterns. Careful substrate preparation and unique deposition conditions particular to our ion beam system are necessary, particularly for the latter two substrates due to surface oxides. The native oxide of silicon inibits the growth of epitaxial thin film growth. Therefore a chemical process was used to form a hydrogen terminated surface on the silicon prior to introducing the substrate into the deposition chamber. Nevertheless, silicon oxidizes upon heating to the MgO deposition temperature of 450-550°C and therefore highly oriented films are difficult to grow. On

GaAs, the substrate is ramped up to 620°C for 2 min. prior to deposition to remove its oxide layer and there after cooled to the MgO deposition temperature for growth. Meanwhile, MgO growth on sapphire gave much more highly oriented films and without a complex surface preparation procedure. We selected the substrate orientation to be (1102) r-cut with a four degree off axis tilt which we calculated from atomic modeling to provide a good lattice match with (100) MgO. In light of the high quality MgO buffer layer on sapphire, silicon-on-sapphire applications will be explored. Appendix 10 reports on these experiments.

5.0 Accomplishments - DuPont/NCSU Collaboration

5.1 Background

The research plan for the NCSU/DuPont collaboration include the following:

1) Transfer of ion beam expertise from NCSU to DuPont to develop an ion beam assisted deposition system and MOCVD deposition system.

2) Deposition and characterization of $KNbO_3$ thin films using the ion beam sputter co-deposition system.

3) Thin film growth of other materials that are applicable to nonlinear optics.

5.2 Development and testing of ion beam sputter co-deposition system.

The ion beam sputter co-deposition system consists of a high vacuum stainless steel chamber containing three independent ion source-target pairs for co-sputtering material onto a single 3 inch substrate. The substrate is heated by quartz lamps to a maximum temperature of 900°C. In addition to the 3 primary sputtering ion sources, a fourth ion source was installed for ion assisted growth. This source provides direct low-energy ion bombardment of the growing film which has been shown by others to be a very useful tool for modifying microstructures and physical properties, and for lowering the deposition temperature for high quality thin film growth. The deposition system also includes three quartz crystal resonators, one of which monitors the sputtered flux from

each of the three sputtering targets. A personal computer monitors the feedback from the resonators and has the ability to change the ion beam current on each target to maintain a desired sputtered flux rate and thus achieve correct chemical stoichiometry.

5.3 Deposition of $KNbO_3$ thin films.

Drawing upon the expertise developed at NCSU, $KNbO_3$ thin films were grown at DuPont using the co-deposition system. Epitaxial (110) oriented single phase $KNbO_3$ thin films were grown on MgO (100) single crystal substrates. A six inch diameter elemental niobium target and a six inch diameter potassium superoxide (KO_2) target were co-sputtered to achieve stoichiometric epitaxial $KNbO_3$ films. Films were deposited between 600°C and 650°C with a background pressure of 1-2 x 10^{-4} torr molecular oxygen. Primary sputtering ion energies were kept in the range of 500-1000 eV to minimize damage to the growing film from high-energy backscattered ions. Rutherford backscattering spectrometry (RBS) was used to determine the cation stoichiometry and thickness of the films. This RBS analysis was performed at the University of Pennsylvania in Philadelphia. Films deposited at NCSU were also analyzed at U. Penn. providing an independent measurement to the analysis done at the University of North Carolina at Chapel Hill. Results of the independent analyses agreed very well.

5.4 Film epitaxy studies using x-ray diffraction.

To use a thin film as a medium for second harmonic generation, phase matching of the fundamental and second harmonic waves must occur. Normally this is only accomplished in certain crystallographic directions of a crystal. Therefore, it is desirable to produce a thin film that is a single crystal, requiring in-plane orientation of the film. The standard x-ray diffractometer theta-two theta scan is a powerful technique for identification of phases and for determining if any preferential orientation exists in a film. However, the standard diffraction pattern reveals nothing about the in-plane orientation of the film. In order to investigate the in-plane orientation of the $KNbO_3$ thin films from both NCSU and DuPont, a pole figure rotation stage in combination with an x-ray diffractometer was used. This apparatus has the ability to probe crystal planes which are not parallel to the substrate surface. Analysis of the films using this apparatus

revealed that the [110] axes of the films are tilted along the cubic directions of the MgO substrate by as much as 1.5 degrees. Films deposited at both NCSU and DuPont exhibit this behavior suggesting that the tilt is a substrate influenced characteristic and not related to the deposition method. The tilt is thought to be a strain accommodation mechanism produced as a result of the relatively large lattice mismatch between $KNbO_3$ and MgO (6%). In addition, the tilt is an indication that in-plane rotation exists in the films. This in-plane rotation must be overcome for efficient phase matching to be possible in these films.

5.5 Optical characterization of the $KNbO_3$ thin films.

The indices of refraction of NCSU and DuPont $KNbO_3$ thin films were measured using the prism coupling m-line technique at DuPont. NCSU and DuPont films supported both TE and TM guided modes. The measured indices (nTE= 2.286 , nTM=2.202 NCSU ; nTE= 2.221 , nTM=2.198 DuPont) compare very closely to the bulk values of $KNbO_3$ for equivalent orientation. Birefringence was not observed in the plane of the films which substantiates the earlier conclusion that in-plane rotation exists in the films.

A fiber probe was prepared at DuPont to measure the optical propagation losses in the $KNbO_3$/MgO films. However, scattering was too large in the films and prevented use of the probe.

5.6 Deposition of KTP films.

DuPont has identified potassium titanyl phosphate ($KTiOPO_4$, KTP) as an important material for non-linear optical applications. Initial work has been done toward depositing thin films of this material using the co-sputtering deposition system. A stoichiometric KTP pressed powder target was used for the initial experiments. Depositions in a molecular oxygen background resulted in potassium and phosphorus deficient films on room temperature and heated y-cut quartz substrates. Potassium superoxide, titanium, and titanium phosphide (TiP) targets have since been obtained and will be used in the future for co-deposition experiments.

5.7 MOCVD

MOCVD is used for the first time to grow $KNbO_3$ thin films. A high deposition rate, large area deposition, and conformal converage are among the technique's attractions. Solid metalorganic source materials are passed through a very sharp temperature gradient allowing them to immediately sublimate, upon which a He carrier gas transports the materials through heated tubes to the reaction chamber. Molecular oxygen is then introduced to the gases prior to entering the chamber to ensure a sufficient amount of oxygen for oxide film growth. The film stoichiometry and growth rate can be controlled by adjusting the flow rate of the sources through the temperature gradient. Appendix 4 and 5 are referred for further information on the work done at DuPont.

6.0 Theses

Ph.D. Thesis: "Ion Beam Sputter Deposition, Optical Characterization, and Modelling of Potassium Niobate Thin Films", by Thomas M Graettinger, Materials Science and Engineering, 1992. (Thesis undertaken primarily under the previous project, but completed under the present).

Ph.D Thesis: "Microstructural and Optical Characterzation of Potassium Niobate Thin Films", by Alice F Chow, Materials Science and Engineering, 1995

7.0 Publications

"Investigation of Optical Loss Mechanisms in Oxide Thin Films", Alice F. Chow, Orlando Auciello, and Angus I. Kingon, Integrated Ferroelectrics **11**, 35-45, 1995. (Appendix 1)

"Second Harmonic Generation in Potassium Niobate Thin Films", A.F. Chow, D.J. Lichtenwalner, J.R. Busch, V.E. Wood, O. Auciello, and A.I. Kingon, J. of Appl. Phys. **78** (1), 1995. (Appendix 2)

"A Study of Microstructures in Ferroelectric $Pb(Zr,Ti)O_3$ and $KNbO_3$ Thin Films, A. I. Kingon, S. H. Rou and Y. L. Chen, Proceedings of the 52nd Annual Meeting of the Microscopy Society of America, 574-575, 1994. (Appendix 3)

"Processing Thin Films of $KNbO_3$ For Optical Waveguides," T. M. Graettinger, D. J. Lichtenwalner, A. F. Chow, O. Auciello, and A. I. Kingon, Integrated Ferroelectrics, **6**, 363-373, 1994. (Appendix 4)

"Growth of Epitaxial $KNbO_3$ Thin Films," Thomas M. Graettinger, P. A. Morris, A. Roshko, A. I. Kingon, O. Auciello, D. J. Lichtenwalner, and A. F. Chow, MRS Symposium Proceedings **341** (Epitaxial Oxide Thin Films and Heterostructures),265-276, 1994. (Appendix 5)

"Epitaxial $KNbO_3$ Thin Films on $KTaO_3$, $MgAl_2O_4$, and MgO Substrates," A. F. Chow, D. J. Lichtenwalner, R. R. Woolcott, Jr., T. M. Graettinger, O. Auciello, and A. I. Kingon, Appl. Phys. Lett. **65**(9), 1073-1075, 1994. (Appendix 6)

"Microstructural and Optical Properties of Potassium Niobate Thin Films," Alice F. Chow, Daniel J. Lichtenwalner, Thomas M. Graettinger, James R. Busch, Orlando Auciello, and Angus I. Kingon, Proceedings of the Ninth International Symposium on Applications of Ferroelectrics, 794-6, 1994. (Appendix 7)

"Growth, Microstructures and Optical Properties of $KNbO_3$ Thin Films," T.M. Graettinger, P.A. Morris, Rene R. Woolcott, F.C. Zumsteg, A.F. Chow, and A.I. Kingon, MRS Symposium Proceedings **310** (Ferroelectric Thin Films III), 301-311, 1993. (Appendix 8)

"Microstructural Characterization of Eptaxial Bottom Electrodes, Buffered Layers, and Ferroelectric Thin Flms", Shan Hsien rou, T. M. Graettinger, A. F. Chow, C. N. Soble II, D. J. Lichtenwalner, O. Auciello and A. I. Kingon, MRS Symposium Proceedings **243** (Ferroelectric Thin Films II), 81-91, 1992. (Appendix 9)

"Ion-Beam Reactive Sputter Deposition of MgO Thin Films on Silicon and Sapphire Substrates," Alice F. Chow, Shang Hsieh Rou, Daniel J. Lichtenwalner, Orlando Auciello, and Angus I. Kingon, MRS Symposium Proceedings **268** (Materials Modification by Energetic Atoms and Ions), 253-258, 1992. (Appendix 10)

"Optical Characterization of Potassium Niobate Thin Film Planar Waveguides," Thomas M. Graettinger and Angus I. Kingon, MRS Symposium Proceedings **243** (Ferroelectric Thin Films II), 557-563, 1992. (Appendix 11)

"Ion-beam Sputter Deposition of $KNbO_3$ Thin Films", contributed to Handbook of Thin Film Technology, Alice F. Chow, D.J. Lichtenwalner, T.M. Graettinger, O. Auciello, and A.I. Kingon, (Institute of Physics Publishing, Williston, VT) 1995.

"Ferroelectric Materials For Nonlinear Optical Devices," P.A. Morris, The Eighth International Meeting on Ferroelectricity, (August 1993), (invited talk).

Appendix 1

"Investigation of Optical Loss Mechanisms in Oxide Thin Films", Alice F. Chow, Orlando Auciello, and Angus I. Kingon, Integrated Ferroelectrics **11**, 35-45, 1995.

Optical -4

Integrated Ferroelectrics, 1995, Vol. 11, pp. 35–45
Reprints available directly from the publisher
Photocopying permitted by license only

INVESTIGATION OF OPTICAL LOSS MECHANISMS IN OXIDE THIN FILMS

ALICE F. CHOW, ORLANDO AUCIELLO*, DAVID B. POKER**, AND ANGUS I. KINGON
North Carolina State University, Raleigh, NC 27695
*Also MCNC, Electronics Technology Division, RTP, NC 27709-2889
**Oak Ridge National Laboratory, Oak Ridge, TN 37831

(Received March 22, 1995)

Abstract $KNbO_3$, $K(Ta,Nb)O_3$, $KTaO_3$, and Ta_2O_5 thin films have been grown by ion-beam sputter deposition. $KNbO_3$ has excellent nonlinear properties for second harmonic generation; however, high optical losses are still characteristic of these films. Several loss mechanisms, such as, high angle grain boundaries, twin domains, interface and surface scattering, and oxygen vacancies can all contribute to the high losses. In order to isolate the various mechanisms, amorphous Ta_2O_5 films, epitaxial cubic $KTaO_3$ and tetragonal $K(Ta,Nb)O_3$ films were grown on MgO and Al_2O_3 substrates subjected to post-deposition annealing treatments and various oxygen pressure conditions. The optical losses and refractive indices were observed to differ depending on the substrate surface and annealing treatments. Resonant scattering experiments were performed to analyze the oxygen composition. The optical properties of these oxide thin film systems are reported and the breakdown of the loss mechanisms is addressed.

INTRODUCTION

The demand for increasing present optical recording densities can be met by blue or green lasers.[1] One of the most promising methods of generating the high frequency is by second harmonic generation (SHG) where an IR laser can frequency double into the blue or green via a nonlinear material. Potassium niobate ($KNbO_3$) is an excellent candidate for SHG due to its high nonlinear coefficients, large birefringence, noncritical

phase-matching, high damage threshold, and transparency in the appropriate wavelengths. Moreover, higher power densities can be achieved in a thin film waveguide configuration due to beam confinement, and direct integration with present semiconductor materials is possible.[2]

Although SHG has been demonstrated recently in $KNbO_3$ thin films,[3] the high losses present in most film-waveguides are problematic and must be overcome for practical device applications. The research focused on the breakdown of loss mechanisms is at a nascent stage; several groups have generated valuable models.[4] We approach the problem of the high $KNbO_3$ losses by studying oxide systems with simpler structures where specific loss mechanisms are eliminated and isolated in order to understand their contribution to losses.

The microstructural and optical properties of the $KNbO_3$ films are summarized as reported by previous work.[5] Basic loss theory is addressed where the relevant mechanisms are noted. Tetragonal potassium tantalum niobate ($K(Ta,Nb)O_3$), cubic potassium tantalate ($KTaO_3$), and amorphous tantalum oxide (Ta_2O_5) films were deposited by ion-beam sputtering and their properties and pertinence to the loss study are discussed. The characterization techniques used include prism-coupling to measure the refractive index, an optical fiber loss method to quantify the optical scattering losses atomic force microscopy (AFM) to probe surface roughness, and elastic resonant scattering to analyze oxygen composition.

$KNbO_3$ FILMS

Ion-beam sputter deposition was used to deposit all the oxide films. For $KNbO_3$ film deposition, two potassium superoxide (KO_2) targets and one niobium target were sequentially sputtered. The details of the deposition process can be found in another paper.[5] The films were grown on MgO, $MgAl_2O_4$, and $KTaO_3$ substrates. X-ray diffraction (XRD) revealed the films to be orthorhombic (110) single orientation. XRD rocking curves, Rutherford backscattering spectrometry (RBS) channeling, and transmission electron microscopy diffraction analyses showed the films to possess a high degree of epitaxy. Small grain sizes (1000 to 5000 Å) were detected and the film surface roughnesses were low with root mean square (rms) values between 9 and 37 Å by AFM. The refractive indices approach bulk values indicating dense films. These results are summarized in Table I.

TABLE I Summary of $KNbO_3$ thin film microstructural and optical properties on $KTaO_3$, $MgAl_2O_4$, and MgO substrates.

$KNbO_3$ on Substrate	$KTaO_3$ (001)	$MgAl_2O_4$ (001)	MgO (001)
FWHM rocking XRD	0.25°	0.30°	0.84°
RBS/channeling χ_{Nb}, χ_K	7%	9%, 15%	18%, 49%
Grain size	~3-5000 Å	~1000 Å	~1200 Å
Grain tilt from TEM	2 to 3°	2 to 3°	10°
Film refractive index, TE, TM	2.27, —	2.28, 2.21	2.28, 2.21
Surface roughness, rms	21 Å	9-19 Å	18-37 Å

The optical losses were measured by an optical fiber method. An optical fiber scans the length of the light streak and measures the scattering intensity where the signal is fed into a photodiode and nanovoltmeter. A longer scattered light streak reflects a lower loss for the waveguide. For the $KNbO_3$ films, longer streaks were observed for thinner films as shown in Figure 1.

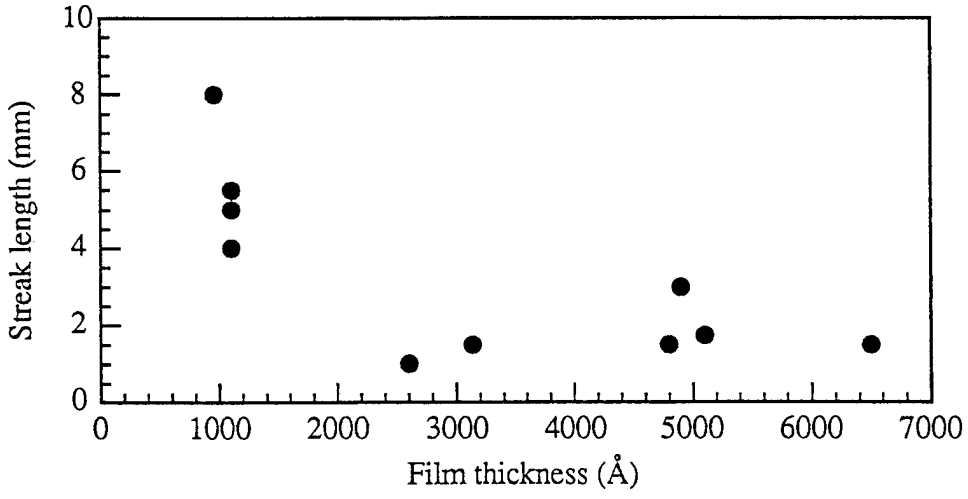

Figure 1 Streak length of $KNbO_3$ waveguide versus film thickness.

According to loss mechanism theory, this would support a volume scattering mechanism rather than a surface scattering mechanism. If the majority of losses took place in the bulk of the film, higher losses would be observed as films became thicker. On the other hand, if interface and film surface scattering were dominating, then thicker films would possess lower losses since there are fewer reflections at the boundaries in the waveguide for an arbitrary distance in thicker films.

Several volume scattering mechanisms could be contributing to the losses in the $KNbO_3$ films. These include twin domains that form in the orthorhombic structure, grain boundary scattering and grain size, and oxygen vacancies. In addition, there is always a surface scattering component that is affected by the interface and film roughness. In order to isolate these various mechanisms, other oxide systems of simpler structures were grown and analyzed where the range of bulk scattering mechanisms gradually narrow as seen in Table II. In the case of amorphous Ta_2O_5 films, the loss due to surface scattering can be focused in the absence of oxygen vacancies which would be significant in determining the minimum surface scattering contribution to losses under optimum conditions (devoid of bulk scattering).

TABLE II Thin film oxide systems and the possible volume scattering sources.

Thin film oxide	Volume scattering source
orthorhombic $KNbO_3$	twin domains, grain boundaries, oxygen vacancies
tetragonal $K(Ta,Nb)O_3$	twin domains? grain boundaries, oxygen vacancies
cubic $KTaO_3$	grain boundaries, oxygen vacancies
amorphous Ta_2O_5	oxygen vacancies

AMORPHOUS Ta_2O_5 FILMS

Ta_2O_5 films were deposited by ion-beam sputter deposition of a tantalum metal target in an oxygen environment. Initial films showed no light streaks and refractive indices higher than the bulk value of 2.20.[6] Oxygen deficiency in the films was suspected and therefore, a film was annealed at 560°C for 20 minutes in oxygen. The post-deposition anneal lowered the refractive index close to that of bulk and a long light streak extending the length of the sample (> 8mm) was observed. Next, the oxygen flow during

deposition was increased to similarly improve the film quality but without post-deposition annealing. Figure 2 shows a plot of the refractive index versus deposition rate. With increasing oxygen flow, both the refractive index and deposition rate decreased as expected.

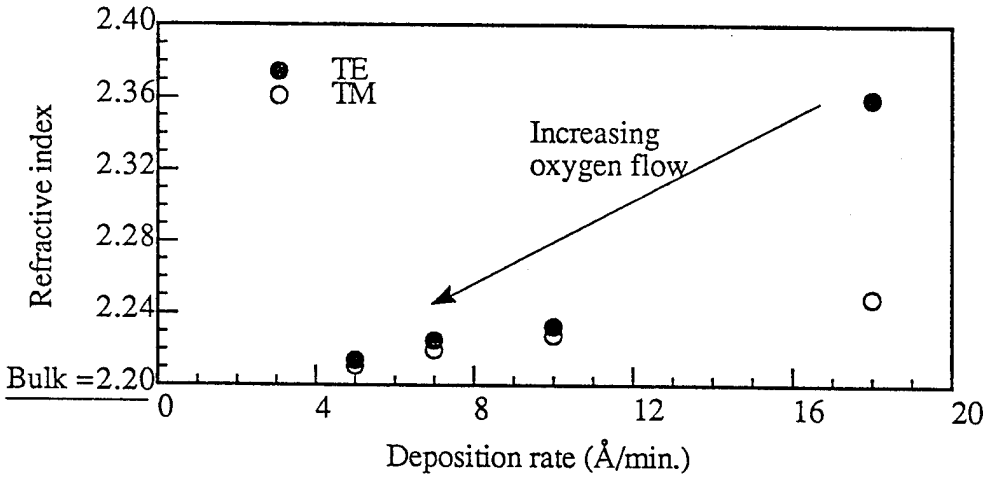

Figure 2 Ta_2O_5 refractive index and deposition rate for increasing oxygen flow during deposition.

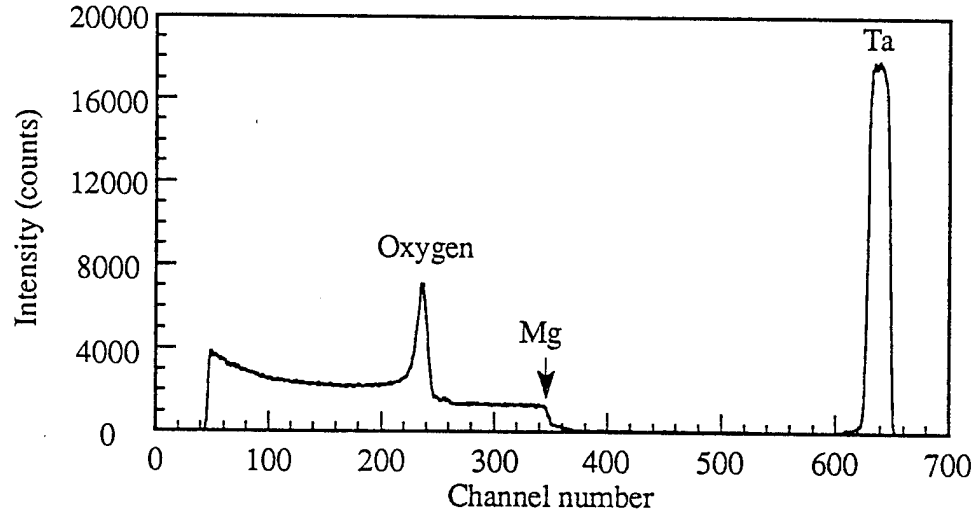

Figure 3 Resonant scattering spectrum for a Ta_2O_5 film on MgO.

Since all the oxide films were deposited on oxide substrates, the oxygen content of the films cannot be quantified by RBS because the oxygen film peak is obscured by the substrate peak. Elastic resonant scattering is one technique that enhances the scattering of the oxygen peak, and thus, oxgyen composition of different films can be compared. Resonant scattering experiments were performed with a 3.09 MeV helium

ion beam energy and a scattering angle of 160.27°. A typical resonant scattering spectrum of a Ta_2O_5 film on a MgO substrate is seen in Figure 3. The normalized oxygen content versus deposition rate of the various Ta_2O_5 films with increasing oxygen flow during deposition is shown in Figure 4. (The oxygen counts were normalized to the film with the highest oxygen flow.) This graph suggests that the original films were indeed oxygen deficient and the films showed long light streaks and lower losses only upon increasing the oxygen flow. A loss of 13 dB/cm was attainable.

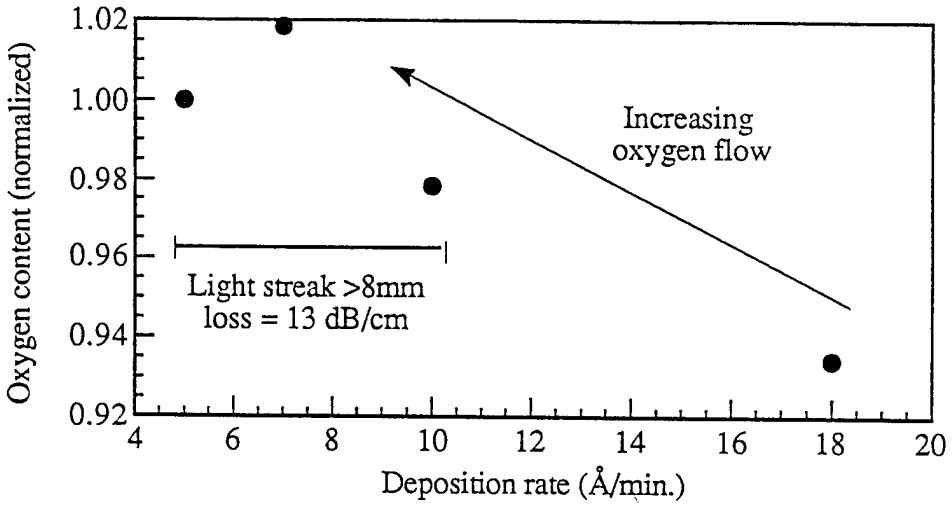

Figure 4 Normalized oxygen content of Ta_2O_5 films with increasing deposition rate and oxygen flow.

In order to further lower the losses and also to evaluate the effect of substrate roughness on losses, an extensive AFM study on various substrates was performed. First, MgO substrates from various vendors were analyzed. The substrate surface roughness seemed to vary depending on the vendor as seen in Table III.

TABLE III AFM data of as-received MgO substrates from four vendors.

MgO substrate vendor	Rms (Å)	Maximum feature height (Å)
Advanced Composite Materials	23	196
ESPI	19	218
Commercial Crystal Lab (C.C.L.)	48	507
Marketech	94	765

One reason for the deviation is the susceptibility to hydroxide growth of the MgO surface. To eliminate the surface hydroxides, the substrates were subjected to a high temperature anneal at 1150°C for 14 hours in oxygen. However, it was important to use the annealed substrate within a few days, otherwise hydroxide growth begins to occur as shown in Table IV.

TABLE IV AFM results of an annealed MgO substrate over 14 days.

MgO substrate	Rms (Å)	Maximum feature height (Å)
Day one of anneal	13	127
Day four after anneal	12	107
Day seven after anneal	32	833
Day ten after anneal	53	1133
Day fourteen after anneal	48	2733

Table V compares the AFM results of other substrates that were analyzed. A sapphire substrate with a novel superpolish was obtained from Crystal Systems that exhibited an rms of only 3.2 Å by AFM. When an amorphous Ta_2O_5 film was deposited on that substrate with the increased oxygen flow conditions, the lowest loss streak was observed as compared to the other Ta_2O_5 films. In fact with our present optical fiber setup, a loss was not measurable due to the low signal to background ratio. A loss of < 5 dB/cm is probable for that film. This result asserts the necessity of a low substrate roughness in obtaining low losses.

TABLE V Surface roughness of various substrates.

Substrate	Rms (Å)	Maximum feature height (Å)
MgO (C.C.L.)	20	184
MgO annealed (C.C.L.)	13	96
quartz	11	643
sapphire (C.C.L.)	12	198
sapphire super polish (Crystal Systems)	3.2	234

TETRAGONAL $K(Ta,Nb)O_3$ FILMS

$K(Ta,Nb)O_3$ (KTN) is a solid solution of $KTaO_3$ and $KNbO_3$. Its curie temperature can be controlled by altering the Ta to Nb concentration and excellent nonlinear properties are observed for particular compositions. $KTa_{0.55}Nb_{0.45}O_3$ is an interesting composition to analyze due to its tetragonal structure which can be grown devoid of twin domains.

Both a Ta and a Nb metal target and one KO_2 target were ion-beam sputtered to deposit KTN films on MgO substrates. The film composition can be precisely controlled by altering the sputtering dwell times on each target as shown in Figure 5.

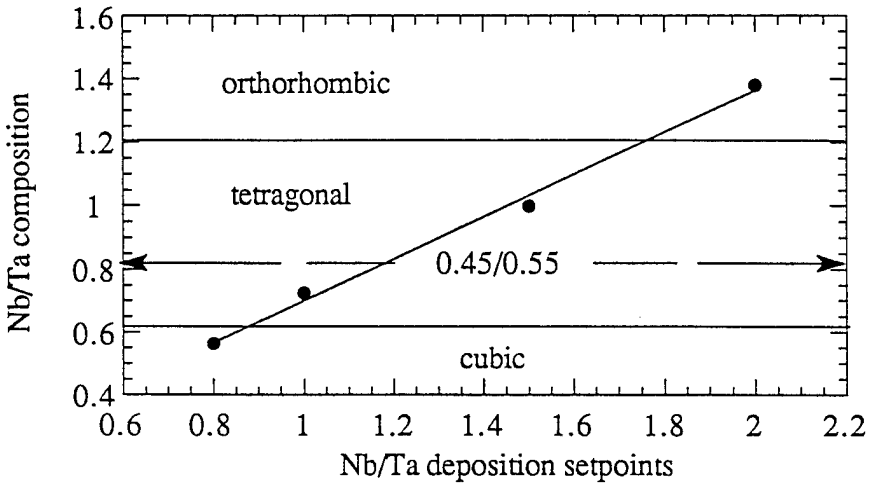

Figure 5 $K(Ta,Nb)O_3$ deposition setpoints versus composition.

The losses of $KTa_{0.55}Nb_{0.45}O_3$ films were analyzed and results similar to those of $KNbO_3$ films were detected. Thinner KTN films showed long light streaks indicative of a bulk scattering phenomenon. The thermal expansion coefficient of the MgO substrate is appreciably larger than that of KTN which would imply that the short axis of the KTN <100> lies in the film plane.[7] This is the desired configuration since the unique or long axis must be perpendicular to the film surface to avoid twin domains. However, the tetragonality of this particular KTN composition is extremely small (difference between the a-axis and c-axis d-spacing is only 0.013 Å)[8] that conventional XRD analysis cannot distinguish between the axes. Consequently, it is highly possible that these KTN films contain both a-axis and c-axis domains and twin domain scattering is present.

CUBIC $KTaO_3$ FILMS

The cubic structure of $KTaO_3$ films would assure a film without twin domains. $KTaO_3$ films were deposited on MgO substrates by sputtering a Ta metal target and two KO_2 targets. At first, no light streaks and low refractive indices were observed. In light of the amorphous Ta_2O_5 results and the possibility of oxygen deficiency, different post-deposition annealing treatments were applied to the $KTaO_3$ films. The first anneal took place at 560°C for 20 minutes in an oxygen environment alone. The film resulted in poor quality visually and light-coupling was not possible. Potassium volatility of the film surface was suspected to be the problem. Consequently, $KNbO_3$ powder placed in the crucible during annealing helped to preserve the original visually translucent film surface. Next, films were annealed at an increased temperature of 850°C for both 2 and 10 hours in O_2 and $KNbO_3$ powder. Again, high losses were present and in this case, the cause was attributed to the increased surface roughness after the high temperature anneal. Figure 6 displays the film roughess in terms of maximum feature height and rms as a function of increasing anneal temperature and time.

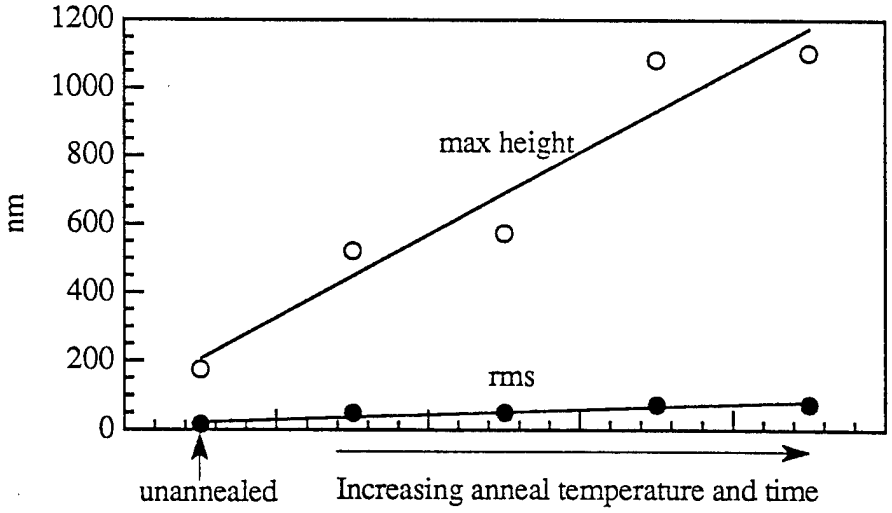

Figure 6 AFM results of $KTaO_3$ films with increasing anneal temperature and time.

These results clearly show that there are critical limits of annealing conditions due to film roughnening. Finally, a $KTaO_3$ film was annealed at a compromised temperature of 650°C for 2 hours in O_2 and $KNbO_3$ powder. The refractive index increased slightly, from 2.178 to 2.185 (bulk value is 2.225) and a long light streak was observed (> 8mm). Therefore, a $KTaO_3$ film was deposited with a higher oxygen pressure during deposition

in order to provide adequate oxygenation and a low film roughness. As expected, the resultant film displayed a > 7mm light streak and the rms was only 16 Å.

In light of these results, preliminary resonant scattering experiments were performed on $KNbO_3$ films with various oxygen flow conditions to explore the possibility of oxygen deficiency in those films. Increasing oxygen composition was observed for films deposited at higher oxygen pressures as seen in Figure 7.

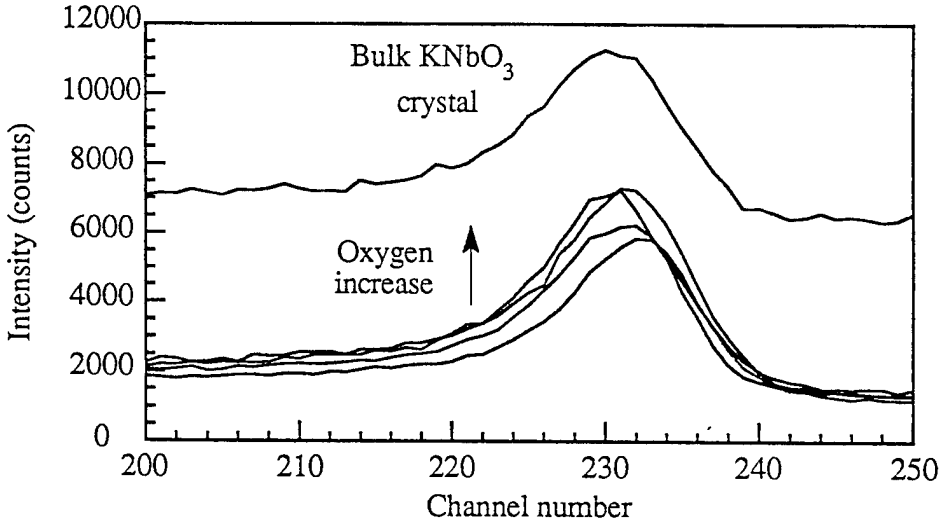

Figure 7 Resonant scattering oxygen peaks of a bulk $KNbO_3$ crystal and $KNbO_3$ films deposited at increasing oxygen flows.

However, the original $KNbO_3$ films appeared to possess near stoichiometric oxygen composition as normalized to a $KNbO_3$ bulk crystal suggesting that oxygen vacancies is not a major factor in the volume losses. The high losses both in the $KNbO_3$ and $K(Ta,Nb)O_3$ films are most likely caused by the twin domains. The effect of grain boundaries and grain size on losses can also be significant and should be investigated.

CONCLUSION

High quality $KNbO_3$, $K(Ta,Nb)O_3$, $KTaO_3$, and Ta_2O_5 films were deposited by ion-beam sputter deposition. The amorphous Ta_2O_5 films, in the absence of oxygen vacancies, offer a study where the sole loss mechanism is attributed to surface scattering. A Ta_2O_5 film was deposited on a super-polished sapphire substrate and the low loss achieved indicated that a low substrate roughness is mandatory for low overall losses. Post-deposition annealing treatments of both the Ta_2O_5 and $KTaO_3$ films showed that the possibility of oxygen vacancies in oxide films should be considered since they can make significant contributions to volume losses. At the same time, post-deposition

anneals are limited due to the increased film roughness that also increases the surface scattering losses. Initial resonant scattering experiments suggest that the $KNbO_3$ films possess near stoichiometric oxygen composition and therefore, the main source for the high bulk scattering losses in these films is likely attributed to twin domains.

ACKNOWLEDGEMENT

This research was supported by the Office of Naval Research under Contract No. N0014-91-1307. The work at ORNL was sponsored by the Division of Materials Sciences, U.S. Department of Energy, under contract DE-AC05-84OR21400 with Martin Marietta Energy Systems, Inc.

REFERENCES

1. W. P. Risk, Optics and Photonics News, 1, 10, (1990).
2. George I. Stegeman and Colin T. Seaton, J. Appl. Phys., 58, R57, (1985).
3. A. F. Chow, D. J. Lichtenwalner, O. Auciello, A. I. Kingon, J. R. Busch, and V. E. Wood, submitted to J. Appl. Phys.
4. D. K. Fork, F. Armani-Leplingard, and J. J. Kingston, submitted to Mat. Res. Soc. Proceedings, Fall (1994).
5. A. F. Chow, D. J. Lichtenwalner, R. R. Woolcott Jr., T. M. Graettinger, N. R. Parikh, L. A. Boatner, O. Auciello, and A. I. Kingon, Applied Physics Letters, 65, 1073, (1994).
6. H. S. Moon, J. S. Lee, S. W. Han, J. W. Park, J. H. Lee, S. K. Yang, and H. H. Park, J. Materials Science, 29, 1545 (1994).
7. Thermal Expansion of Nonmetallic Solids, Vol. 13 of Thermophysical Properties of Matter, edited by Y. S. Touloukian, R. K. Kirby, R. E. Taylor, and T. Y. R. Lee (Plenum, New York, 1977).
8. A. W. Hewat, K. D. Rouse, and G. Zaccai, Ferroelectrics, 4, 153, (1972).

Appendix 2

Second Harmonic Generation in Potassium Niobate Thin Films", A.F. Chow, D.J. Lichtenwalner, J.R. Busch, V.E. Wood, O. Auciello, and A.I. Kingon, J. of Appl. Phys. **78** (1), 1995.

Second harmonic generation in potassium niobate thin films

A. F. Chow, D. J. Lichtenwalner, O. Auciello,[a] and A. I. Kingon
Department of Materials Science and Engineering, North Carolina State University, Raleigh, North Carolina 27695-7919

J. R. Busch and V. E. Wood
Battelle Memorial Institute, Columbus, Ohio 43201-2693

(Received 24 October 1994; accepted for publication 5 March 1995)

Green light produced by second harmonic generation has been observed in an epitaxial orthorhombic $KNbO_3$ thin film planar waveguide produced by ion-beam sputter deposition on a (100)-oriented MgO single crystal substrate. A Nd:YLF laser beam, with a wavelength of 1.053 μm and ~80 ps, 100 MHz pulses under mode-locked operation, was coupled into the waveguide using a rutile prism, and a green light streak 3–4 mm long was seen in the guide. The TM_0 mode of the input beam was phase matched to the TE_1 mode of the second harmonic for a film thickness of 2300 Å. Second harmonic generation was also observed in a nonwaveguided configuration on thicker (4600–6500 Å) films on both MgO and $KTaO_3$ substrates. © *1995 American Institute of Physics.*

I. INTRODUCTION

Currently, red laser beams of wavelengths of ~780 nm are used to read optical disks. A source of shorter wavelength, having a smaller minimum beam size, would allow for denser packing of data on the disk. The drive for increasing optical recording density has stimulated the development of nonlinear materials for frequency doubling. Using such materials, an infrared source laser can be used to produce blue or green light via second harmonic generation (SHG). Up to four times greater disk storage capacity has been demonstrated using SHG from a potassium niobate single crystal.[1]

For reasons of compactness, ruggedness, and high conversion efficiency, it is desirable in optical disk applications for the SHG to take place in an optical waveguide.[2] The confinement offered by the waveguide structure allows high optical power densities to be maintained over long interaction lengths; both these factors increase the SHG conversion efficiency. In addition, if the effective waveguide thickness can be appropriately adjusted, the modal dispersion of the guide can be utilized to achieve phase matching under a wider variety of conditions than possible in the bulk material.[3,4] The deposition of waveguide films suitable for SHG on crystalline substrates of lower refractive index is of particular interest for hybrid integration of the guide with diode lasers and other optical components.[5] Among SHG materials, crystalline $KNbO_3$ is notable for its large figure of merit for SHG, broad transparency range, high resistance to optical damage, and suitability for noncritical phase matching of laser diodes.[6] Some properties of $KNbO_3$ are summarized in Table I. High quality $KNbO_3$ crystals are expensive to grow and prepare, and it is difficult to form waveguides in crystals of this material by simple diffusive or ion-exchange processes, although both planar and channel $KNbO_3$ waveguides formed by ion implantation have been achieved.[7,8] Moreover, it is not possible, using bulk crystals, to obtain noncritical phase matching at room temperature for wavelengths below 857 nm.[9] Thus it is not surprising that there has been considerable interest in obtaining thin crystalline films of $KNbO_3$ by various deposition methods. Relatively thick, multimode films have been prepared by liquid phase epitaxy.[10] Epitaxial films have been made by the sol-gel method on (211) $SrTiO_3$ (Ref. 11) and on Pt-coated (100) MgO,[12] but no optical properties have been reported. Recently the pulsed-laser deposition technique has been used to grow epitaxially oriented, stoichiometric $KNbO_3$ films on (100) MgO substrates using K-rich targets,[13] again no optical properties have been reported. Thöny and co-workers prepared waveguiding $KNbO_3$ layers by rf sputtering on MgO and magnesia-alumina spinel substrates.[14] Their films retained the tetragonal high-temperature $KNbO_3$ phase. They also observed SHG in these films in the bulk configuration (i.e., nonwaveguiding). SHG in channel waveguides formed by ion implantation has been reported.[15,16] We have recently prepared epitaxial $KNbO_3$ films of the orthorhombic phase on several different substrates using ion-beam sputtering,[17] and have observed waveguiding in these films.[18] In this paper, we report on SHG in these samples.

$KNbO_3$ thin films were deposited on MgO and $KTaO_3$ single crystal substrates. Film orientation, epitaxial quality, and substrate and film roughness were characterized by x-ray diffraction and rocking curves, Rutherford backscattering spectroscopy (RBS), ion channeling, and atomic force microscopy. Refractive indices were determined by the prism-coupling technique.[19] Second harmonic generation experiments were conducted in the transverse nonwaveguided configuration by placing the sample perpendicular to the direction of a Nd:YLF source beam, and also in a waveguided mode using prism-coupling. Waveguiding and modal dispersion phase matching conditions and calculations of overlap integrals for different mode conversions are presented.

II. EXPERIMENT

An ion-beam sputter deposition technique featuring a computer-controlled rotating target assembly was used to

[a]Also MCNC, Electronics Technology Division, Research Triangle Park, NC 27709-2889.

 0021-8979/95/78(1)/435/4/$6.00

TABLE I. Properties of $KNbO_3$.

Nonlinear coefficient at 1.064 μm[a]	−15.8 to −27.4 pm/V
Refractive index[b]	n_a=2.1687, n_b=2.2801, n_c=2.3297
Lattice parameters[c]	a=5.721 Å, b=5.695 Å, c=3.973 Å
Crystallographic structure	mm2 orthorhombic
Transparency range[a]	0.4–4.5 μm
Damage threshold[a] for 100 ps pulse, 20 Hz, at 1.064 μm	>100 GW/cm^2

[a]Ref. 24.
[b]Ref. 8.
[c]Ref. 25.

synthesize $KNbO_3$ thin films using a layer by layer deposition technique described in detail elsewhere.[20] Two KO_2 targets and one Nb metal target were sequentially sputtered using a xenon ion source. Deposition temperatures of 650–700 °C and oxygen pressures of about 1×10^{-4} Torr were used. All substrates were cleaned in acetone, methanol, and followed by de-ionized water. The MgO substrates were annealed (at 1150 °C for 14 h) after the cleaning to remove any hydroxide that may have formed on the surface.[14] The deposited films were visually transparent.

III. RESULTS AND DISCUSSION

X-ray diffraction revealed a $KNbO_3$ (110) orthorhombic orientation for films on all substrates. No other orientations or phases were detected. Both x-ray rocking curves and RBS/channeling analyses determined the films to possess good epitaxial orientation. Films on MgO and $KTaO_3$ showed rocking curve FWHM values as low as 0.84° and 0.35°, and minimum channeling yields of 18% and 7% for the Nb peak, respectively. The single orientation of $KNbO_3$ is critical, for any second phases or other orientations are potential sources of light scattering. The small amount of grain tilt as inferred from the rocking curves and ion-channeling results also suggests that some grain-boundary scattering may occur. More details concerning the $KNbO_3$ film epitaxy and microstructure can be found in a previous paper.[17]

Substrate and film surface roughnesses were measured by atomic force microscopy. The interface and film surface can be significant contributors to scattering losses as nonuniformity of these boundaries causes light to scatter incoherently. Low substrate roughnesses with root-mean-square (rms) values of 8–10 Å can be achieved for both as-received $KTaO_3$ substrates and annealed MgO substrates. The $KNbO_3$ film surface roughnesses are also low, varying in rms values from 18–37 Å.

Refractive indices were determined using a prism-coupling apparatus in which a He-Ne (632.8 nm) laser is focused onto a rutile prism clamped to the thin film sample. The measured refractive indices are about 2.21 and 2.28 for the TM (light polarized along the $KNbO_3$ (110)) and the TE modes (light polarized in the film plane), respectively. The bulk refractive index values for the $KNbO_3$ (110) orientation are 2.225 for the TM mode and 2.278 for the TE mode. Because of the presence of 90° domains in the film plane, the TE value is calculated as an average of the $KNbO_3$ [$\bar{1}$10] and [001] values.[14] The fact that the film indices are so close to the bulk values suggests that the films are very dense.

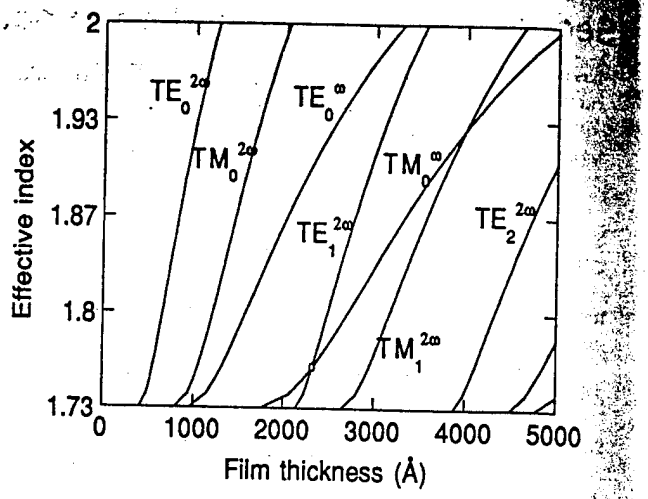

FIG. 1. Modal dispersion curves of the fundamental (1.053 μm) and second harmonic (5265 Å) waveguide modes for $KNbO_3$ thin film on an MgO substrate.

Phase matching of the fundamental wavelength with the second harmonic can be achieved by using modal dispersion in thin films.[3] First, the refractive index of $KNbO_3$ as a function of wavelength must be known.[8] The effective index of the film for different modes varies with respect to the film thickness. Thus, by plotting the modal dispersion curves for both the fundamental and second harmonic wavelengths, the thicknesses where phase-matching occurs for particular modes can be pinpointed. Figure 1 displays the modal dispersion curves for a $KNbO_3$ thin film on an MgO substrate at the Nd:YLF laser wavelength of 1.053 μm and the frequency doubled wavelength of 5265 Å. As an example, for a film thickness of 2300 Å, the effective index of the TM_0 mode at 1.053 μm matches that of the TE_1 mode at 5265 Å (Fig. 1). Therefore, thin film waveguides permit a simpler phase-matching scheme whereby growing films to specific thicknesses allows phase-matching of particular modes to be accomplished.

Figure 2 shows a schematic of the SHG experimental setup. A Nd:YLF laser with a wavelength of 1.053 μm, ~80 ps pulse duration, and 100 MHz frequency was used as the source beam under mode-locked operation. A harmonic beam splitter transmits the fundamental wavelength to a beam block, and reflects the second harmonic through a tilted 532 nm bandpass filter onto a ground-glass screen. First, $KNbO_3$ samples of thickness varying from 4600 to 6500 Å were placed perpendicular to the beam direction in a nonwaveguiding mode. Three samples of $KNbO_3$ thin films on MgO substrates and one on a $KTaO_3$ substrate displayed green light as visually detected on the screen. Laser drive currents of 28 to 30 A (power at 30 A was calibrated at 275 W/pulse) were necessary to generate green light. The signal appeared to saturate at 30 A. Next, we measured SHG in the waveguide configuration. Light was coupled into a $KNbO_3$ film on an MgO substrate with thickness varying from 2200–

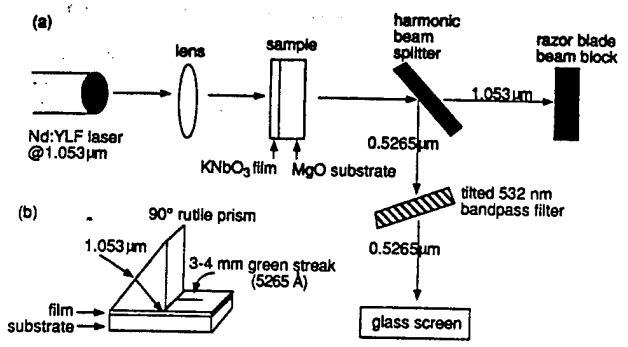

FIG. 2. SHG experimental setup for $KNbO_3$ (a) mounted perpendicular to the laser beam and (b) in coupling mode.

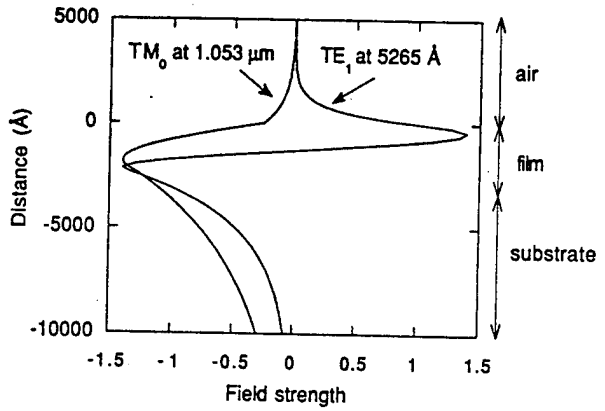

FIG. 3. Field distribution of the TM_0 mode at 1.053 μm and the TE_1 mode at 5265 Å.

2800 Å using a 90° rutile prism. The $KNbO_3$ film was purposely grown with a thickness gradient so that the critical phase-matching thickness could be assured at some area of the sample.[21] A 3–4 mm green light streak was observed at the coupling angle for the TM_0 mode using a fundamental wavelength of 1.053 μm. Currents of 31–33 A were used. We believe that phase matching is occurring for a film thickness close to 2300 Å for the TM_0 mode (at 1.053 μm) and the TE_1 mode (at 5265 Å). No previous reports on SHG in $KNbO_3$ thin film waveguides are known to the authors.

Since modal dispersion allows phase matching to occur without using crystal birefringence, different orders of modes must be used. The effective refractive index decreases with increasing mode number and wavelength. Therefore, a lower order mode of the fundamental wavelength matches a higher order mode of the second harmonic. The figure of merit for SHG efficiency in a waveguide can generally be expressed as $d_{\text{eff}}{}^2 S_{ij}{}^2/n^3$, where d_{eff} is the effective nonlinear coefficient, n is the refractive index, and S_{ij} is the mode overlap integral. Since all the nonlinear coefficients are comparable in magnitude and of the same sign for potassium niobate, the mode overlap integral gives an indication of the SHG efficiency between mode conversions.[22] For a slab waveguide and for a uniform beam intensity in the film plane, the overlap integral can be expressed as

$$S_{ij}=\int_0^a (F_i^{\omega})^2 F_j^{2\omega} dx \left[\int_{-\infty}^{\infty} (F_i^{\omega})^2 dx \left[\int_{-\infty}^{\infty} (F_j^{2\omega})^2 dx\right]\right]^{1/2},$$

where F_m^{ω} is the amplitude of the transverse field of the mth mode at frequency ω, and the variable a is the thickness of the nonlinear layer.[23] Table II lists the overlap integrals calculated for four different mode conversions for a $KNbO_3$ film on MgO substrate at the fundamental and second harmonic wavelengths of 1.053 μm and 5265 Å, respectively. On the basis of bulk symmetry and film orientation, certain mode conversions are forbidden, such as TM_0^{ω} to $TM_1^{2\omega}$ mode, although nonlinearities could arise from strains in the film. These calculations suggest that the most efficient conversion does occur for the TM_0 mode (at 1.053 μm) to TE_1 mode (at 5265 Å). The overlap of this modal conversion can be seen in Fig. 3. Work to measure the SHG efficiency of different mode configurations is presently in progress.

TABLE II. Overlap integrals of mode conversions for 1.053 μm to 5265 Å wavelengths for a $KNbO_3$ film on MgO substrate.

Mode conversion (1.053 μm to 5265 Å)	Phase-matching thickness, Å	Overlap integral, $Å^{-1/2}$
TM_0^{ω} to $TE_1^{2\omega}$	2326	2.78×10^{-3}
TE_0^{ω} to $TE_1^{2\omega}$	3866	1.86×10^{-3}
TM_0^{ω} to $TM_1^{2\omega}$	3980	0.66×10^{-3}
TM_0^{ω} to $TE_2^{2\omega}$	6718	2.16×10^{-3}

IV. CONCLUSIONS

High quality epitaxial $KNbO_3$ thin film planar waveguides have been grown by ion-beam sputter deposition. An infrared laser has been used to produce green light by SHG from $KNbO_3$ thin films on both MgO and $KTaO_3$ substrates. Film thicknesses of only 4600–6500 Å exhibited green light when placed perpendicular to the beam. A green light streak 3–4 mm in length was also observed when light was coupled in the TM_0 mode into a $KNbO_3$ thin film on MgO. The film thickness was close to 2300 Å, where modal dispersion phase-matching occurs for the TM_0 mode at 1.053 μm and the TE_1 mode at 5265 Å.

ACKNOWLEDGMENTS

This research is supported in part by the Office of Naval Research under Contract No. N0014-91-J-1307. We thank Dr. N. R. Parikh at the University of North Carolina, Chapel Hill, for use of the RBS equipment and Dr. L. A. Boatner for the $KTaO_3$ substrates.

[1] I. Stambler, Research and Development Magazine, September 1993.
[2] J. Ohya, G. Tohmon, K. Yamamoto, T. Taniuchi, and M. Kume, Appl. Phys. Lett. **56**, 2270 (1990).
[3] G. H. Hewig and K. Jain, J. Appl. Phys. **54**, 57 (1983).
[4] D. B. Anderson and J. T. Boyd, Appl. Phys. Lett. **19**, 266 (1971).
[5] D. K. Fork and G. B. Anderson, Appl. Phys. Lett. **63**, 1029 (1993).
[6] P. Günter, Proc. SPIE **236**, 8 (1980).
[7] T. Bremer, W. Heiland, B. Hellermann, P. Hertel, E. Kratzig, and D. Kollewe, Ferroelectrics Lett. **9**, 11 (1988).
[8] D. Fluck, P. Günter, R. Irmscher, and Ch. Buchal, Appl. Phys. Lett. **59**, 3213 (1991).
[9] B. Zysset, I. Biaggio, and P. Günter, J. Opt. Soc. Am. B **9**, 380 (1992).

[10]O. A. Khachaturyan and R. S. Madoyan, Crystal Res. Technol. **19**, 461 (1984).
[11]S. L. Swartz, P. L. Melling, and C. S. Grant, Mater. Res. Soc. Symp. Proc. **152**, 227 (1989).
[12]D. Roy, G. Derderian, J. Barrie, K. Aitchinson, and M. Mecartney, 6th International Symposium Integrated Ferroelectrics, Monterey, CA, 1994, paper 53c.
[13]C. Zaldo, D. S. Gill, R. W. Eason, J. Mendiola, and P. J. Chandler, Appl. Phys. Lett. **65**, 502 (1994).
[14]S. Schwyn Thöny, H. W. Lehmann, and P. Günter, Appl. Phys. Lett. **62**, 373 (1992).
[15]D. Fluck, B. Binder, M. Kupfer, H. Looser, C. Buchal, and P. Günter, Opt. Commun. **90**, 304 (1992).
[16]D. Fluck, J. Moll, P. Günter, M. Fleuster, and Ch. Buchal, Electron. Lett. **28**, 1092 (1992).
[17]A. F. Chow, D. J. Lichtenwalner, R. R. Woolcott, Jr., T. M. Graettinger, O. Auciello, A. I. Kingon, L. A. Boatner, and N. R. Parikh, Appl. Phys. L[illegible] **65**, 1073 (1994).
[18]A. F. Chow, D. J. Lichtenwalner, T. M. Graettinger, J. R. Busch[illegible] Auciello, and A. I. Kingon, IEEE Proceedings of the Ninth International Symposium on the Applications of Ferroelectrics (ISAF 94), p. 791.
[19]R. Ulrich and R. Torge, Appl. Opt. **12**, 2901 (1973).
[20]T. M. Graettinger, S. H. Rou, M. S. Ameen, O. Auciello, and A. I. Kingon, Appl. Phys. Lett. **58**, 1964 (1991).
[21]Y. Suematsu, Y. Sasaki, K. Furuya, K. Shibata, and S. Ibukuro, IEEE J. Quantum Electron. **10**, 222 (1974).
[22]G. I. Stegeman and C. T. Seaton, J. Appl. Phys. **58**, R57 (1985).
[23]G. L. J. A. Rikken, Opt. Lett. **18**, 1916 (1993).
[24]I. Biaggio, P. Kerkoc, L.-S. Wu, P. Günter, and B. Zysset, J. Opt. Soc. Am. B **9**, 507 (1992).
[25]Landolt-Bornstein, *New Series, Group III* (Springer, New York, 1981), Vol. 16, Part A.

Appendix 3

"A Study of Microstructures in Ferroelectric Pb(Zr,Ti)O3 and $KNbO_3$ Thin Films, A. I. Kingon, S. H. Rou and Y. L. Chen, Proceedings of the 52nd Annual Meeting of the Microscopy Society of America, 574-575, 1994.

G. W. Bailey and A. J. Garratt-Reed, Eds., Proc. 52nd Annual Meeting of the Microscopy Society of America
Held jointly with the 29th Annual Meeting of the Microbeam Analysis Society
 Published by San Francisco Press, Inc., Box 426800, San Francisco, CA 94142-6800, USA

A STUDY OF MICROSTUCTURES IN FERROELECTRIC $Pb(Zr,Ti)O_3$ AND $KNbO_3$ THIN FILMS

A.I. Kingon, S.H. Rou, and Y.L. Chen

Department of Materials Science and Engineering, *North Carolina State University*,
Raleigh, NC 27695-7919

Oxide ferroelectric thin films are receiving considerable attention due to their potential application in a wide range of devices including ferroelectric nonvolatile memory, dynamic random access memory (DRAMs) electrooptic phase modulators, and laser light source frequency doublers. However, the complexity of the oxide materials has resulted in a relatively slow development of structure-processing property relationships. In this paper, we review in turn how the microstructures of epitaxial $KNbO_3$ and $Pb(Zr,Ti)O_3$ have been significantly improved over a period of time.

In the case of epitaxial $KNbO_3$ on oxide single crystal substrates, defect types which need to be controlled include 221-type misorientations, low angle boundaries, multiposition domains, and inversion domains[1-3]. Several of these defect types are controlled *via* the substrate surface preparation. The role of lattice mismatch between film and substrate on the formation of the low angle boundaries remains an unresolved issue. We are currently comparing *via* TEM the $KNbO_3$(100) films on (100)MgO, (100)$MGAl_2O_4$, (100)$NdGaO_3$ and (100)$KTaO_3$ substrates; these substrates covering a range of values of lattice mismatch between 0.1% and 5.0%.

Some special features have been noted $KNbO_3$ epitaxial films[4]. 1.) We have seen that the first atomic layer which is deposited can have a large impact on the microstructure. If the BO_2 layer of the (100)ABO_3 perovskite is deposited first on the MgO substrate,, good epitaxy is maintained. However, if the AO layer is deposited first, then the structure can be rotated 45°, despite a large mismatch of >33%[6]. This phenomenon can be explained in terms of electrostatic interactions across the interface. 2.)Smooth interfaces are critically important for optical waveguides. For the perovskites, this practically eliminates all orientations except (pseudocubic) (100). For example, growth of (110) $KNbO_3$ (in pseudocubic axes) results in strong (100) faceting. A practical procedure for eliminating this tendency has not been developed. 3.) A surprisingly common feature which has been observed in the $KNbO_3$ films has been the observation of an amorphous layer at the substrate-film interface, which grows after the epitaxial nucleation has been established. Examples include $KNbO_3$/Pt, $KNbO_3$/y$Ba_2Cu_3O_7$, as well as the analogous $Pb(Mg_{0.33}Nb_{0.67})O_3$/$Sr,TiO_3$.

In the case of epitaxial $Pb(Zr,Ti)O_3$ PZT films, the microstructures are dominated by the presence of competing pyrochlore-type phases. As a result, properties are dominated by nucleation phenomena at the substrate. In these cases, the substrate is usually a conducting epitaxial metal or oxide, such as (100)Pt/(100)MgO, (100)La(SrCo)O_3/(100)MgO, or (1$\bar{1}$0)RuO_2/(100)MgO[5]. For example, nucleation of the desired perovskite phase appears to be far easier on Pt than on RuO_2. Even if steps are taken to increase the nucleation rate of perovskite $Pb(Zr,Ti)O_3$, the effect of this nucleation phenomenon can still be observed. The microstructures of the epitaxial PZT/RuO_2 films all show signs of second phases of the pyrochlore type located at the perovskite grain boundaries. This impacts the properties.

1. S.H. Rou et al ,*Mat. Res. Soc. Symp. Proc.* 243(1992)81
2. M.S.Ameen et al *Mat. Res. Soc. Symp.Proc.* 200(1990)65
3. S.H. Rou et al *Mat. Res. Soc. Symp Proc.*.183(1990)285
4. T.M. Graettinger et al *Mat. Res. Soc. Symp.Proc.* 310(1993)301
5. P.D.Hren et al *Integrated Ferroelectrics* 2(1992)311
6. S.H.Rou et al *Mat. Res. Soc. Symp Proc.* 221(1991)65
7. A.F. Chow et al submitted *Appl. Phys. Lett.* (1994)
8. H.N.Al-Shareef et al *IMF8* (1993), acceptd for publication in *Ferroelectrics*, 1994
9. H.N.Al-Shareef et al *Integrated Ferroelctrics* 3(1993)259
10. This research was supported by the Office of Naval Research under contract N00014-91-J-1307, and Advanced Research Projects Agency under contract N00014-93-1-0591

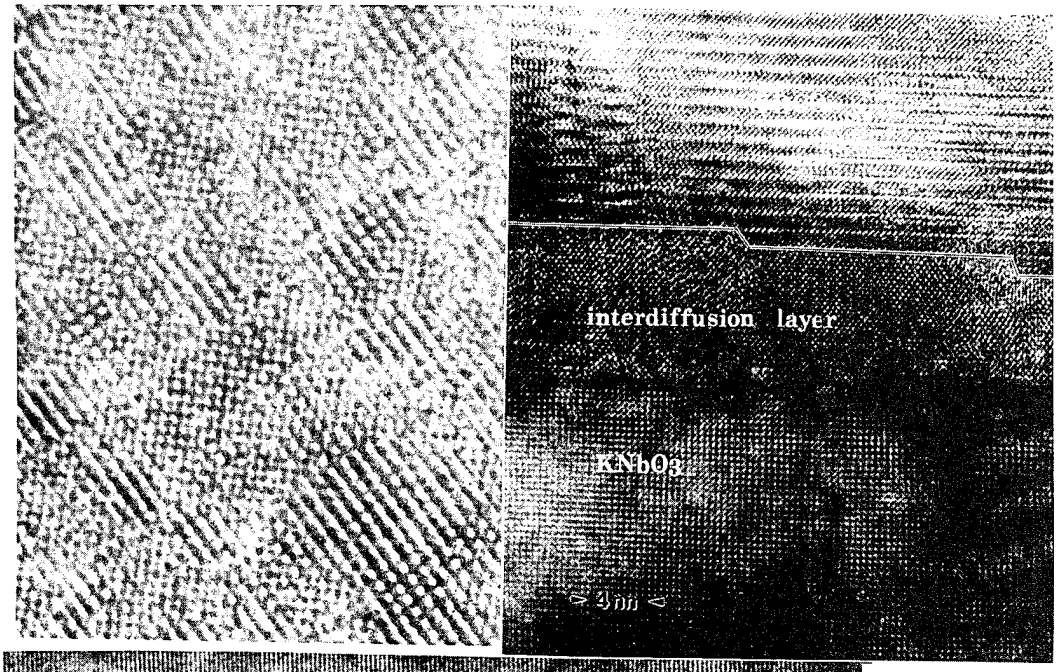

Figures 1 and 2

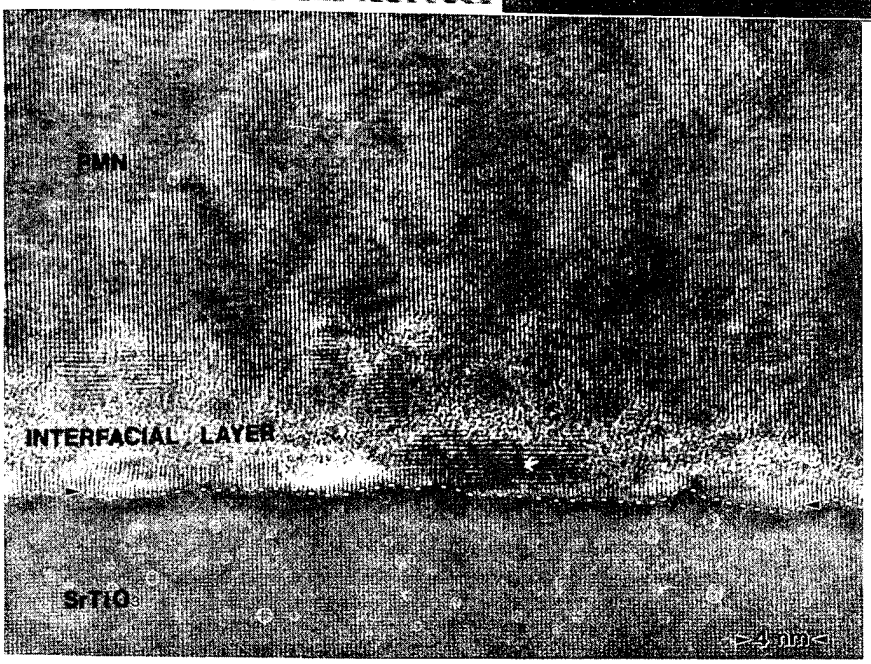

Figure 3

Figure 1 Defective $KNbO_3$ showing very high density of inversion domain boundaries.
Figure 2 $YBa_2Cu_3O_7$ on $KNbO^3$/MgO showing interdiffusion layer
Figure 3 $Pb(Mg0_{.33}Nb_{0.67})O_3$ on $SrTi)_3$ showing interfacial layer.

Appendix 4

"Processing Thin Films of $KNbO_3$ For Optical Waveguides," T. M. Graettinger, D. J. Lichtenwalner, A. F. Chow, O. Auciello, and A. I. Kingon, Integrated Ferroelectrics, Vol. 6, p. 363, 1994.

Integrated Ferroelectrics, 1995, Vol. 6, pp. 363–373
Reprints available directly from the publisher
Photocopying permitted by license only

PROCESSING THIN FILMS OF $KNbO_3$ FOR OPTICAL WAVEGUIDES

T. M. GRAETTINGER*, D. J. LICHTENWALNER*,
A. F. CHOW*, O. AUCIELLO*,**, AND A. I. KINGON*
*North Carolina State University, Raleigh, NC 27695-7919.
**MCNC, Electronics Technology Division, RTP, NC 27709-2889.

P. A. MORRIS
DuPont Central Research and Development, Wilmington, DE.

(Received April 6, 1994; in final form May 16, 1994)

Abstract Thin film waveguides of ferroelectric materials hold great promise for use in active integrated optics devices because of the high optical confinement possible in a thin film structure. $KNbO_3$ is an attractive material for active devices because it possesses large nonlinear optical susceptibilities and large electro-optic coefficients. $KNbO_3$ films with low optical losses are required to produce efficient devices. Epitaxial films of $KNbO_3$ (110) have previously been deposited on single crystal MgO (100) using ion beam sputtering techniques. However, these films contained microstructural defects due to the large lattice mismatch (>4.0%) between $KNbO_3$ and MgO which resulted in high optical losses. Recent work has focused on determining the relationships between microstructure and optical loss through the use of lattice matched substrates. Film composition, epitaxial quality and optical properties of $KNbO_3$ films deposited on MgO and $MgAl_2O_4$ have been investigated and are compared.

INTRODUCTION

Crystalline optical waveguides hold great promise for use in integrated optics because high power densities can be maintained over long interaction lengths. Waveguides of ferroelectric materials are of special interest because of their generally strong nonlinear optical, electro-optic, and photorefractive effects. Currently one application of technological importance which uses the nonlinear optical properties of these materials

is second harmonic generation (SHG). SHG has been proposed as a viable route to producing a compact, blue laser. Blue light is considered necessary for the next generation of optical storage devices, and has many uses in the laser writing and medical fields because the smaller wavelength means increased resolution. Efficient SHG of GaAs lasers is possible in ferroelectric materials and has been demonstrated in thin films of $LiNbO_3$[1,2] and $BaTiO_3$,[3] among others. Many technological challenges to producing a commercial device based on thin film materials still remain. The greatest of these challenges is fabricating a thin film waveguide with low enough optical loss to permit blue light generation of sufficient power for applications. This paper presents an investigation of the processing of $KNbO_3$ thin films and relates the optical properties to growth characteristics.

PROCESSING OF $KNbO_3$ FILMS

Bulk crystal growth of $KNbO_3$ has been studied for nearly 45 years. The phase diagram of the Nb_2O_5-K_2O system, first reported by Reisman and Holtzberg,[4] reveals that $KNbO_3$ melts incongruently. Thus solution growth techniques have been limited to growth from K_2O-rich melt compositions. Little is therefore known about the effects of composition on the structure and properties of $KNbO_3$. Thin film processing techniques, many of which are non-equilibrium processes, promise the ability to surpass the limits of solution crystal growth. The region of the phase diagram around stoichiometric $KNbO_3$ can then be studied.

Determining the limits of the solid solubility region for $KNbO_3$ are an important first step toward understanding the effects of composition on the perovskite structure of $KNbO_3$. Thin films of $KNbO_3$ with K/Nb cation ratios ranging from 1.35 to 0.66 were grown on single crystal MgO (100) substrates using an ion beam co-sputter deposition system which has been described in detail previously.[5] During film growth a niobium target and a potassium superoxide, KO_2, target were sputtered simultaneously in the presence of molecular oxygen. Changes in the cation ratio were achieved by independently controlling the ion beam energy and current on each target. Typical growth conditions for near stoichiometric $KNbO_3$ films are given in Table I.

X-ray diffraction was used to determine the limits of the single phase region of $KNbO_3$. A selected group of theta-two theta diffraction patterns from this study are shown in Figure 1. Figures 1(a) and 1(b) show the diffraction patterns of potassium-rich films with cation ratios (K/Nb), determined from Rutherford backscattering spectroscopy (RBS),

Table I Processing conditions for $KNbO_3$ thin films.

Parameter	Value
KO_2: Ion Beam Energy	500 eV
KO_2: Ion Beam Current	11 mA
Nb: Ion Beam Energy	750 eV
Nb: Ion Beam Current	16 mA
Xe Pressure (Sputtering Gas)	2.0×10^{-4} torr
O_2 Pressure	1.0×10^{-4} torr
Growth Temperature	600-700°C

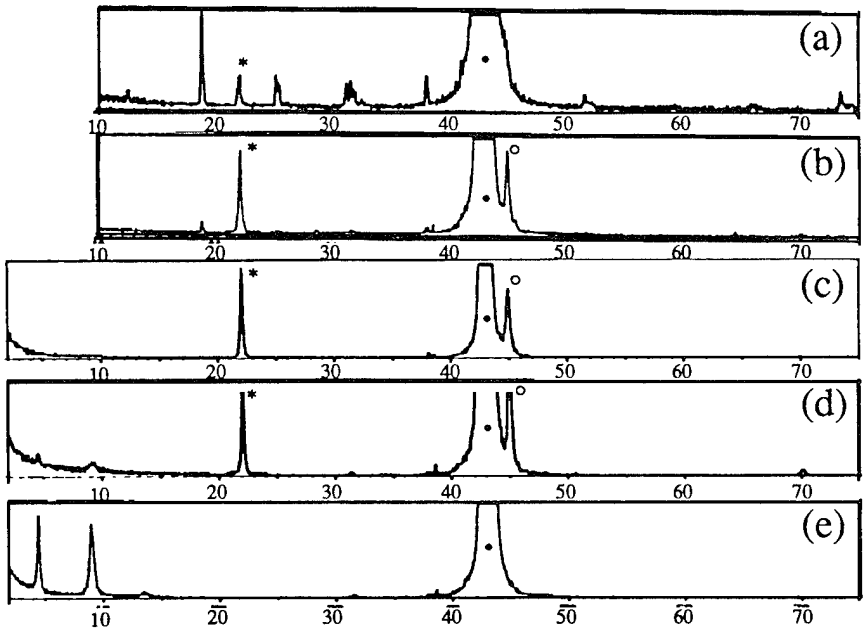

Figure 1 X-ray diffraction patterns of potassium niobium oxide thin films showing the phase evolution as the cation ratio (K/Nb) changes from (a) 1.35, (b) 1.18, (c) 1.00, (d) 0.77, to (e) 0.66. [* $KNbO_3$ (110), • MgO (200), ° $KNbO_3$ (220)]

of 1.35 and 1.18, respectively. Figure 1(b) reveals the presence of second phases in the thin film. As the composition becomes further potassium rich, as shown in Figure 1(a), more second phase(s) form as evidenced by more, and more intense, diffraction peaks not due to the $KNbO_3$ phase. The limit of the single phase region of $KNbO_3$ on the potassium-rich side can be conservatively estimated to be reached at a cation ratio of 1.10±5%. The second phase(s) which form above this limit can not be matched to those expected from Reisman and Holtzberg's

phase diagram.[4] Instead, metastable phases have apparently formed during the non-equilibrium growth process.

Figures 1(d) and 1(e) represent x-ray diffraction patterns of niobium-rich, potassium niobium oxide thin films. As seen in Figure 1(e), the $KNbO_3$ phase disappears entirely from the diffraction pattern as the cation ratio reaches 0.66. The limit of the single phase region of $KNbO_3$ was reached at 0.80±5%. Thus the $KNbO_3$ perovskite structure will tolerate a larger potassium deficiency than niobium deficiency before second phases begin forming. It should be noted that the limits of the single phase $KNbO_3$ region determined in this study may differ when using other processing parameters, or for other growth techniques.

The $KNbO_3$ phase which appears in Figures 1(a) through 1(d) is highly oriented (110) normal to the substrate. The following sections present results of our investigation of the epitaxial quality of these (110) oriented $KNbO_3$ films.

Epitaxy of Ion Beam Sputter Deposited $KNbO_3$

Thin films of $KNbO_3$ were grown on single crystal MgO (100) and single crystal $MgAl_2O_4$ (100) substrates using the ion beam sputter deposition process described above. MgO and $MgAl_2O_4$ were chosen for this study for their reasonably small lattice mismatch and chemical inertness to the perovskite $KNbO_3$. Table II summarizes the lattice parameters of these two substrates and their lattice mismatch with (110) oriented $KNbO_3$. Since $KNbO_3$ is orthorhombic at room temperature, the lattice mismatch between the cubic substrates and both in-plane lattice parameters of $KNbO_3$ (3.973Å and 4.035Å) are given in the table. It is clear from the table that $MgAl_2O_4$ is much better lattice matched to $KNbO_3$ than MgO. Thus it was expected that films deposited on $MgAl_2O_4$ would show a higher degree of epitaxy.

All $KNbO_3$ films grown on MgO (100) and $MgAl_2O_4$ (100) were highly oriented (110) normal to the substrate. Typical x-ray diffraction patterns of these films are shown in Figure 2(a) and Figure 3(a). It was discovered previously through pole figure measurements that $KNbO_3$ films on MgO display a lattice tilt of 1-1.5° about the substrate normal.[5]

Table II Physical properties of substrates used for $KNbO_3$ film growth.

	MgO (100)	$MgAl_2O_4$ (100)
Lattice Parameter, Å	4.213	8.083
Lattice mismatch, %	6.0, 4.4	1.7, 0.1
Bulk refractive index	1.736	1.723

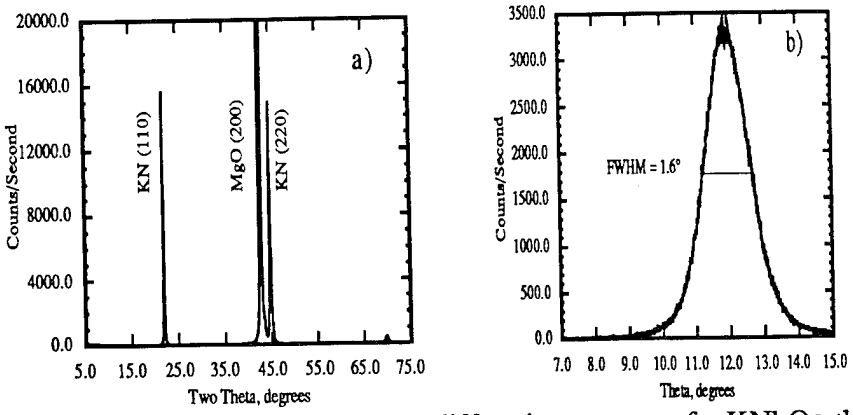

Figure 2 (a) A typical x-ray diffraction pattern of a KNbO3 thin film on MgO, and (b) a rocking curve measurement of the KNbO3 (110) diffraction peak for the film in (a).

In addition, the tilt occurs along all four in-plane substrate [100] directions, evidencing the presence of 90°, 180°, and 270° rotated grains. The x-ray rocking curve measurement of the (110) diffraction peak of a typical KNbO3 film on MgO is shown in Figure 2(b). The width of the rocking curve, FWHM=1.5°, also confirms the misorientation of KNbO3 films on MgO. The lattice tilt and grain rotations accommodate the strain induced in the films on MgO due to the >4% lattice mismatch. Much less lattice tilting is expected for films on $MgAl_2O_4$ whose lattice mismatch is less than 2%. Figure 3(b) shows the rocking curve measurement of the (110) KNbO3 diffraction peak of a film on $MgAl_2O_4$. The FWHM=0.6 is indeed much smaller than the films on MgO, indicating a higher degree of epitaxy for these films. The optical properties of KNbO3 / $MgAl_2O_4$ films which will be discussed below indicate that the grain rotations seen in films deposited on MgO exist in these films as well.

Epitaxy of Ion-assisted Ion Beam Sputter Deposited KNbO3

The ion beam co-sputter-deposition process described above was modified by the addition of a filamentless rf ion source. The rf ion source was used to bombard the growth surface at normal incidence with low energy oxygen ions. Ion-assisted film growth can provide many beneficial effects for film growth including increasing the activity of depositing species which promotes compositional homogeneity and film adherence. In addition, lower processing temperatures may be possible

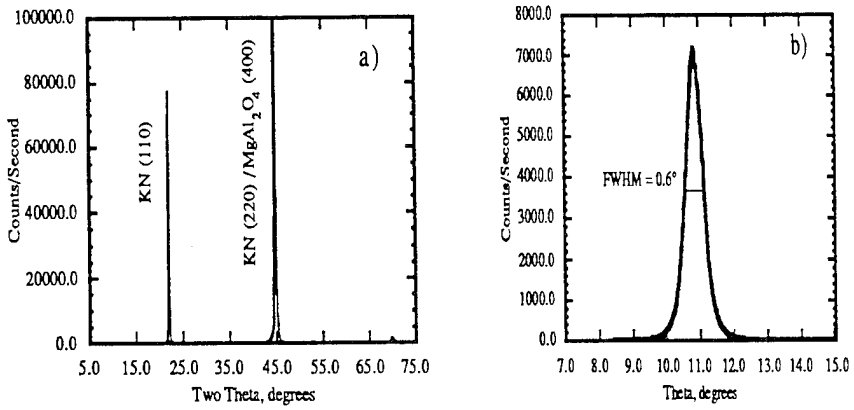

Figure 3 (a) X-ray diffraction pattern of a (110) $KNbO_3$ thin film on $MgAl_2O_4$, and (b) a rocking curve measurement of the $KNbO_3$ (110) diffraction peak for the film in (a).

with ion-assisted growth which may be necessary for integration with semiconductor processing. Nucleation and growth mechanisms can also change, modifying film morphology and microstructure. However, the current study focused on investigating the effects of ion-assisted growth on film orientation and epitaxial quality.

For this study $KNbO_3$ films were again grown on MgO and $MgAl_2O_4$ substrates. Typical processing conditions are shown in Table III. X-ray diffraction patterns reveal that the film (110) axis is normal to the substrate as it was for films deposited without ion-assist. However, the lattice spacing is slightly enlarged compared to the (110) spacing of unassisted films. This comparison is shown in the x-ray diffraction patterns in Figure 4(a) where the (110) peak for the ion-assisted film has shifted to a slightly lower angle. It can also been seen in Figure 4(a) that the (110) diffraction peak of the ion-assisted film is much broader and less symmetrical than the peak of the unassisted film. This is a qualitative indication that the oxygen ion-assist beam has worsened the quality of the $KNbO_3$ films. The rocking curve measurement, shown in Figure 4(b), quantitatively reveals in dramatic fashion that the epitaxial quality of the ion-assisted $KNbO_3$ films is inferior to that of films deposited without ion-assistance. The FWHM of the rocking curve of a $KNbO_3$/ $MgAl_2O_4$ film has increased to over 2° compared to a value of 0.6° for an unassisted film [Figure 3(b)].

The increase in lattice parameter for ion assisted films has been attributed to impurity incorporation. The RBS spectrum shown in Figure

Table III Process parameters for ion-assisted growth of KNbO3 thin films.

Process Parameter	Value
KO2: Ion Beam Energy	850 eV
KO2: Ion Beam Current	13 mA
Nb: Ion Beam Energy	1000 eV
Nb: Ion Beam Current	10 mA
Xe Pressure (Sputtering Gas)	2.0×10^{-4} torr
O_2^+ Energy	50 eV
O_2^+ Current	10 mA
O_2 Pressure	1.0×10^{-4} torr
Growth Temperature	600-700°C

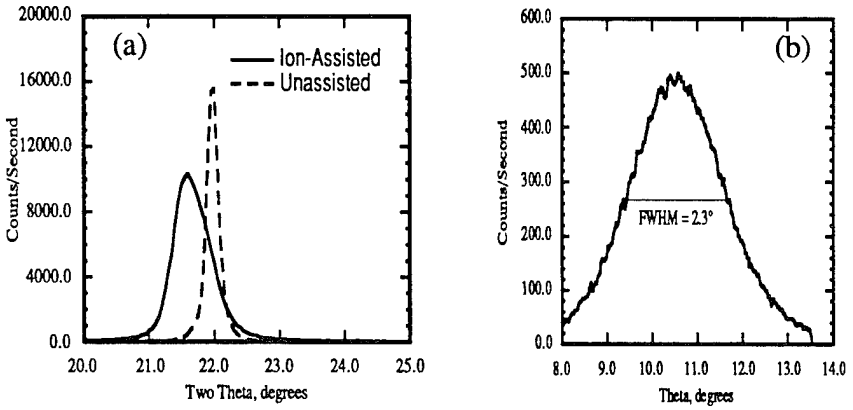

Figure 4 (a)KNbO3 (110) diffraction peaks for ion-assisted and unassisted films. (b) A rocking curve measurement of the KNbO3 (110) diffraction peak for an ion-assisted film.

5 reveals that the ion-assisted films contain Fe and Xe impurities. The Fe impurity has been traced to the stainless steel ring electrode inside the discharge chamber of the rf ion source. For future work it may be possible to replace this electrode with a niobium electrode which would eliminate the source of contamination. The Xe detected is trapped primary sputtering gas that has been trapped in the film during growth. Changing the incidence angle of the oxygen ion-assist beam may reduce this gas incorporation. However, the position of the rf ion source is fixed in the current deposition system. Morphology and microstructure of ion-assisted films has yet to be studied. If the impurities can be eliminated the ion-assisted KNbO3 films may yet show improved characteristics.

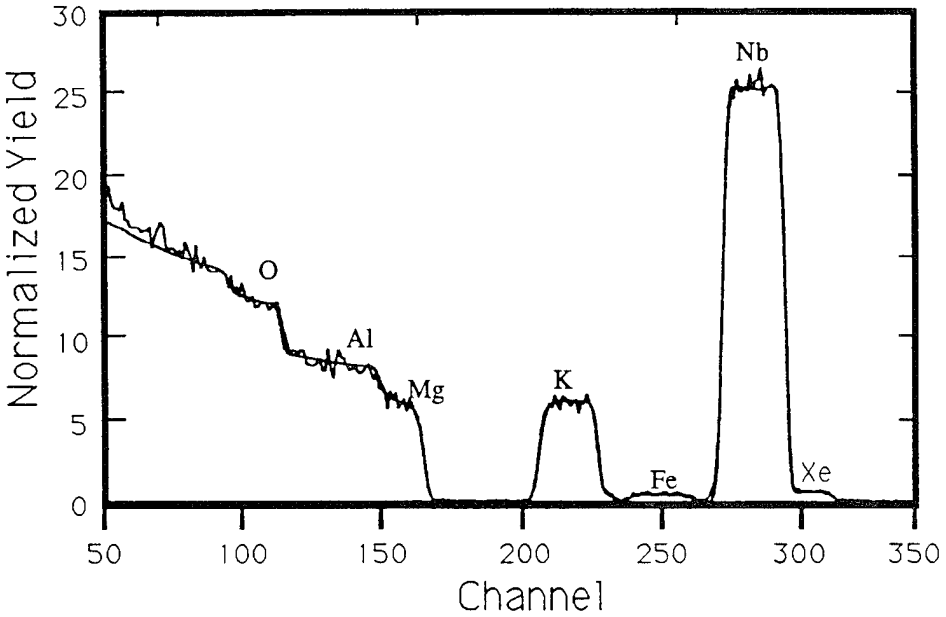

Figure 5 A Rutherford backscattering spectrum of an ion-assisted $KNbO_3$ film showing the presence of Fe and Xe impurities.

OPTICAL CHARACTERIZATION

Optical properties of both ion-assisted and unassisted ion beam sputter deposited $KNbO_3$ thin films were measured using a rutile prism coupler. The refractive indices of the films were determined using the numerical technique developed by Ulrich and Torge.[6] Unassisted $KNbO_3$ films on both MgO and $MgAl_2O_4$ substrates had refractive indices of 2.28 for TE modes and 2.22 for TM modes. The value for the TM modes is very near the bulk value of 2.2221 expected for a (110) oriented crystal. A single crystal $KNbO_3$ film would be expected to have birefringence between orthogonal TE modes. However, no birefringence was observed for orthogonal TE modes in these films. The grain rotations that were observed in the x-ray analyses above lead to a single, averaged refractive index for TE modes in the films.

The refractive indices measured for ion-assisted deposited films were slightly lower than the indices measured for unassisted films. The refractive index for TE modes was 2.26 while the index for TM modes was 2.18. Again no birefringence was observed for TE modes. The decrease in the refractive indices results from the presence of Fe and Xe impurities in the films as discussed above. These impurities increased

the lattice parameter of the films thereby lowering the density of the films which is known to reduce the refractive indices.

Optical losses were measured by optically coupling to the $KNbO_3$ thin films with a rutile prism and observing the light streak traveling through the films. These observations lead to several qualitative conclusions about the $KNbO_3$ thin films. First it was found that TM modes have lower losses than TE modes. Second, thin films (1000-1300Å) have significantly lower losses than thicker films (>1500Å). Third, films on MgO have lower optical loss than films on $MgAl_2O_4$; and finally, that losses were so high in ion-assisted thin films that no light streaks could be observed. An analysis of each of these conclusions will follow below.

The high optical loss of guided TE modes relative to TM modes can be understood from an analysis of reflection and refraction at grain boundaries. In the x-ray analysis above, it was found that grain rotations of 90°, 180°, and 270° exist in $KNbO_3$ films. While there is no change in refractive index as a TM mode crosses a grain boundary, there is a refractive index change of 0.11 that occurs as a TE mode crosses a boundary. This index change causes reflection and refraction to occur at these boundaries depending on the angle of incidence of the guided light. The grain size of the $KNbO_3$ films is on the order of 1000Å, so thousands of these boundaries must be crossed in order for a TE mode to propagate an appreciable distance in the film. Therefore propagation is prohibited by light scattering due to reflection and refraction, leading to high optical loss.

The second conclusion above stated that thin films had lower optical loss than thick films. This statement is more evident for TM modes since losses for TE modes in all films are high and are dominated by reflection and refraction at grain boundaries as discussed above. To determine the nature of this observation, the electric field distributions for a thin film (1180Å) and for a thick film (1965Å) were plotted. The field distributions normalized to the Poynting vector are shown in Figure 6. It is clear from the field distributions that much of the optical energy of the guided mode is traveling through the substrate in the thin film. Since the substrate is a single crystal of high optical quality, naturally the thinner film has lower total optical loss for the guided light. Work is currently in progress to determine whether the source of optical loss in the films is due to interface or bulk effects.

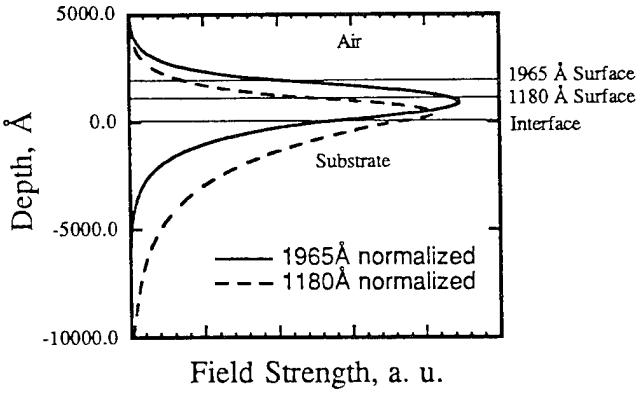

Figure 6 Optical field distributions in $KNbO_3$ thin films.

It is currently unclear why films on MgO have lower optical loss than films on $MgAl_2O_4$. Initially films on $MgAl_2O_4$ were expected to have lower optical loss because of the higher degree of epitaxy discussed earlier in this work. It is suspected that interface effects which do not impair the epitaxial relationship, possibly diffusion between film and substrate, are the source of the higher optical loss. Finally, the high optical losses in ion-assisted $KNbO_3$ thin films are attributed to defects in the film resulting from impurity incorporation and to possible interface damage resulting from bombardment by oxygen ions. Work is continuing to separate and quantify these effects.

SUMMARY

In summary, the single phase region of $KNbO_3$ was investigated to understand the effect of composition on phase formation. The single phase region was determined by x-ray diffraction measurements and RBS spectra to lie between the K/Nb cation ratios of 1.10±5% and 0.80±5%. The epitaxial quality of stoichiometric $KNbO_3$ films deposited on single crystal MgO (100) and single crystal $MgAl_2O_4$ (100) substrates was analyzed through x-ray rocking curve measurements. Films on $MgAl_2O_4$ were found to possess much less misorientation as evidenced by a rocking curve FWHM of 0.6 compared to a FWHM of 1.6 for films on MgO. The addition of a low-energy oxygen ion-assist source to the deposition process was found to degrade the quality of epitaxy on both substrates due to impurity incorporation.

The waveguiding properties of the $KNbO_3$ films were also studied. The refractive indices were measured using a rutile prism coupler and were found to be near bulk values, TE=2.28 and TM=2.20. No in-plane birefringence was observed due to grain rotations which result from lattice mismatch between film and substrate. The refractive indices of ion-assisted films were reduced to TE=2.26 and TM=2.18 by the incorporation of Fe and Xe impurities during processing. Optical losses were also observed in these films. Thin $KNbO_3$ films (1000-1250Å) on MgO substrates demonstrated the lowest optical losses of the films studied.

ACKNOWLEDGMENTS

The authors would like to acknowledge: the Office of Naval Research for partial support of this work under contract N00014-91-J-1307; and Bruce Rothman and the Laboratory for Research on the Structure of Matter at the University of Pennsylvania for assistance and use of their equipment in making the RBS measurements under NSF#DMR91-20668.

REFERENCES

1. K. Nunomura, A. Ishitani, T. Matsubara, and I Hayashi, J. Cryst. Growth, 45, 355 (1978).
2. G. H. Hewig and K. Jain, J. Appl. Phys., 54, 57 (1983)
3. H. Lu, L. Wills, B. Wessels, W. Lin, T. Zhang, G. Wong, D. Neumayer, and T. Marks, Appl. Phys. Lett., 62, 1314 (1993).
4. A. Reisman and F. Holtzberg, J. Am. Chem. Soc., 77, 2115 (1955).
5. T. M. Graettinger, P. A. Morris, R. R. Woolcott, F. C. Zumsteg, A. F. Chow, and A. I. Kingon, in Ferroelectric Thin Films III, MRS Symposium Proceedings, Vol. 310 (MRS, Pittsburgh, PA, 1993), p. 301.
6. R. Ulrich and R. Torge, Applied Optics, 12, 2901 (1973).

Appendix 5

"Growth of Epitaxial $KNbO_3$ Thin Films," Thomas M. Graettinger, P. A. Morris, A. Roshko, A. I. Kingon, O. Auciello, D. J. Lichtenwalner, and A. F. Chow, MRS Symposium Proceedings **341** (Epitaxial Oxide Thin Films and Heterostructures),265-276, 1994.

Preprint: Submitted to MRS Proceedings "Epitaxial Oxide Thin Films and Heterostructures," Spring 1994.

GROWTH OF EPITAXIAL $KNbO_3$ THIN FILMS

THOMAS M. GRAETTINGER,* P.A. MORRIS,** A. ROSHKO,*** A. I. KINGON,* O. AUCIELLO,*,**** D.J. LICHTENWALNER,* AND A.F. CHOW*
*North Carolina State University, Department of Materials Science and Engineering, Raleigh, NC 27695-7919
**DuPont Company, Wilmington, DE 19880-0356
***National Institute of Standards and Technology, Boulder, CO 80303-3328
****MCNC, Electronics Technology Division, Research Triangle Park, NC 27709-2889

ABSTRACT

$KNbO_3$ possesses high nonlinear optical coefficients making it a promising material for frequency conversion of infrared light into the visible wavelength range using integrated optical devices. While epitaxial thin films of $KNbO_3$ have previously been grown using ion beam sputtering,[1] defects (i.e. grain boundaries, domains, surface roughness) in these films resulted in high optical losses and no measurable in-plane birefringence. Previous films were grown on MgO substrates, which have a >4% lattice mismatch with $KNbO_3$. In the work reported here, we have grown films on MgO, $MgAl_2O_4$, $NdGaO_3$, and $KTaO_3$ to investigate the role of lattice mismatch on the resulting film quality. Films have also been grown with and without oxygen ion assistance. The orientations, morphologies, and defects in the films were examined using x-ray diffraction and AFM to determine their relationships to the growth conditions and substrate lattice mismatch.

INTRODUCTION

Applications for ferroelectric oxide thin films have increased rapidly in the last ten years. One application that is currently receiving much attention is second harmonic generation, SHG, which allows infrared laser diode wavelengths to be frequency doubled to the blue region of the visible spectrum. Coherent blue light is desired for many next-generation applications, such as optical recording and laser printing, where the smaller wavelength leads to increased resolution. Ferroelectric oxides are an important class of materials for SHG because of their generally large nonlinear optical coefficients. High quality thin films of these oxides are desirable for integrating active waveguides with current laser diode technology. However, many technological challenges remain to be solved to produce device quality ferroelectric thin films. These challenges include producing a low optical loss thin film and, additionally, meeting the requirements for SHG. SHG has been demonstrated in thin films of $LiNbO_3$[2,3] and $BaTiO_3$,[4] among others, but few have met the additional requirements of a low loss waveguide which is necessary for efficient SHG. It is becoming clear to researchers in this field that controlling the microstructure of these films will be necessary to achieving the goal of efficient SHG. The deposition process and the epitaxial quality and surface morphology of $KNbO_3$ thin films are investigated in this work as a step toward understanding the influences of microstructure on optical properties.

ION BEAM SPUTTER DEPOSITION

An ion beam co-sputter deposition system, which has been described previously,[1] was developed for the growth of complex oxide thin films. Ion beam sputtering is well known to produce dense, smooth films, which are very important criteria for optical quality films. A co-deposition route was chosen for the ability to independently control the cation stoichiometry. A niobium and a potassium superoxide, KO_2, target were sputtered simultaneously by Xe ion beams from 3 cm Kaufmann-type ion sources. By independently controlling the ion energy and ion current on each target, the desired film composition could be achieved. Figure 1 clearly illustrates this ability of the deposition system. In Figure 1(a) the ion energy of the beam sputtering the KO_2 target was varied from 500 to 750 eV while all other deposition parameters remained constant. These changes in ion energy resulted in changes in the K/Nb cation ratio from 0.9 to 1.85, determined from Rutherford backscattering spectra (RBS), as shown. Similarly, Figure 1(b) shows the control of cation stoichiometry by changing the ion current on the Nb target. It was experimentally determined that single phase $KNbO_3$ thin films resulted for cation ratios between 0.80 and 1.10 (±0.05). This single phase region is considerably wider than expected from the phase diagram determined by Reisman and Holtzberg[5] for the Nb_2O_5-K_2O system. Table I lists the typical processing parameters for the growth of stoichiometric $KNbO_3$.

EPITAXIAL GROWTH OF $KNbO_3$

$KNbO_3$ thin films were grown on single crystal MgO (100) and single crystal $MgAl_2O_4$ (100) substrates because of the reasonably good lattice match that exists between $KNbO_3$ and

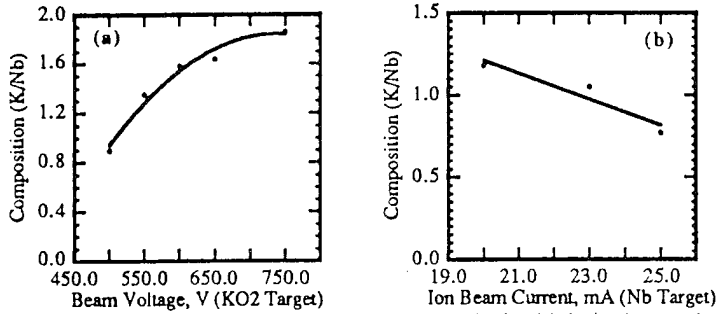

Figure 1 Cation stoichiometry can be controlled by adjusting (a) the ion beam voltage, or (b) the ion beam current.

Table I Typical processing parameters for ion beam sputter deposition of $KNbO_3$ thin films.

Parameter	Unassisted Deposition	Ion-assisted Deposition
KO_2: Ion Beam Energy	500 eV	850 eV
KO_2: Ion Beam Current	11 mA	13 mA
Nb: Ion Beam Energy	750 eV	1000 eV
Nb: Ion Beam Current	16 mA	10 mA
Xe Pressure (Sputtering Gas)	2.0×10^{-4} torr	2.0×10^{-4} torr
O_2 Pressure	1.0×10^{-4} torr	1.0×10^{-4} torr
O_2^+ Energy	N. A.	50 eV
O_2^+ Current	N. A.	10 mA
Substrate Temperature	600-700 °C	600-700 °C
Growth Rate	0.30 nm/min.	0.25 nm/min.

Table II Summary of lattice parameters of $KNbO_3$ and substrate materials, including lattice mismatch.

	Lattice Parameter, nm	Lattice Mismatch, %†
$KNbO_3$ ($\bar{1}10$)	0.4036	N.A.
$KNbO_3$ (001)	0.3973	N.A.
MgO (100)	0.4213	4.4, 6.0
$MgAl_2O_4$ (100)	0.8083	0.1, 1.7
$KTaO_3$ (100)	0.3989	0.4, -1.2
$NdGaO_3$ (001)	0.3863	-2.8, -4.3

†First number listed is the lattice mismatch with $KNbO_3$ ($\bar{1}10$). Second number listed is lattice mismatch with $KNbO_3$ (001).

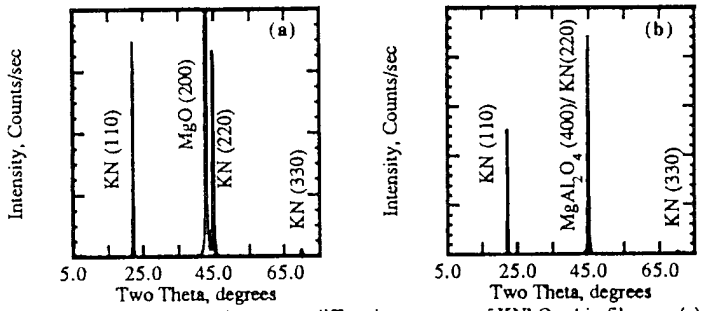

Figure 2 Theta-two theta x-ray diffraction patterns of $KNbO_3$ thin films on (a) MgO (100), and (b) $MgAl_2O_4$ (100).

these materials. Table II summarizes the lattice mismatch between the in-plane lattice parameters of (110) oriented $KNbO_3$ and those of the MgO and $MgAl_2O_4$ substrates. Theta-two theta x-ray diffraction patterns of all films show that the $KNbO_3$ grows highly (110) oriented on these substrates. Figure 2 shows typical diffraction patterns of $KNbO_3$ films on both these substrates. It is important to note that all films were (110) oriented in contrast to the (001) orientation which is the other pseudo-cubic direction of the perovskite unit cell. At the growth temperature, >600 °C, $KNbO_3$ is cubic, so it would be reasonable to expect some (001) orientation to occur. However, no (001) orientation has been observed in x-ray diffraction patterns for any $KNbO_3$ films grown in this study. An analysis of the structural transformations that occur during cooling from the growth temperature reveals why the (110) orientation is preferred.[6] X-ray diffraction rocking curve measurements were used to investigate the epitaxial quality of the $KNbO_3$ thin films. The rocking curve yields a quantitative measure of the misorientation of the thin films due to lattice tilting that results from defects in the microstructure. However, it does not measure in-plane misorientations, or twist, which are also common in heteroepitaxial growth of oxides. Typical rocking curves of $KNbO_3$ thin films on MgO (100) and $MgAl_2O_4$ (100) are shown in Figure 3. It is clear from the FWHM of the rocking curves that the films on $MgAl_2O_4$ possess higher epitaxial quality than those on MgO. This result is expected from the much smaller lattice mismatch between $KNbO_3$ and $MgAl_2O_4$ that was shown in Table II. In addition to the larger lattice mismatch, it is believed that the quality of the MgO surface prior to deposition plays a very important role in determining the

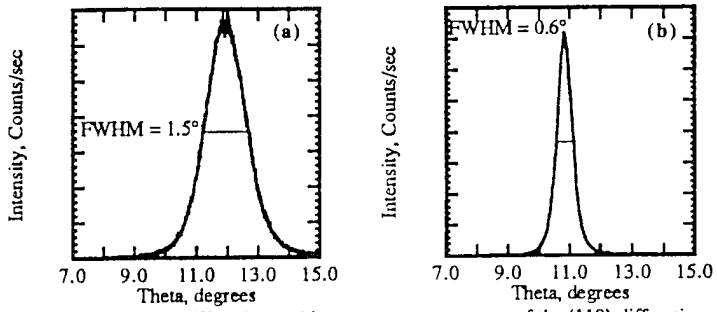

Figure 3 X-ray diffraction rocking curve measurements of the (110) diffraction peak of $KNbO_3$ thin films on (a) MgO (100), and (b) $MgAl_2O_4$ (100).

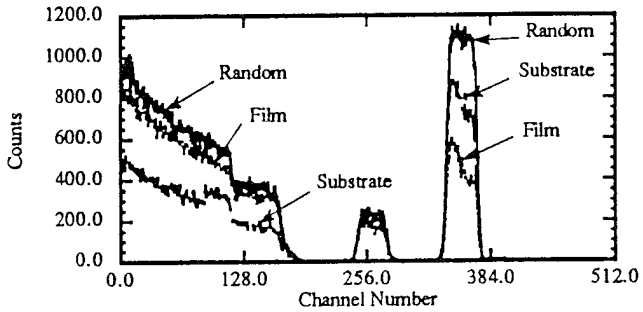

Figure 4 Rutherford backscattering spectra of a $KNbO_3$ thin film on MgO (100), including the spectra showing minimum channeling yields for the film and the substrate.

FWHM of the rocking curve. The rocking curve measurements also reveal that the [110] axis of most $KNbO_3$ films grown on MgO is tilted 1.0-1.5° away from the substrate normal.

RBS channeling was also used to determine the epitaxial quality of $KNbO_3$ films deposited on MgO. Figure 4 shows the random and channeled spectra of one of these films. By determining the minimum scattering yield, χ_{min}, of the film, the misorientation of the film with respect to a single crystal can be quantified. Experimentally it was found that more imperfections exist on the K sublattice than on the Nb sublattice. χ_{min} of the Nb signal was measured to be 37% while χ_{min} of the K signal was calculated to be only 71%. Although the channeling measurement is more sensitive to imperfections on the K sublattice,[7] the cause(s) of the greater imperfection on the K sublattice is unclear at this time. The tilt of the [110] axis is also evident in this measurement. The minimum scattering yields of the substrate and film do not occur at the same beam incidence angle. In fact the minimum yields are found one degree apart, as expected from the rocking curve measurements.

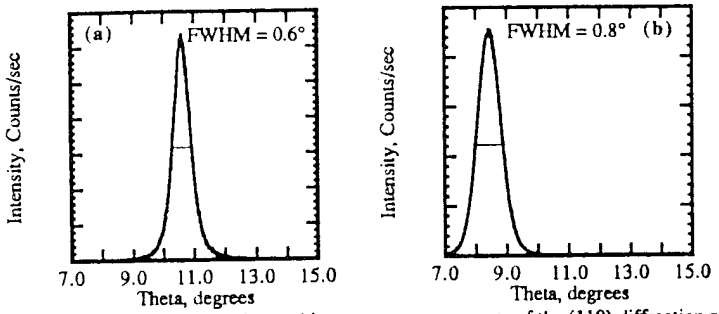

Figure 5 X-ray diffraction rocking curve measurements of the (110) diffraction peaks of (a) a $KNbO_3$ film deposited on Nb_xO_y/MgO, and (b) a $KNbO_3$ thin film deposited on MgO (100)-2°.

MgO is an important substrate for the growth of active optical waveguides because MgO can be grown on GaAs. High quality $KNbO_3$ thin films grown on MgO could then be easily integrated into planar optical device structures which would include both the AlGaAs laser source and the active element. It is thus necessary to improve the epitaxial quality of the $KNbO_3$ films on MgO. Two routes to improving the epitaxial quality of these films have been undertaken and show encouraging results. The first involves the deposition of a niobium oxide transition layer between the MgO substrate and the $KNbO_3$ film. It was shown previously that rotations of the $KNbO_3$ unit cell on top of the MgO surface.[8] In the present study, approximately 5 nm of niobium oxide was first deposited on the MgO (100) surface at the $KNbO_3$ growth temperature. $KNbO_3$ growth was initiated immediately after this layer was complete. The rocking curve of a $KNbO_3$ film grown on top of a niobium oxide transition layer is shown in Figure 5(a). Figure 5(a) reveals a marked improvement in the quality of the $KNbO_3$ film. The FWHM of the rocking curve has been reduced from 1.5° to 0.64°. The structure of the niobium oxide layer has not yet been investigated, but it is believed that this layer eases the lattice mismatch between $KNbO_3$ and MgO resulting in a better oriented film.

The second route to improving the quality of $KNbO_3$ on MgO involves the use of MgO substrates polished slightly off-axis. Polishing the substrate slightly off-axis may induce some anisotropy in the $KNbO_3$ film growth which is not present when films are grown on the on-axis cubic MgO surface. Figure 5(b) shows the rocking curve of a $KNbO_3$ film grown on an MgO substrate whose surface was polished approximately two degrees off the (100) surface. Once again the FWHM of the rocking curve was improved (FWHM = 0.87°), although not to the extent of the improvement seen with the niobium oxide transition layer. It should be emphasized that these are initial results and further improvement in the epitaxial quality of the $KNbO_3$ films on MgO may be realized by optimizing the growth conditions.

Surface quality and optical properties of epitaxial $KNbO_3$ thin films

The quality of the surface of a waveguiding thin film must be very high to prevent optical loss due to modal conversion and surface scattering. An atomic force microscope (AFM) was used to quantify the surface roughness of $KNbO_3$ thin films deposited on MgO. Figure 6 shows the evolution of the surface morphology as film thickness increases. Figure 6(a) is an AFM

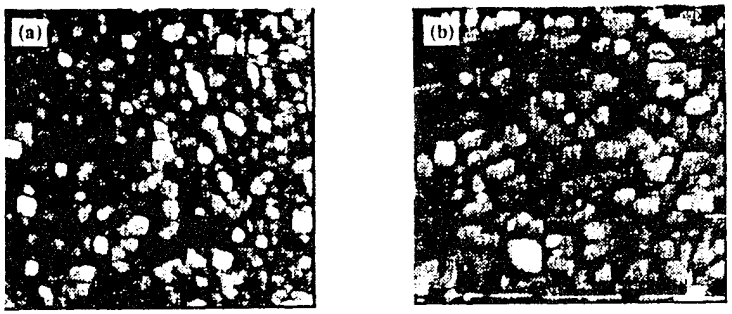

Figure 6 AFM images of the surfaces of $KNbO_3$ thin films (a) 100 nm thick, and (b) 200 nm thick. The images are 2 μm square and the gray scale is 30 nm.

image of the surface of a $KNbO_3$ film which is slightly less than 100 nm thick. This image shows that the peak-to-valley surface roughness is approximately 30 nm. The average grain size of this film, as seen in the image, is approximately 100 nm. Figure 6(b) shows an AFM image of a 200 nm thick film. While the peak-to-valley roughness has remained nearly constant, the grain size of the film has more than doubled. The increased grain size can lead to a degradation of waveguiding properties because light scattering is known to increase as grain size gets nearer to the wavelength of the propagating light. Control of grain size may thus be necessary to achieve high quality waveguides for integrated optical applications.

The refractive indices and waveguide losses of sputtered $KNbO_3$ thin films were measured using prism coupling techniques and the details of these measurements have been reported previously.[9] While no in-plane birefringence was observed, the measured refractive indices, TE = 2.28 and TM = 2.20, are very near the expected bulk refractive indices of 2.277 and 2.222, respectively. Optical waveguiding losses were measured to be as low as 10 dB/cm for films 100-120 nm thick. However, no correlation could be determined between the AFM measurements and the optical loss. It is believed that optical losses due to microstructural defects and surface imperfections are very large, and the low-loss waveguiding is simply the result of a weakly confined mode propagating through the thin film/substrate waveguide structure.

ION-ASSISTED EPITAXIAL GROWTH OF $KNbO_3$

Thin films of $KNbO_3$ were also grown using an ion-assisted deposition process. A filamentless rf ion source was used to bombard the growth surface with 50 eV oxygen ions. Ion-assisted deposition is known to provide many beneficial effects to film quality. Among the potential advantages of incorporating ion-assisted growth with the ion beam sputter deposition process described above are modifications to the nucleation and growth mechanisms, lower growth temperature, and increased activity at the growth surface. Through ion-assisted growth it may be possible to control the film microstructure including the grain size. A lower growth temperature could be advantageous for integrating these films with current semiconductor processing, and increased activity of the depositing species may improve compositional homogeneity which is important for low-loss optical waveguiding.

The first studies of ion-assisted $KNbO_3$ film growth focused on determining the epitaxial quality achievable using the technique. Typical processing parameters are shown in Table I. $KNbO_3$ films were grown on MgO (100), $MgAl_2O_4$ (100), $KTaO_3$ (100), and $NdGaO_3$ (001) substrates. Lattice constants of these substrates and their lattice mismatch with $KNbO_3$ are shown in Table II. $KTaO_3$, and $NdGaO_3$ were chosen in addition to the MgO and $MgAl_2O_4$ substrates for their unique lattice matching to $KNbO_3$. $KTaO_3$ possesses the smallest lattice

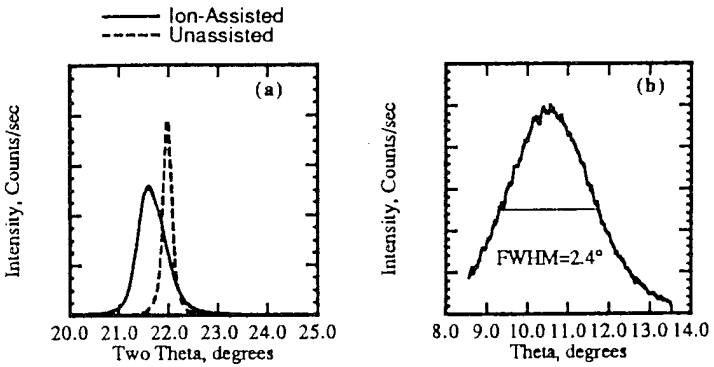

Figure 7 (a) A comparison of the $KNbO_3$ (110) diffraction peaks for films grown with and without ion assistance. (b) The x-ray diffraction rocking curve measurement of the $KNbO_3$ (110) diffraction peak for a film deposited with ion assistance.

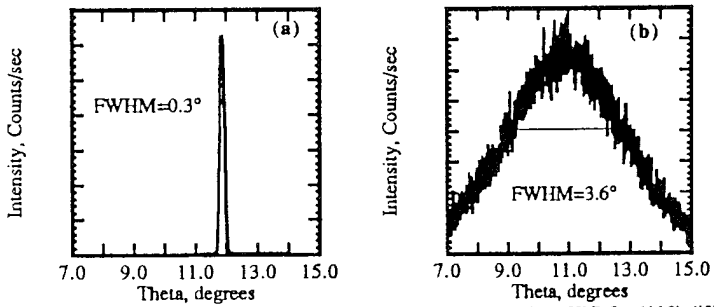

Figure 8 X-ray diffraction rocking curve measurements of the $KNbO_3$ (110) diffraction peak for films deposited on (a) $KTaO_3$ (100), and (b) $NdGaO_3$ (001).

mismatch of any of the substrates used in this study providing the potential for very high quality $KNbO_3$ film growth. The lattice parameters of $NdGaO_3$, on the other hand, are strictly smaller than those of $KNbO_3$ which is unique to the group of substrates used in this study. The deposition temperature during film growth was kept in the 600-700°C range, so that results could be easily compared to films grown without ion assistance.

All $KNbO_3$ films grown with ion assistance were highly (110) oriented. However, the lattice parameter of $KNbO_3$ films on MgO, $MgAl_2O_4$, and $NdGaO_3$ was found to be slightly enlarged. Figure 7(a) shows a comparison of the (110) diffraction peaks of an ion-assisted film and an unassisted film. The lattice parameter of the ion-assisted film has increased by 1.4%, as seen by the shift to a lower two-theta angle. The broadening of the (110) peak of the ion-assisted films is also indicative of a smaller grain size or film strain. The rocking curve of this film, shown in Figure 7(b), reveals that the epitaxial quality has diminished. The FWHM of the rocking curve has increased to more than two degrees compared to 0.6 degrees for the film shown in Figure 3(b). RBS analysis of ion-assisted $KNbO_3$ films revealed the presence of Xe and Fe impurities. These impurities are believed to be responsible for the lower film quality. The Xe in the films is trapped primary sputtering gas, while the Fe is believed to come from sputtering of the stainless steel ring electrode inside the discharge chamber of the rf ion source. The impurity incorporation may be substantially reduced by changing the incidence angle of the oxygen ion bombardment and replacing the stainless steel electrode with another metal such as niobium which would minimize film contamination.

The $KNbO_3$ films on single crystal $KTaO_3$ (100) exhibited the highest epitaxial quality of all of the films deposited with ion assistance. The x-ray rocking curve measurement of one of these films is shown in Figure 8(a). The FWHM of the rocking curve is 0.3° which is at the limit of resolution of the diffractometer used for the measurement. Xe and Fe impurities were also observed in the films on $KTaO_3$. However, due to the very low lattice mismatch between film and substrate these impurities did not diminish the crystal quality as determined by x-ray measurements. In contrast, $KNbO_3$ films deposited on $NdGaO_3$ (001) were of poor epitaxial quality. Figure 8(b) shows the x-ray rocking curve of a film on $NdGaO_3$. The FWHM of the rocking curve is well over three degrees, the largest of all film/substrate combinations. In addition, the films grown on $NdGaO_3$ adhered poorly and exhibited a tendency to peel off the substrate.

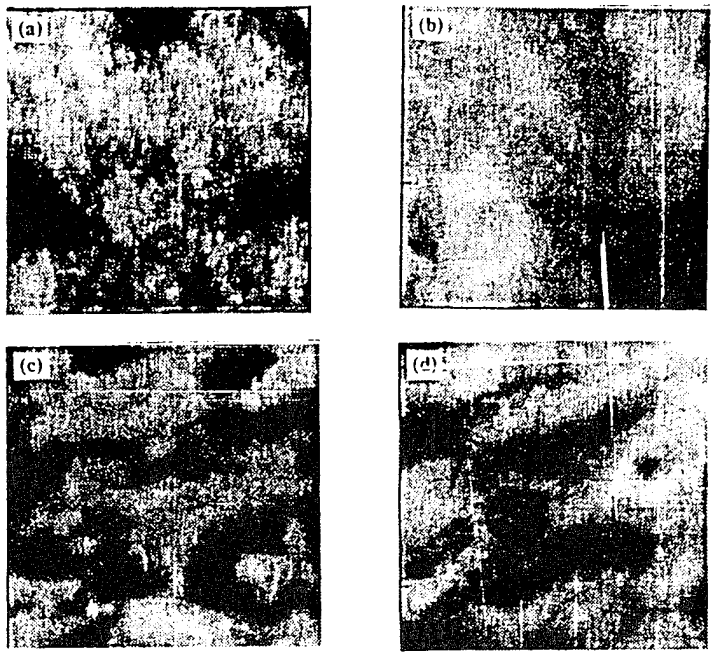

Figure 9 AFM images of $KNbO_3$ thin films deposited with ion assistance on (a) MgO (100), (b) $MgAl_2O_4$ (100), (c) $KTaO_3$ (100), and (d) $NdGaO_3$ (001). The images are 1.25 x1.25 μm square and the gray scales are 5, 100, 30, and 10 nm,respectively.

Surface quality and optical properties of epitaxial ion-assisted $KNbO_3$ thin films

The surface quality of $KNbO_3$ films grown with ion assistance was also investigated using the atomic force microscope. AFM images of films grown on MgO (100), $MgAl_2O_4$ (100), $KTaO_3$ (100), and $NdGaO_3$ (001) substrates are shown in Figure 9. $KNbO_3$ films grown on MgO are shown to have the smoothest surface with a peak-to-valley roughness of 5 nm. This result is an improvement over unassisted films, but it must be further improved for optical waveguiding applications which require very smooth interfaces to prevent scattering and modal conversion. Films on the other substrates were rougher, with a 400 nm thick film on $MgAl_2O_4$ the roughest, 100 nm peak-to-valley. The surfaces of films deposited on $KTaO_3$ and $NdGaO_3$ had intermediate values of roughness, 30 and 20 nm, respectively. The grain size of the films grown with ion assistance is difficult to determine from the AFM images, but it is believed to be smaller than that of the films grown without ion assistance. This smaller grain size may reduce optical scattering in waveguides, as discussed above. If the smaller grain size can be combined with a smoother surface, the films on MgO deposited with ion assistance may be favorable for waveguiding applications if impurity incorporation can also be minimized.

The optical properties of ion-assisted $KNbO_3$ films were also measured with prism coupling techniques and were also reported previously.[9] The measured refractive indices were 2.26 for TE modes and 2.18 for TM modes which are slighlty lower than the indices measured for unassisted films. The lower indices are attributed to a small decrease in density caused by the presence of Fe and Xe impurities which increased the lattice parameter of the assisted films. Optical losses were greater than 50 dB/cm and could not be measured using the fiber probe technique, and thus no correlation with the AFM measurements could be made.

MOCVD GROWTH OF ORIENTED $KNbO_3$ FILMS

$KNbO_3$ thin films were grown for the first time using an MOCVD process.[10] The deposition system, shown schematically in Figure 10, uses solid metalorganic sources. These sources are passed through a very sharp temperature gradient where they sublimate immediately and are transported with He carrier gas to the reaction chamber through heated tubes. The use of the sharp temperature gradient ensures that the source is not exposed to high temperatures over long periods of time, avoiding the difficulty of maintaining a stable vapor pressure over the source during the entire growth process. The cation stoichiometry is controlled by adjusting the feed rate of the metalorganic sources through the temperature gradient. Similarly, the deposition rate can be controlled by scaling the feed rate of both sources. Molecular oxygen, O_2, is added to the gas mixture before entering the reaction chamber so that sufficient oxygen is available for oxide film growth. Typical processing parameters for MOCVD film growth are given in Table III.

Table III Process parameters for MOCVD growth of $KNbO_3$ thin films.

Process Parameter	Value
Source 1	$K(C_{11}H_{19}O_2)$
Source 1: T_{sub}	450 °C
Source 1: Feed Rate	$7.3\text{-}9.7 \times 10^{-5}$ mol/min.
Source 2	$Nb(C_{11}H_{19}O_2)4$
Source 2: T_{sub}	325 °C
Source 2: Feed Rate	1.2×10^{-5} mol/min.
Base Pressure	100 mtorr
Operating Pressure	10 torr
He (1) Flow	300 sccm
He (2) Flow	15 sccm
O_2 Flow	300 sccm
Substrate Temperature	650-700 °C
Growth Rate	3.0 nm/min.

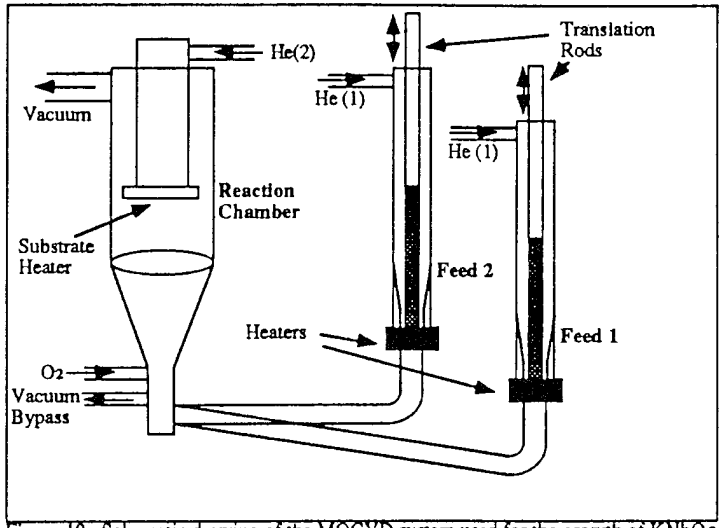

Figure 10 Schematic drawing of the MOCVD system used for the growth of $KNbO_3$ thin films.

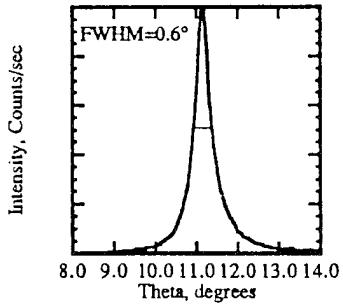

Figure 11 X-ray diffraction rockin curve measurement of the $KNbO_3$ (110) diffraction peak of an MOCVD $KNbO_3$ thin film.

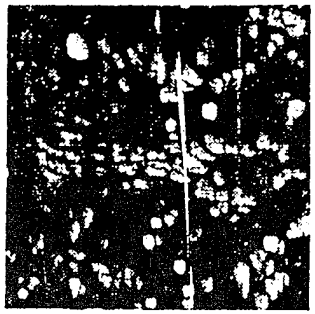

Figure 12 An AFM image of the surface of an MOCVD $KNbO_3$ thin film. The image is 3μm square and the gray scale is 100 nm.

MOCVD $KNbO_3$ films were grown only on $MgAl_2O_4$ (100) substrates, and were found to be highly (110) oriented. Figure 11 shows the rocking curve of a MOCVD $KNbO_3$ film. The FWHM of the rocking curve is 0.6° in keeping with the ion beam deposited films on $MgAl_2O_4$ without ion assistance. However, the surface quality of these initial MOCVD films was found to be considerably below the quality of all the ion beam sputtered films. Figure 12 shows the AFM

image of an MOCVD film surface. The peak to valley roughness is 100 nm, nearly equal to the thickness of the film. It is believed that the surface quality of the MOCVD films may be improved by optimizing the processing parameters, particularly the substrate temperature and the deposition rate which was 10 times greater than the deposition rate of the sputtered films.

SUMMARY

The epitaxial quality of $KNbO_3$ thin films grown using ion-assisted and unassisted ion beam sputter deposition was investigated. Key influences of processing conditions on the epitaxial quality were identified. Of these influences, the lattice mismatch between film and substrate was found to have the most prominent effect on epitaxial quality. $KNbO_3$ thin films on $KTaO_3$ (mismatch $\leq$ 1.2%) deposited with ion assistance were found to have the narrowest x-ray rocking curve, 0.3°. However, Fe and Xe impurities were incorporated into the films during the deposition process as a result of the oxygen ion bombardment. Films deposited with ion assistance on MgO, $MgAl_2O_4$, and $NdGaO_3$ substrates had wider rocking curves than films deposited without ion assistance. Two routes were found to further improve the epitaxy of $KNbO_3$ films deposited on MgO without ion assistance. A niobium oxide interlayer and the use of off-axis MgO substrates were found to reduce the width of the rocking curves of $KNbO_3$ films by 60% and 47%, respectively. The surface quality of the films deposited by ion beam sputtering was investigated using atomic force microscopy. Peak-to-valley roughness as low as 5 nm was measured for $KNbO_3$ films deposited on MgO with ion assistance.

$KNbO_3$ thin films were grown for the first time using a solid source MOCVD growth process. Cation stoichiometry and growth rate were controlled by individually adjusting the feed rates of the potassium and niobium metalorganic sources. A rocking curve FWHM of 0.6° was measured for films deposited on $MgAl_2O_4$ which is comparable to the results achieved using sputter deposition. The AFM image of an MOCVD film surface revealed the film was very rough. By optimization of the process parameters it is hoped that surface roughness can be improved in the future.

ACKNOWLEDGMENTS

The authors would like to acknowledge the following contributions to this work; the Office of Naval Research for support under contract N0014-91-J-1307, Dr. L.A. Boatner in the Solid State Division of Oak Ridge National Laboratories for supplying the $KTaO_3$ substrates, Dr. N.R. Parikh at the University of North Carolina and Bruce Rothman and the Laboratory for Research on the Structure of Matter at the University of Pennsylvania for assistance in making the RBS measurements.

REFERENCES

1. T.M. Graettinger,.P.A. Morris, R.R. Woolcott, F.C. Zumsteg, A.F. Chow, and A.I. Kingon in Ferroelectric Thin Films III, (Mater. Res. Soc. Proc. 310, Pittsburgh, PA, 1993) 301.
2. K. Nunomura, A. Ishitani, T. Matsubara, and I Hayashi, J. Cryst. Growth 45, 355 (1978).
3. G.H. Hewig and K. Jain, J. Appl. Phys. 54, 57 (1983).
4. H. Lu, L. Wills, B. Wessels, W. Lin, T. Zhang, G. Wong, D. Neumayer, and T. Marks, Appl. Phys. Lett. 62, 1314 (1993).
5. A. Reisman and F. Holtzberg, J. Am. Chem. Soc. 77, 2115 (1955).
6. A.F. Chow, D. J. Lichtenwalner, R.R. Woolcott Jr., T.M. Graettinger, L.A. Boatner, N.R. Parikh, O. Auciello, and A.I. Kingon, (submitted to Applied Physics Letters, 1994).
7. S. Schwyn Thöny, H.W. Lehmann, and P. Günter, Appl. Phys. Lett. 61, 373 (1992).
8. S.H. Rou, T.M. Graettinger, O. Auciello, and A.I. Kingon in Heteroepitaxy of Dissimilar Materials, (Mater. Res. Soc. Proc., Pittsburgh, PA, 1991).
9. T.M. Graettinger, D.J. Lichtenwalner, A.F. Chow, O. Auciello, A.I. Kingon, and P. Morris, presented at the 8th ISIF, Monterey, CA, 1994. (To be published in Integrated Ferroelectrics).
10. R. Hiskes, S.A. DiCarolis, J.L. Young, S.S. Laderman R.D. Jacowitz, and R.C. Taber, Appl. Phys. Lett. 59, 606 (1991).

Appendix 6

"Epitaxial $KNbO_3$ Thin Films on $KTaO_3$, $MgAl_2O_4$, and MgO Substrates," A. F. Chow, D. J. Lichtenwalner, R. R. Woolcott, Jr., T. M. Graettinger, O. Auciello, and A. I. Kingon, Appl. Phys. Lett. **65**(9), 1073, 1994.

Epitaxial $KNbO_3$ thin films on $KTaO_3$, $MgAl_2O_4$, and MgO substrates

A. F. Chow, D. J. Lichtenwalner, R. R. Woolcott, Jr., T. M. Graettinger, O. Auciello,[a] and A. I. Kingon
Department of Materials Science and Engineering, North Carolina State University, Raleigh, North Carolina 27695-7919

L. A. Boatner
Oak Ridge National Laboratory, Solid State Division, Oak Ridge, Tennessee 37831-6056

N. R. Parikh
Department of Physics, University of North Carolina, Chapel Hill, North Carolina 27599-3255

(Received 31 March 1994; accepted for publication 19 June 1994)

Epitaxial potassium niobate ($KNbO_3$) thin films have been deposited on $KTaO_3$ (100), $MgAl_2O_4$ (100), and MgO (100) substrates using ion-beam sputter deposition. X-ray-diffraction results show that $KNbO_3$ films have orthorhombic (110) orientation on all three substrates. Rutherford backscattering channeling analysis of $KNbO_3$ films on $KTaO_3$, $MgAl_2O_4$, and MgO exhibits minimum scattering yields (χ_{min}) of 7%, 9%, and 18% for the Nb peak, respectively. This illustrates how the quality of epitaxy improves as the lattice mismatch decreases. Prism-coupling measurements reveal near-bulk refractive indices of about 2.27 for TE modes and 2.22 for TM modes for films on each substrate.

$KNbO_3$ is a promising material for nonlinear-optical (NLO) and electro-optical (EO) applications. It possesses large nonlinear-optical coefficients, and its high electro-optic figure of merit makes it superior to the widely used material, lithium niobate, for integrated-optical phase and amplitude modulators.[1,2]

Several groups have demonstrated the growth of $KNbO_3$ thin films;[3–6] however, films of good optical quality, critical for competitive optical-waveguide devices, are difficult to produce. Thin films used for optical applications should generally be single phase, dense, smooth, stoichiometric, and epitaxial, with as few structural defects as possible. All these properties are important for minimizing light-propagation losses and maximizing NLO and EO effects. An understanding of $KNbO_3$ epitaxial film growth mechanisms is important for optimizing film properties.

In this work, the properties of epitaxial $KNbO_3$ thin films on $KTaO_3$ (perovskite), $MgAl_2O_4$ (spinel), and MgO (rock-salt) substrates are investigated in order to clarify the substrate effects on the epitaxial growth of $KNbO_3$. All three substrates have cubic symmetry. The orthorhombic $KNbO_3$ phase has lattice parameters of $a=5.721$ Å, $b=5.695$ Å, $c=3.973$ Å, and corresponding refractive indices of $n_a=2.168$, $n_b=2.279$, and $n_c=2.329$.[1,7] The three substrates used here provide different lattice and refractive-index mismatches with potassium niobate, as listed in Table I. The properties of $KNbO_3$ films grown on each substrate are presented, and key factors that control film growth, microstructure, and optical properties are discussed.

Ion-beam sputter deposition of $KNbO_3$ thin films has been accomplished using a computer-controlled, sequential layer-by-layer growth technique.[6] A single ion source is used to sequentially sputter targets of niobium and potassium superoxide (KO_2). Substrate temperatures range from 650 to 700 °C, and the oxygen pressure is held at 1×10^{-4} Torr. The MgO and spinel substrates were purchased from Advanced Composite Materials and Commercial Crystal Systems, respectively, while the $KTaO_3$ substrates were provided by Oak Ridge National Laboratory.

The deposited films and substrate materials were analyzed using a variety of techniques. Substrate roughness was measured using atomic force microscopy (AFM). X-ray diffraction (XRD) was used to determine the lattice parameter, phase, and orientation of the $KNbO_3$ films. X-ray-diffraction rocking curve measurements were used to measure grain tilt of the films. Rutherford backscattering spectrometry (RBS) provided film composition and thickness, while ion channeling revealed the epitaxial quality of the $KNbO_3$ films. A prism-coupling technique was used to obtain refractive indices.[10]

Substrate surface roughness can not only directly influence the film surface but impede the epitaxial growth process, since surface steps can induce the growth of (041) tetrahedral twin domains.[11] Atomic force microscopy of the

TABLE I. Bulk properties of $KTaO_3$, $MgAl_2O_4$, and MgO, with comparison to those of $KNbO_3$ (110). Measured properties of $KNbO_3$ (110) films on each substrate are also included.

Substrate	$KTaO_3$ (100)	$MgAl_2O_4$ (100)	MgO (100)
Bulk lattice parameter[a] (Å)	3.989	8.083	4.213
Bulk refractive index[b]	2.225	1.723	1.736
Bulk lattice mismatch, $KNbO_3$ [$\bar{1}$10], [001]	−1.2%, 0.4%	0.1%, 1.7%	4.4%, 6.0%
Measured FWHM XRD rocking curve	0.25°	0.30°	0.84°
Measured film RBS/channeling, χ_{Nb}	7%	9%	18%
Measured film refractive index,TE, TM	2.27, ···	2.27, 2.23	2.28, 2.21

[a]Reference 8.
[b]Reference 9.

[a]Also at MCNC, Electronics Technology Division, Research Triangle Park, NC 27709-2889.

 0003-6951/94/65(9)/1073/3/$6.00

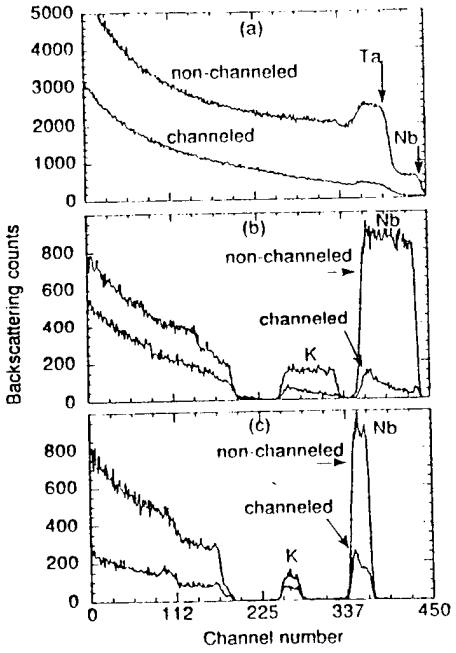

FIG. 1. RBS spectra obtained using unchanneled and channeled configurations are plotted for $KNbO_3$ (110) films on (a) $KTaO_3$ (100), (b) $MgAl_2O_4$ (100), and (c) MgO (100).

substrate surfaces shows that $KTaO_3$ had the lowest surface roughness, with rms roughness of 8 Å, while the rms roughness of the spinel and MgO surfaces was 10 and 26 Å, respectively. The as-received MgO surface contains arrays of "columns" which can be 100 Å or more in height. These are believed to be due to magnesium hydroxide growth. Annealing the MgO substrate at a temperature of ~1200 °C improves the roughness to a rms value of 9 Å. Therefore, a similar roughness can be achieved on each substrate. AFM also detected typical grain sizes of 1000–3000 Å for the $KNbO_3$ films.

X-ray diffraction showed that the $KNbO_3$ films on all substrates are single phase and the orthorhombic [110] is normal to the substrate surface. For the $KNbO_3$ (110) orientation a lattice parameter of 4.036 Å is expected perpendicular to the surface plane. The (110)-plane spacing measured for all films ranged from 4.02 to 4.05 Å. Rocking curve measurements of the $KNbO_3$ (110) peak revealed a full width at half maximum (FWHM) value of 0.84° for $KNbO_3$ on MgO substrates, 0.25° for films on $KTaO_3$, and 0.30° for films on $MgAl_2O_4$, as listed in Table I.

RBS/channeling spectra are shown in Fig. 1 for $KNbO_3$ films on $KTaO_3$ [Fig. 1(a)], $MgAl_2O_4$ [Fig. 1(b)], and MgO [Fig. 1(c)]. Values of minimum channeling, χ_{min}, were obtained in a 10-channel energy window by comparing the lowest point in the channeled spectra, just below the surface peak, with an unchanneled spectrum. $KNbO_3$ on $KTaO_3$ had a χ_{min} of 7% for the Nb peak. Films on spinel show slightly higher χ_{min} values, 9% for Nb, while results for $KNbO_3$ on MgO showed the highest χ_{min}, 18% for Nb. The higher χ_{min} values for $KNbO_3$ on MgO suggest a larger amount of either grain tilt, grain misorientation, or other defects.

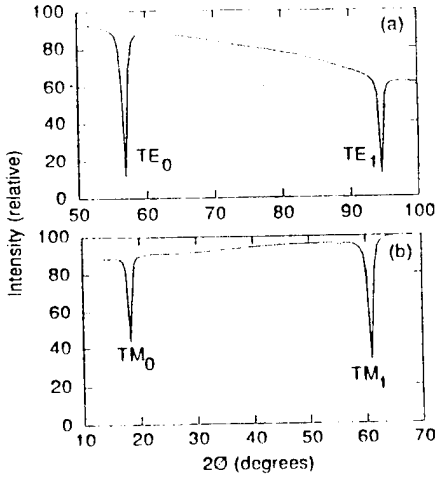

FIG. 2. Coupling curves of uncoupled, reflected intensity vs coupling angle for $KNbO_3$ (110) films on $MgAl_2O_4$ (100), are shown for (a) TE modes and (b) TM modes.

RBS also showed that all of the films are deficient in potassium, with a K to Nb cation ratio in the range of 0.7–0.95. Increasing the amount of KO_2 sputtered does not cause a composition change when deposited at 650–700 °C, although at lower temperatures, 550–600 °C, the films can become potassium rich and not optically translucent. Energy-dispersive x-ray analysis reveals the presence of sodium in some films, which may partially compensate for the potassium deficiency and allow the films to possess a single orientation and near-bulk refractive indices as shown later. A possible source for the sodium is the superoxide pressed KO_2 targets. Potassium vacancies might also be filled by hydrogen atoms.

The refractive indices were measured by coupling a He-Ne (6328 Å) laser beam into the films using the prism-coupling method.[10] Coupling curves for a $KNbO_3$ film with a thickness of 5000 Å on a spinel substrate are shown in Fig. 2. The narrow coupling width is indicative of a smooth film with uniform thickness. Typical refractive indices measured for all films are 2.22 and 2.27 in the TM (light polarized along $KNbO_3$ [110]) and TE modes (light polarized in the film plane), respectively, as shown in Table I. The index of $KNbO_3$ (110) films is smaller than $KTaO_3$ in the TM mode, so TM-mode film coupling is not possible for this case. The measured refractive index for TM modes compares very favorably with the bulk refractive index of $KNbO_3$ [110], 2.222. The refractive indices of the TE modes of our films were measured in two orthogonal propagation directions and were found to be similar in each direction, which indicates that 90° domain orientations exist on all substrates. Therefore, the refractive index for the TE modes should reflect an average value (2.274) between the indices of $KNbO_3$ [$\bar{1}$10] and [001], 2.222 and 2.329, respectively. The fact that our indices so closely approach the bulk values indicates that the films are very dense over a range of film compositions. No dependence of refractive index on composition was detected.

In-plane lattice spacings for single-crystal $KNbO_3$ with (110) orientation would be 3.973 Å [001] and 4.036 Å [$\bar{1}$10].

Table I lists the calculated lattice mismatches for each film/substrate system. The x-ray-diffraction rocking curve and RBS/channeling data show that a smaller amount of grain tilt (higher degree of epitaxy) was observed for the $KNbO_3$ films on $KTaO_3$ and spinel substrates, where a smaller lattice mismatch occurs, compared to films on MgO substrates. This is a clear indication that lattice mismatch is a key factor in achieving good epitaxial quality. Better epitaxial quality suggests fewer structural defects, which should improve the optical quality of the films.

The reason why the $KNbO_3$ (110)-film orientation occurs can be explained based on the following discussion. The lattice parameter of ~4.02–4.05 Å observed for all $KNbO_3$ films by x-ray diffraction indicates that the shortest ⟨100⟩ axis ([001], c=3.973 Å) is parallel to the substrate surface plane (in-plane). At the growth temperature, the fact that both our film and substrate are cubic suggests that the film is (001) oriented with the in-plane ⟨100⟩ axes aligned parallel to those of the substrate. The cubic-to-tetragonal transformation results in two "short" axes and one "long" axis of $KNbO_3$.[1] At least one of the short axes must lie along the substrate surface.

As the film transforms to the orthorhombic phase, there is a slight lattice distortion that leads to the lengthening of one of the original short axes, which becomes the [110] orthorhombic direction. The other short axis remains essentially unchanged, becoming the [001] direction. Since there are no stresses perpendicular to the growth direction, the short axis normal to the substrate plane would be less energetically inhibited to lengthen, thus leaving the remaining short axis to be in the film plane. Similarly, in the other case where if both the short axes were in the film plane, one axis will lengthen and leave the other short axis still in the plane. Thus a short axis would always lie in the plane of the substrate, resulting in the (110)-oriented orthorhombic $KNbO_3$ we observe.

The occurrence of grain tilts and 90° domain orientations can be further understood by considering the $KNbO_3$ phase transformations from cubic (at growth temperature) to tetragonal (~435 °C), and then to orthorhombic (~225 °C) during cooling. During deposition, misfit dislocations are expected to form to accommodate the lattice mismatch between the film and substrate. This may result in "tilts" and "twists" of the film grains with respect to the substrate. Upon cooling, more tilting may occur depending on the thermal-expansion-coefficient mismatch. The phase transformation can induce twin formation and also can affect the magnitude of the grain tilt. Due to the $KNbO_3$ (110) orientation and its orthorhombic structure, in which there is a slight asymmetry of the two ⟨100⟩ long axes, an additional tilt of 0.13° from the normal towards one of the two in-plane $KNbO_3$ ⟨110⟩ directions occurs. The cubic nature of the substrates allows for the tilts and twins to occur in any of the equivalent 90° directions. This limits the x-ray-diffraction rocking curve to a minimum FWHM value of ~0.26° for the fine-grained, unpoled thin films.

Both the XRD rocking curves and RBS/channeling data show a higher quality of epitaxy for $KNbO_3$ on $KTaO_3$ and $MgAl_2O_4$ compared with films on MgO, indicating that a smaller lattice mismatch is the key to improving epitaxy and minimizing low-angle boundaries. Tilts and twins may be a significant factor limiting propagation losses. The lower substrate roughnesses of $KTaO_3$ and $MgAl_2O_4$ substrates and the corresponding lower film roughnesses should result in lower surface scattering losses due to a smoother interface and film surface.

We have deposited high-quality, dense, epitaxial $KNbO_3$ films on $KTaO_3$, $MgAl_2O_4$, and MgO substrates. Despite the observed potassium deficiency, the $KNbO_3$ films are dense as suggested by the bulk refractive indices observed. $KNbO_3$ films on $KTaO_3$ and $MgAl_2O_4$ have better epitaxial orientation than those on MgO, confirming that lattice mismatch is a key issue in producing high-quality epitaxial films. The varying quality of epitaxy of the films and the refractive-index differences between substrates should provide information regarding the dominant loss mechanisms for $KNbO_3$ thin-film waveguides on different substrates. The optical losses are presently being investigated and the results will be reported in a forthcoming publication.

The present work is supported by the Office of Naval Research under Contract No. N0014-91-J-1307. Research at ORNL is sponsored by the Division of Materials Sciences, U. S. Department of Energy under Contract No. DE-AC05-84OR21400 with Martin Marietta Energy Systems, Inc.

[1] *Landolt-Bornstein, New Series, Group III* (Springer, New York, 1981), Vol. **16**, Part A.
[2] B. Tuttle, MRS Bull. **40**, Oct./Nov., 40 (1987).
[3] R. Guttmann and J. Hulliger, Cryst. Prop. Prep. **32–34**, 117 (1991).
[4] M. Amini and M. D. Sacks, Mater. Res. Soc. Symp. Proc. **180**, 675 (1990).
[5] S. Schwyn Thony, H. W. Lehmann, and P. Gunter, Appl. Phys. Lett. **61**, 373 (1992).
[6] T. M. Graettinger, S. H. Rou, M. S. Ameen, O. Auciello, and A. I. Kingon, Appl. Phys. Lett. **58**, 1964 (1991).
[7] M. Zgonik, R. Schlesser, I. Biaggio, E. Voit, J. Tscherry, and P. Gunter, J. Appl. Phys. **74**, 1287 (1993).
[8] Y. Fujii and T. Sakudo, J. Phys. Soc. Jpn. **41**, 888 (1976).
[9] *CRC Handbook of Chemistry and Physics*, 73rd ed. (CRC, Boca Rotan, Florida, 1993).
[10] R. Ulrich and R. Torge, Appl. Opt. **12**, 2901 (1973).
[11] S. H. Rou, P. H. Hren, J. J. Hren, T. M. Graettinger, M. S. Ameen, O. H. Auciello, and A. I. Kingon, Mater. Res. Soc. Symp. Proc. **183**, 285 (1990).

Appendix 7

"Microstructural and Optical Properties of Potassium Niobate Thin Films," Alice F. Chow, Daniel J. Lichtenwalner, Thomas M. Graettinger, James R. Busch, Orlando Auciello, and Angus I. Kingon, Proceedings of the Ninth International Symposium on Applications of Ferroelectrics, 794-6, 1994.

ISAF '94

PROCEEDINGS
of the
Ninth
IEEE

International Symposium on
Applications of Ferroelectrics

Editors:

R. K. Pandey
Michael Liu
Ahmad Safari

Penn State Scanticon Conference Center
The Pennsylvania State University
University Park, Pennsylvania
USA
August 7 - August 10, 1994

IEEE Catalog Number 94CH3416-5

MICROSTRUCTURAL AND OPTICAL PROPERTIES OF POTASSIUM NIOBATE THIN FILMS

Alice F. Chow, Daniel J. Lichtenwalner, Thomas M. Graettinger,
James R. Busch*, Orlando Auciello**, and Angus I. Kingon

North Carolina State University, Department of Materials Science and Engineering, Raleigh, NC 27695-7919
*Battelle Memorial Institute, Columbus, OH 43201-2693
**Also MCNC, Electronics Technology Division, Research Triangle Park, NC 27709-2889

ABSTRACT

A potassium niobate thin film waveguide is an ideal candidate for producing a compact blue laser source by second harmonic generation. However, good epitaxial quality films are difficult to produce and high optical losses are a continuing problem. A report is presented in this paper on the investigations of the microstructural and optical properties of $KNbO_3$ thin films to better understand the origin of optical waveguide losses. Epitaxial, dense $KNbO_3$ thin films have been grown on MgO, $MgAl_2O_4$, and $KTaO_3$ substrates by ion-beam sputter deposition. X-ray diffraction, rocking curves, Rutherford backscattering spectroscopy, ion-channelling, field emission scanning electron microscopy, and atomic force microscopy were used to analyze the orientation, epitaxial quality, grain size, and surface roughness of the films. Optical properties including refractive index and optical scattering losses have been characterized by prism-coupling and an optical fiber loss measurement method. The dominant loss mechanism in these film waveguides is discussed. Green light by second harmonic generation has been produced in the transverse and waveguide modes in $KNbO_3$ films.

INTRODUCTION

A short wavelength laser source is necessary to increase the density of present optical recording systems. Green or blue light can be generated from an IR laser by second harmonic generation (SHG) using a nonlinear optical material. Several problems continue to hinder efficient frequency doubling. First, few materials posess high nonlinearity and can be easily phase-matched for the appropriate wavelengths. In addition, bulk crystals that have demonstrated SHG in the blue or green spectral region produce too little power. (At least 5 mW of power is necessary for many practical applications.) [1]

Potassium niobate posesses very high nonlinear constants and one of the highest figures of merit for producing SHG. [2] Also, $KNbO_3$ thin films offer field confinement and thus, high conversion efficiency as well as ease of phase-matching by use of normal dispersion. Lithium niobate thin films have demonstrated SHG blue light. However, its bulk nonlinear optical properties are inferior to those of $KNbO_3$ and the second harmonic power produced was weak. [3] Ultimately, thin film waveguides will be desired for high power conversion. Nevertheless, high quality $KNbO_3$ thin films are difficult to grow due to potassium volatility at the growth temperature. A high degree of epitaxy and defect minimization are necessary for low waveguide losses. Thus, the origin of losses must be pinpointed, and microstructure and film processing must be synergistically controlled.

We report the growth of $KNbO_3$ thin films with a high degree of epitaxy, and correlate film microstructures with optical properties. Films were grown by ion-beam sputter deposition. X-ray diffraction (XRD) and x-ray rocking curves were performed to analyze film orientation and grain tilt, respectively. Rutherford backscattering spectroscopy (RBS) revealed film composition information while RBS/channelling detected the grain tilt and misorientation of the films. Substrate and film surface roughnesses were determined by atomic force microscopy (AFM). Field emission scanning electron microscopy displayed the film surface morphology. Refractive indices were calculated from prism-coupling measurements and an optical fiber attachment allowed optical scattering losses to be measured. Highly epitaxial, dense $KNbO_3$ thin films have produced green light by SHG in the transverse and waveguide modes.

ION-BEAM SPUTTER DEPOSITION

Ion-beam sputter deposition was used to produce $KNbO_3$ thin films on MgO (100), $MgAl_2O_4$ (100), and $KTaO_3$ (100) substrates. A computer-controlled, sequential rotating target assembly consists of potassium superoxide (KO_2) and niobium targets that are alternately sputtered by an xenon ion beam. [4] Thus, composition is controlled by programming the ion beam dwell time on each target. Each layer deposited in one rotation of the targets is only 5-10 Å to allow for interdiffusion to form a homogeneous film. The deposition rate is about 10 Å/min. and film growth occurs at 650-700°C. Table 1 summarizes the important sputter deposition parameters.

Table 1. Ion-beam deposition parameters for $KNbO_3$ thin film growth.

Beam energy	800 eV
Beam current	15 mA
Xe^+ source gas pressure	1.4×10^{-4} torr
O_2 gas pressure	2.5 x 10-4 torr
Deposition temperature	650-700°C
Deposition rate	10 Å/min.

MICROSTRUCTURAL PROPERTIES

Orientation

The d-spacings of the planes parallel to the sample surface can be detected through standard theta-two theta x-ray diffraction. $KNbO_3$ films on all substrates under typical growth conditions show a single $KNbO_3$ (110) orientation with d-spacings in the range of 4.02-4.04Å. This corresponds to one of the longer axes of the orthorhombic $KNbO_3$ cell. Films deposited at temperatures lower than 600°C often contain additional grain orientations such as the $KNbO_3$ (111).

X-ray diffraction rocking curve analysis provides information about the grain tilt of the films. The samples were 'rocked' about the $KNbO_3$ [110]. Any misorientation of the film grains will result in detection of planes slightly off the two-theta bragg angle. Figure 1 reveal FWHM values of 0.25, 0.30, and 0.84° on $KTaO_3$, $MgAl_2O_4$, and MgO, respectively.

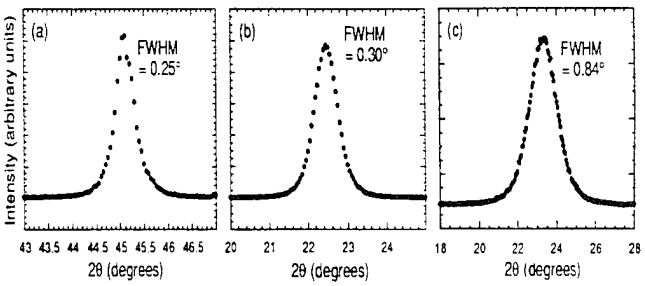

Figure 1. X-ray diffraction rocking curves of $KNbO_3$ [110] on (a) $KTaO_3$, (b) $MgAl_2O_4$, and (c) MgO substrates.

Composition and grain tilt

Rutherford backscattering spectroscopy was used to analyze the composition and thickness of the films. $KNbO_3$ films are found to posess K to Nb ratios in the range of 0.60 to 0.90. The potassium deficiency does not seem to affect the bulk properties of the films. For instance, in XRD, only the $KNbO_3$ (110) orientation exists and near bulk refractive index values are measured (as discussed later) for all films despite the K deficiency. It is believed that Na atoms arising from impurities in the KO_2 targets compensate for the K deficiency. A $KNbO_3$ film was deposited on a beryllium substrate to allow sodium to be detected in the RBS spectrum without being obscured by the substrate peak. Sodium was found to exist throughout the thickness of the film. Thus, it is likely that Na substitution on the K sub-lattice preserves the integrity of the $KNbO_3$ unit cell and further, has the little influence on some film properties such as the refractive index.

RBS/channeling measurements were performed by aligning the beam along the [110] film direction. The amount of scattering from the film would reveal the amount of film misorientation, defects, and other scattering centers. Channelling can only occur if films are of good epitaxial quality. In all cases the film was found to be aligned with the substrate in the perpendicular growth direction as the minimum film channeling direction corresponds to that of the substrate. $KNbO_3$ films on $KTaO_3$ and spinel substrates displayed the lowest

channeling yields with χ_{min} of only 7% and 9% for the Nb peak, respectively, while $KNbO_3$ films on MgO showed a χ_{min} of 18 %. A single crystal $KTaO_3$ substrate displayed a χ_{min} of 3% which illustrates the high degree of epitaxy of these films. However, films on MgO posess significantly more grain tilt. These results seem to correlate with the XRD rocking curve data shown above.

Surface morphology

Field emission scanning electron microscopy was used to characterize the surface microstructure and grain size of the films. $KNbO_3$ films on MgO and spinel contained grains of 1000 to 1200 Å in size as shown in Figure 2. Larger grain sizes of ~ 3000Å and also 90° oriented domain structures were found for films on $KTaO_3$.

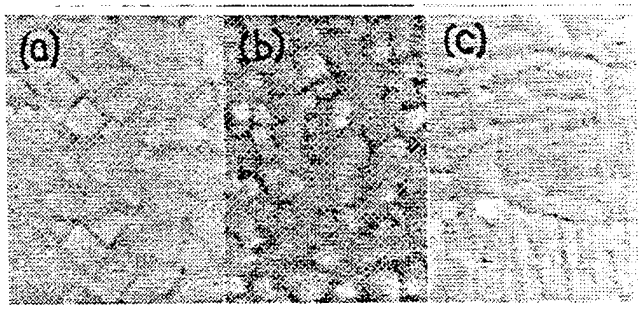

Figure 2. FESEM micrographs of $KNbO_3$ on (a) MgO, (b) $MgAl_2O_4$, and (c) $KTaO_3$ substrates

MgO and spinel substrates were purchased from Advanced Composited Materials and Commercial Crystal Systems, respectively. Oak Ridge National Laboratories provided the $KTaO_3$ substrates.

Surface roughness of both the films and substrates were analyzed by atomic force microscopy. Substrate surface roughness minimization is key for lowering optical scattering at the interfaces and for optimizing epitaxial film growth. Regions of 5 by 5 microns were scanned for all samples. MgO substrates displayed a root mean square (rms) roughness value of 23 Å with maximum features of 196 Å in height. These periodic large structures are believed to be due to hydroxide formation on the MgO surface. Annealing of the MgO substrates for 14 hours at 1150°C resulted in an rms value of only 13 Å with maximum features of 95 Å. Spinel substrates presented rms values of 14 Å and large features of 270 Å. Upon annealing both the rms and the maximum feature height increased appreciably. The rougher spinel surface can be attributed to either the nature of the more complex spinel structure where several different atomic surfaces are possible, or due to vendor preparation. $KTaO_3$ substrates exhibited the lowest surface roughness with an rms of 8 Å and a maximum height of 56 Å. The surface roughness of the $KNbO_3$ films were found to be low, with rms values varying from 13 to 37 Å.

OPTICAL PROPERTIES

Refractive index

The prism coupling technique was used to evaluate the refractive index of the thin films. [5] A He-Ne laser (6328 Å) is focused on a rutile prism clamped to the sample. The beam can be either polarized in the TE (polarized in the plane of the film) or TM (polarized perpendicular to the film) mode. When the propagation constant of the He-Ne beam in the prism matches that of the film, the overlap of the light waves in the airgap between the prism and film allows the light to couple into the film/waveguide. The incident angles which produce coupling conditions are used to calculate the refractive index and thickness of the film. If two coupling angles (two waveguide modes) can be detected, both the thickness and refractive index can be calculated independently. Otherwise, one parameter must be known to calculate the other. Refractive indices measured for all films are 2.21 and 2.28 in the TM (light polarized along $KNbO_3$ [110]) and TE modes (light polarized in the film plane), respectively. The bulk refractive index of $KNbO_3$ [110] in the TM orientation is 2.222. The refractive indices of the TE modes of our films were measured in two orthogonal propagation directions, but no birefringence was measured, which indicates that 90° domain orientations exist on all substrates. Therefore, the bulk refractive index for the TE modes should reflect an average value between the indices of $KNbO_3$ [$\bar{1}$10] and [001], 2.222 and 2.329. Figure 3 displays the $KNbO_3$ film refractive indices as a function of composition. Consequently, the fact that the refractive indices fall so close to the bulk values suggest $KNbO_3$ films are dense despite the potassium deficiency.

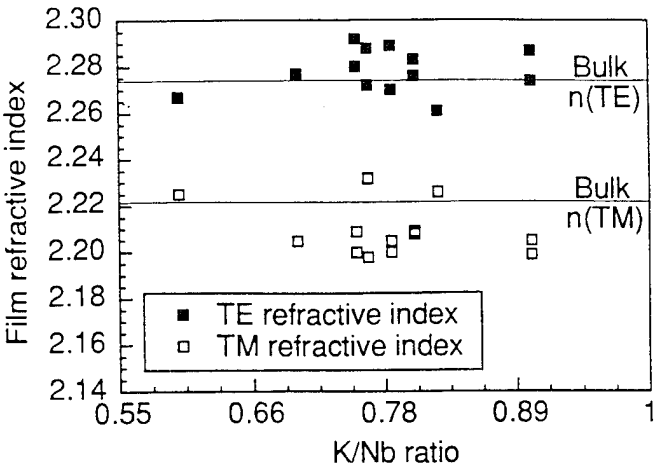

Figure 3. Refractive index of $KNbO_3$ (110) measured in the TE and TM modes versus composition

Scattering losses

Optical waveguide losses can be measured by analyzing the light streak observed in the film when coupling occurs. Longer light streaks suggest lower scattering losses. $KNbO_3$ films on MgO and spinel show higher losses for thick films (>1500 Å) than thinner (~1000 Å) films. Streak lengths of >8 mm can be observed for the latter cases as compared to only 2-3 mm for the thicker films. For our apparatus, losses can only be measured by those films with streak lengths of >5 mm. An optical fiber is mounted on a micrometer that allows movement along the length of the streak. The intensity of the light scattered at the surface of the streak is detected and quantified by a photodiode and connected to a nanovoltmeter. The losses can then be calculated by taking the slope of the 10log(I/Io) versus distance along the light streak where I = intensity of the measurement point and Io = initial intensity collected by the first point near the prism. Optical waveguide losses of ~34 dB/cm were found for $KNbO_3$ films of ~1100 Å. While even higher losses of >50 dB/cm were detected for thicker (>1500 Å) films .

Second harmonic generation

A Nd:YLF laser source with a wavelength of 1.053 μm with ~80psec, 100 MHz pulses under mode-locked operation was used as the source beam for SHG measurements. A harmonic beam splitter transmits the fundamental wavelength to a razor blade beam block, and reflects the second harmonic through a tilted 532 nm bandpass filter onto a ground-glass screen. First, $KNbO_3$ samples of thicknesses varying from 4600 to 6500 Å were placed perpendicular to the beam direction. By visual inspection of the screen, strong green light was observed for four samples of $KNbO_3$ thin films on both MgO and $KTaO_3$ substrates. Currents of only 28 to 30 A (at 30A, 275 watt/pulse was detected) were necessary to generate strong green light. Saturation of the signal seem to occur at 30 A. A $KNbO_3$ sample of ~2400 Å in thickness was then coupled with a 90° rutile prism. A 3-4 mm green light streak was seen in the TM_0 mode using currents of 31 to 33 A.

DISCUSSION

Three types of loss mechanisms exist: scattering, absorption, and radiation.[6] However, for dielectric thin films, the predominant contribution to losses are scattering losses. Scattering is subdivided into volume and surface scattering. Surface scattering losses are attributed to both light scattered from the film surface and the film/substrate interface. As the thickness of the film increases, the surface scattering losses decrease for a given coupling angle and arbitrary propagation length. As the mode number increases, the surface scattering will likewise increase, for the number of reflections within the waveguide increases duly. Therefore, properties that affect these losses are film and substrate roughness, and the particular mode or coupling angle.

Volume losses originate from scattering due to imperfections such as point defects, dislocations, and grain boundaries, found in the bulk of the waveguide. Figure 4 illustrates the phenomenon of volume scattering. Our data shows that the optical waveguide losses increase as the thickness of the film increases in the case of $KNbO_3$ films on MgO and spinel. This indicates that volume scattering losses are indeed dominating. When the films are just above the thickness

criterion for waveguiding of the first mode, the majority of the field is propagating in the low loss single crystal substrate, and thus, low scattering losses are observed. As the film thickness increases, the amount of the optical field propagating in the film increases, and thus volume losses bcome a greater proportion of the total losses.

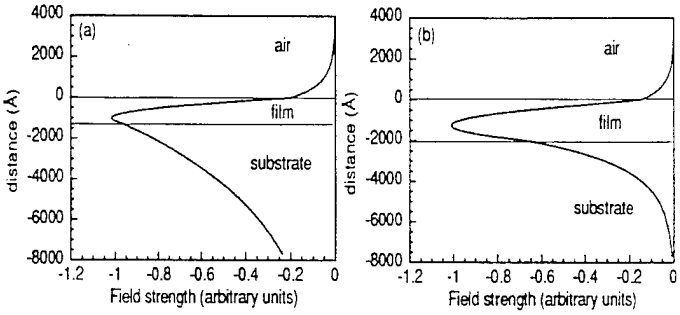

Figure 4. Modal distribution versus distance at the TM=0 mode and wavelength 6328 Å for a $KNbO_3$ waveguide on MgO substrate for film thickness (a) 1200 Å and (b) 2000 Å

The x-ray diffraction rocking curve and RBS/channeling data show a correlation between lattice mismatch and grain tilt. $KNbO_3$ films on spinel and $KTaO_3$, where a smaller lattice mismatch exists, exhibited less grain tilt as compared to films on MgO. At the deposition temperature, the $KNbO_3$ film is cubic. Misfit dislocations form to accomodate the lattice mismatch which may result in 'tilts' and 'twists' of the grains. These lattice imperfections can be a significant contributor to bulk scattering. During cooling, the film first transforms to the tetragonal phase at ~435°C. It is during the second transformation to the orthorhombic structure (~225°C) where twin domains may form. The cubic symmetry of the substrates allows the in-plane orientations to be accomodated in any of the four equivalent 90° directions. Light waves travelling in the film will therefore experience refractive index changes as they traverse the twin domains resulting in attenuation. The coarse and fine grain structure as seen in the FESEM micrographs gives additional evidence of the bulk scattering that is occurring in the films.

SUMMARY

Epitaxial dense $KNbO_3$ thin films have been grown on MgO, $MgAl_2O_4$, and $KTaO_3$ substrates by ion-beam sputter deposition. X-ray diffraction scans show a single $KNbO_3$ (110) orientation for all films. RBS revealed K to Nb ratios ranging from 0.60 to 0.90. The potassium deficiency of the $KNbO_3$ films can be explained by sodium incorporation from impurities found in the KO_2 sputtering targets. AFM measurements reveal smooth films when grown on high quality substrate surfaces. Prism coupling measurements show films to possess near bulk TE and TM refractive indices of 2.28 and 2.21, respectively. The optical waveguide losses in the films can be attributed primarily to volume scattering, possibly originating from the coarse and fine grain structure and/or twins formed during structural transformations. $KNbO_3$ thin films have demonstrated SHG of green light from a Nd:YLF laser source in the transverse and waveguide modes with film thicknesses of 4600-6500 Å and ~2400 Å, respectively. The strong green light seen at low currents and small film thicknesses indicate the high nonlinearity of the $KNbO_3$ films, the high quality of these $KNbO_3$ thin films, and the potential for producing a blue laser source.

ACKNOWLEDGEMENTS

This research is supported by the Office of Naval Research under Contract No. N0014-91-1307. We thank Dr. N. R. Parikh at University of North Carolina-Chapel Hill for providing the Rutherford backscattering spectroscopy equipment, and Dr. L. A. Boatner at Oak Ridge National Laboratory for supplying the $KTaO_3$ substrates.

REFERENCES

[1] J. J. E. Reid, M. Ouwerkerk, and L. J. A. M. Beckers, "Potassium Lithium Niobate and its Application to Intercavity Frequency Doubling," Philips Journal of Research, vol. 46, nos. 4-5, pp. 199-213, 1992.

[2] V. G. Dmitriev, G. G. Gurzadyan, and D. N. Nikogosyan, Handbook of Nonlinear Optical Crystals. Berlin Heidelberg: Springer-Verlag, 1991.

[3] G. H. Hewig and K. Jain, "Frequency Doubling in a $LiNbO_3$ Thin Film Deposited on Sapphire," J. Appl. Phys., 54(1), pp. 57-61, January 1983.

[4] T. M. Graettinger, S. H. Rou, M. S. Ameen, O. Auciello, and A. I. Kingon, "Electro-optic Characterization of Ion Beam Sputter-Deposited $KNbO_3$ Thin Films," Appl. Phys. Lett., 58, p.p. 1964-1966, May 1991.

[5] R. Ulrich and R. Torge, "Measurement of Thin Film Parameters with a Prism Coupler," Appl. Opt. 12, p.p. 2901-2908, December 1973.

[6] R. G. Hunsperger, Integrated Optics: Theory and Technology. Berlin Heidelberg: Springer-Verlag, 1991.

Appendix 8

"Growth, Microstructures and Optical Properties of $KNbO_3$ Thin Films," T.M. Graettinger, P.A. Morris, Rene R. Woolcott, F.C. Zumsteg, A.F. Chow, and A.I. Kingon, MRS Symposium Proceedings **310** (Ferroelectric Thin Films III), 301-311, 1993.

GROWTH, MICROSTRUCTURES AND OPTICAL PROPERTIES OF $KNbO_3$ THIN FILMS

THOMAS M. GRAETTINGER*, P. A. MORRIS**, R. R. WOOLCOTT*, F. C. ZUMSTEG**, A. F. CHOW*, AND A. I. KINGON*
*North Carolina State University, 1001 Capability Dr., Raleigh, NC 27695-7919
**DuPont Company, Experimental Station, Wilmington, DE 19880-0356

ABSTRACT

Potassium niobate, $KNbO_3$, possesses high nonlinear optical coefficients making it a promising material for frequency conversion into the visible wavelength range. While epitaxial thin films of $KNbO_3$ have been reported [1,2], only limited data exists concerning the optical loss mechanisms and nonlinear optical properties of these films. In this study, epitaxial thin films of $KNbO_3$ have been grown using ion beam sputter deposition and evaluated in terms of their microstructures and optical properties. Characterization of the microstructures of these films includes the in-plane epitaxial relationship to the substrate. The relationships between the growth parameters and microstructures developed to the indices of refraction and the optical losses (absorption and scattering) are discussed.

INTRODUCTION

The next generation of laser writing and optical storage devices will require a high resolution coherent light source. The resolution necessary can be achieved by using a blue light source where high resolution is achieved because of the short wavelength. Currently no compact blue laser source is commercially available, but the production of blue laser radiation through second harmonic generation (SHG) in a nonlinear optical material presents the most promising approach demonstrated thus far. Achieving the necessary second harmonic power (1-5 mW) from a relatively low power semiconductor laser diode requires high conversion efficiency in the nonlinear material.

Many factors influence the SHG efficiency including the nonlinear susceptibility of the material (**dijk**), the refractive index (**n**), the optical pathlength (**L**), and the waveguide width and thickness (**w**,**t**) as shown in the following equation.

$$\frac{P^{(2\omega)}}{P^{(\omega)}} \propto \frac{d_{ijk}^2}{n^3} L^2 \frac{P^{(\omega)}}{w \cdot t} \qquad (1)$$

Mat. Res. Soc. Symp. Proc. Vol. 310. ©1993 Materials Research Society

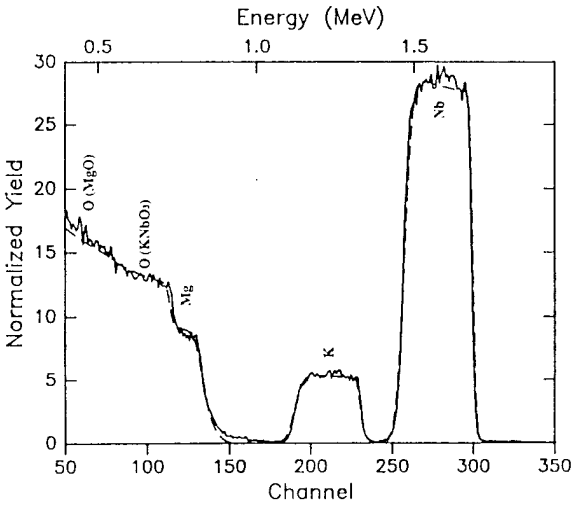

Fig. 4. RBS spectrum of a KNbO3 thin film grown on MgO. The dashed line represents the simulated spectrum of a stoichiometric KNBO3 film.

EPITAXY STUDY

Crystal orientation is critically important to SHG performance. Phase matching of the fundamental and second harmonic waves can normally be accomplished only in certain crystallographic directions in a crystal. Therefore, it is desirable to produce a thin film that is a single crystal, requiring epitaxy in both planar directions of the thin film and no microstructural defects. In practice it is very difficult to grow a true heteroepitaxial film. Lattice mismatch between film and substrate is often accommodated by the formation of microstructural defects such as high and low-angle grain boundaries and the formation of domain walls in ferroelectric thin films. For these reasons, neighboring grains or domains may not have the same crystallographic orientation across the boundary or wall, ruining the phase matching conditions as the fundamental and second harmonic waves cross these boundaries.

The standard x-ray diffractometer theta-two theta scan is a powerful technique for determining the crystalline structure of thin films and for determining if any preferential orientation exists. The resulting pattern is also useful in identifying the crystalline phases present. Fig. 5 shows a typical x-ray diffraction pattern for a KNbO3 thin film deposited on MgO. From this diffraction pattern it is clear that the film is single phase KNbO3 and highly

oriented with (110)KNbO3||(001)MgO where the indices given for KNbO3 are for the orthorhombic phase. This orientation of the orthorhombic unit cell is pictured in Fig. 6. As shown in the figure, the [001]KNbO3 is in the plane of the film. However, it can not be determined from the standard diffraction pattern if the [001]KNbO3 is parallel to the [100]MgO or the [010]MgO. The in-plane orientation of the film, is necessary for phase matching considerations as discussed earlier.

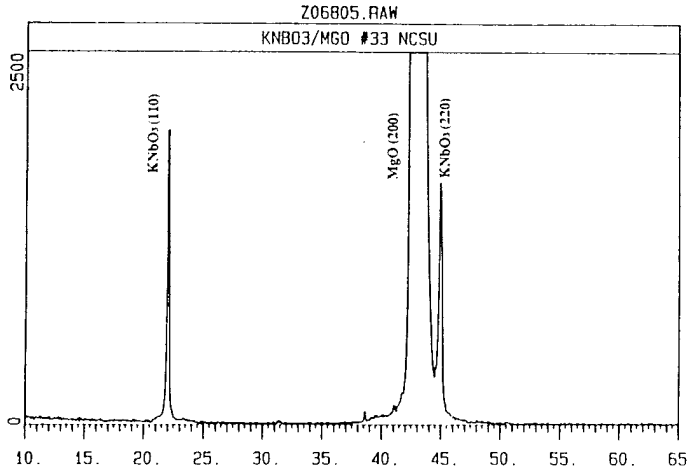

Fig. 5. X-ray diffraction pattern of a KNbO3 thin film deposited on MgO(001).

In order to investigate the in-plane orientation of the KNbO3 thin films, a pole figure rotation stage in combination with an x-ray diffractometer was used. This apparatus has the ability to probe crystal planes which are not parallel to the substrate surface. First, (110) pole figures were constructed for the KNbO3 thin films and a representative figure is shown in Fig. 7. This figure makes it clear that the film is tilted along the MgO [100], [010], [$\bar{1}$00], and [0$\bar{1}$0] directions. Samples deposited by both ion beam sputtering methods exhibited this behavior, suggesting that the tilt is a substrate influenced characteristic and is not related to deposition method. Lattice tilt is a well known mechanism for accommodating lattice mismatch between film and substrate. The lattice mismatch between the (001)KNbO3 and [100]MgO planes is 6.0%. This mismatch is relatively large for achieving high quality heteroepitaxial growth. In addition to tilt, low angle grain boundaries twinning, and inversion domain

boundaries have been observed previously in KNbO3 thin films grown by ion beam sputtering.[12]

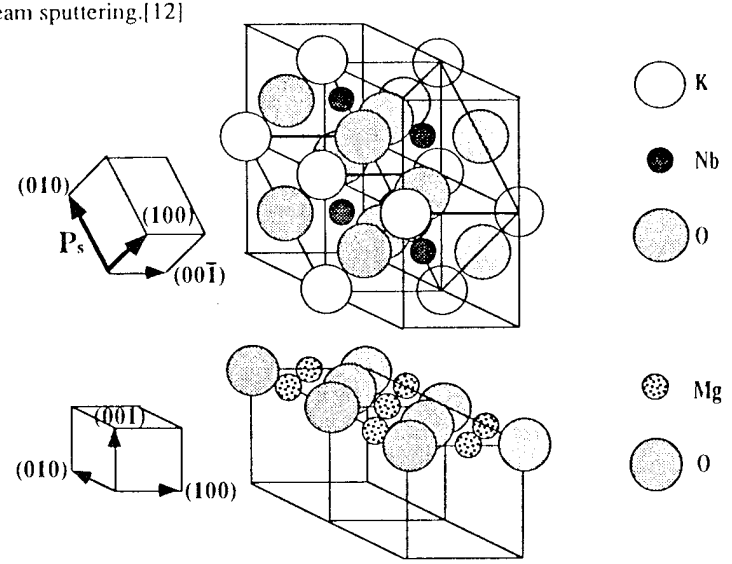

Fig. 6. The orientation of the orthorhombic unit cell of KNbO3 on MgO(001).

With this knowledge it is probable that complete in-plane epitaxy has not been achieved. The films may be best described as textured with in-plane rotation.

Due to the large lattice mismatch between KNbO3 and MgO the films may be highly strained. Others have reported the growth of tetragonal KNbO3 films[2] which may be a result of strain in those films. The (110) and (220) reflections of orthorhombic KNbO3 match closely the peaks observed for the ion beam sputtered films grown in this study. To confirm that the films grown by ion beam sputtering were indeed orthorhombic, the pole figure rotation stage was used to rotate the samples so that planes which are not parallel to the substrate surface would reflect in the standard diffractometer geometry. In this manner, the (131) and (311) planes, among others, were identified and their d-spacings are consistent with orthorhombic KNbO3. Further, these planes also exhibited tilt about the expected positions which were based on alignment of the [110]KNbO3 and [001]MgO directions.

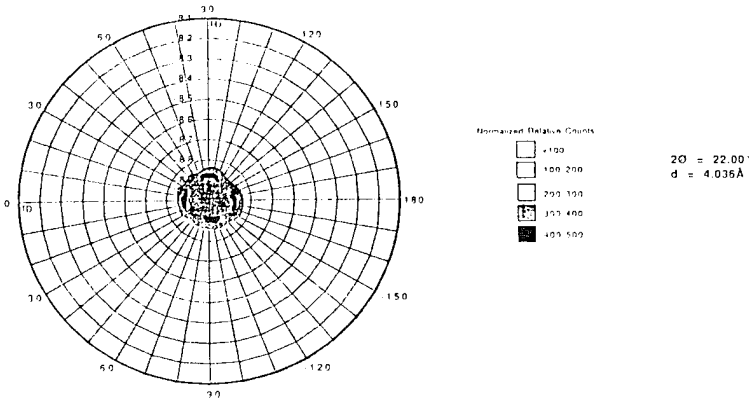

Fig. 7. (110) pole figure for a KNbO3 thin film deposited on MgO.

OPTICAL PROPERTIES

The indices of refraction of layer-by layer deposited and cosputtered KNbO3 thin films were measured using the prism coupling m-line technique. The mode lines appeared relatively sharp as shown in Fig. 8 which shows the measurement of a layer-by layer deposited film. Both types of films supported TE and TM guided modes. The results of these measurements are presented in Table II along with the indices of bulk KNbO3 for orientations which correspond to the guided modes. The film indices for TE modes should be compared to the (001) and (1 $\bar{1}$0) indices of bulk KNbO3, 2.3291 and 2.2242, respectively, since these are the major and minor axes of the index ellipsoid in the plane of the film. If the films were single crystal, both values should have been observed as the films were rotated 90 degrees during the measurements. This birefringence was not observed, however. Instead, the measured TE indices match closely with the average of the bulk (001) and (1 $\bar{1}$0) indices. The fact that birefringence was not seen in the TE measurements supports the conclusion that the films are textured with in-plane rotation as stated above. However, strain effects and twinning could also account for the lack of birefringence in the TE index. The TM indices of both types of ion beam sputtered films, on the other hand, are in good agreement with the expected (110) bulk index.

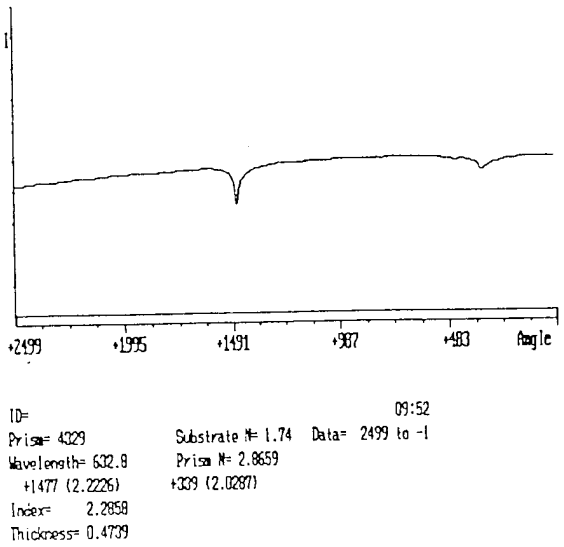

Fig. 8. Guided mode spectrum for an ion beam sputter deposited $KNbO_3$ film.

Table II. Refractive indices of thin films and bulk $KNbO_3$.

Film	Substrate	Mode/Orientation	Refractive Index
Layer-by-layer	MgO	TE	2.2856±.0003
		TM	2.2021±.0012
Cosputtered	MgO	TE	2.2207±.0041
		TM	2.1975±.0046
Bulk $KNbO_3$		(001)	2.3291
		(110), (1$\bar{1}$0)	2.2242

A fiber probe was used to measure the optical propagation loss in the $KNbO_3$ films. A large degree of scattering prevented the measurement of propagation loss in the films using the fiber probe. As discussed earlier, microstructural features such as grain boundaries and interface roughness can be major contributors to scattering loss. These features are found in the sputtered films and must be controlled in the future to yield low-loss waveguides.

SUMMARY

Thin films of $KNbO_3$ were fabricated by ion beam sputtering using both layer-by-layer and cosputtering ion beam deposition methods. Both methods have demonstrated good compositional control and stoichiometric $KNbO_3$ thin films have been produced. However, in-plane epitaxy is necessary to achieve efficient SHG in a thin film. To investigate the in-plane epitaxy of the films a pole figure rotation stage in combination with a standard x-ray diffractometer was used. The results of this study show that the $KNbO_3$ films are tilted 1-1.5° about the substrate normal along the MgO cubic directions. This is an indication that the films are textured with in-plane rotation. The refractive indices of the thin films were measured using the prism coupling m-line technique and compare favorably with bulk values. Birefringence was observed between TE and TM modes, but was not observed in TE measurements at 90° supporting the conclusion that the films are textured and true in-plane epitaxy has not been achieved. Further work to understand the relationships between growth, microstructure, and loss mechanisms is needed to achieve a thin film material suitable for an efficient SHG device.

ACKNOWLEDGMENTS

The authors would like to acknowledge; the Office of Naval Research for partial support of this work under contract N00014-91-J-1307, and Bruce Rothman and the Laboratory for Research on the Structure of Matter at the University of Pennsylvania for assistance and use of their equipment in making the RBS measurements under NSF #DMR91-20668.

[1]T. M. Graettinger, S. H. Rou, M. S. Ameen, O. Auciello, and A. I. Kingon, Appl. Phys. Lett **58**, 1964 (1991).
[2]S. Schwyn Thöny and H. W. Lehmann, and P. Günter, Appl. Phys. Lett. **61**, 373 (1992).
[3]W. J. Kozlovsky, W. Lenth, E. E. Latta, A. Moser, and G. L. Bona, Appl. Phys. Lett. **56**, 2291 (1990).
[4]C. Zimmermann, T. W. Hänsch, R. Byer, S. O'Brien, and D. Welch, Appl. Phys. Lett. **61**, 2741 (1992).
[5]C. J. van der Poel, J. D. Bierlein, J. B. Brown, and S. Colak, Appl. Phys. Lett. **57**, 2074 (1990).
[6]K. Yamamoto, K. Mizuuchi, and T. Taniuchi, Optics Lett. **16**,1156 (1991).
[7]M. Fujimura, T. Suhara, and H. Nishihara, Electronics Lett. **27**, 1207 (1991).
[8]P. Günter, Appl. Phys. Lett. **34**, 650 (1979).
[9]M. Amini and M. D. Sacks in Better Ceramics through Chemistry IV, (Mater. Res. Soc. Proc. **180**, Pittsburgh, PA, 1990) p. 675.
[10]R. Gutmann and J. Hulliger, Cryst. Prop. Prep. **32-34**, 117 (1991).
[11]D. Marcuse, Theory of Dielectric Optical Waveguides, (Academic Press, New York, 1974), p.138.
[12]A. I. Kingon, S. H. Rou, M. S. Ameen, T. M. Graettinger, K. Gifford, and O. Auciello in Electro-Optics and Non-linear Optic Materials, edited by A. S. Bhalla, E. M. Vogel, and K. M. Nair (Ceramic Transactions **14**, Westerville, OH, 1990) pp. 179-196.

Appendix 9

"Microstructural Characterization of Eptaxial Bottom Electrodes, Buffered Layers, and Ferroelectric Thin Flms", Shan Hsien rou, T. M. Graettinger, A. F. Chow, C. N. Soble II, D. J. Lichtenwalner, O. Auciello and A. I. Kingon, MRS Symposium Proceedings **243** (Ferroelectric Thin Films II), 81-91, 1992.

MICROSTRUCTURAL CHARACTERIZATION OF EPITAXIAL BOTTOM ELECTRODES, BUFFERED LAYERS, AND FERROELECTRIC THIN FILMS

Shang Hsien Rou, T. M. Graettinger, A. F. Chow, C. N. Soble, II, D. J. Lichtenwalner, O. Auciello*, and A. I. Kingon, Department of Materials Science and Engineering, NCSU, Raleigh, NC., *Also, MCNC, RTP, NC

ABSTRACT

Three subjects are covered in this paper. First, a set of criteria are established to explain how epitaxial growth can be achieved for sol-gel processed ferroelectric thin films. These criteria describe the conversion of amorphous films to epitaxial films. Second, we report the microstructures of ion beam sputtered buffer layers, (100) MgO on (100) Si, and epitaxial bottom electrodes, (100) Pt on (100) MgO and (111) Pt on (0001) Al_2O_3, for the integration of ferroelectric films with various types of substrates. Third, microstructures of the multilayered epitaxial films, (001) $YBa_2Cu_3O_{7-\delta}$ on (100) $KNbO_3$/(100) MgO and (100) $KNbO_3$ on (100) MgO/(100) Si, are characterized. The results indicate that high quality epitaxial multilayered films can be obtained under the proper processing conditions.

I. INTRODUCTION

Microstructural characterization plays an important role in both material and process developments. The relative importance of microstructural characterization is even greater for epitaxial films, because epitaxial films offer unique microstructures and particular defect structures not often observed in randomly oriented films or bulk materials. The understanding of microstructures enables us to develop mechanisms for epitaxial nucleation and growth, and to rationalize energetic criteria for defect formation. Thereafter, the processing-structure-property relationships can be correlated.

Epitaxial ferroelectric thin films have been shown to offer unique characteristics compared to randomly oriented films [1,2]. It is recognized that epitaxial films are required for optical and electro-optic applications [2]. Furthermore, ferroelectric materials [3] have been identified as one of the high permittivity materials which may replace SiO_2-based dielectric layers for memory capacitors. Epitaxial films, which can have fewer defects and, therefore, smaller leakage currents, may have technological advantages in device performance. Therefore, it is important to investigate the processing issues and to understand the nucleation and growth mechanisms for epitaxial ferroelectric films.

In this paper, transmission electron microscopy (TEM) was employed for microstructural characterization. Highly oriented buffer layers and epitaxial bottom electrodes were investigated for the integration of epitaxial ferroelectric films with various types of substrates. Microstructural characterization was performed on these epitaxial layers. Also, two multilayer structures containing epitaxial ferroelectric $KNbO_3$ films were characterized.

Mat. Res. Soc. Symp. Proc. Vol. 243. ©1992 Materials Research Society

. EXPERIMENTAL PROCEDURE

The ferroelectric films, $KNbO_3$ and $Pb(Mg_{2/3}Nb_{1/3})O_3$ (PMN), characterized this paper were deposited utilizing ion beam sputter deposition [4] and sol-gel rocessing techniques [5], respectively. The buffer layers, bottom electrodes, and ıperconducting $YBa_2Cu_3O_{7-\delta}$ (YBCO) films were all ion beam sputtered utilizing ngle metallic or multicomponent targets. The processing parameters for these lms are briefly described and properly referenced when mentioned.

Plan view and cross sectional TEM samples were prepared employing a ıriety of procedures [6-8]. These specimens were examined utilizing a Hitachi H-)0 transmission electron microscope equipped with an energy dispersive ɔectroscope for compositional analysis, and a JEOL 200CX transmission electron ıicroscope equipped with a high resolution pole piece for high resolution naging.

I. RESULTS AND DISCUSSION

I.1. Solid phase epitaxy of ol-gel processed PMN on rTiO$_3$

PMN films were ıbricated on the (111) rTiO$_3$ substrates utilizing a ɔl-gel processing technique 5]. Because the sol-gel rocess utilizes metalorganic ɔrecursors and organic olvents, a large volume hrinkage occurs during hermal processing. As a esult, most sol-gel processed hin films contain porosity 9] or even microcracks. 'herefore, it is challenging ɔ produce a dense film or a ıigh quality epitaxial film ıtilizing the sol-gel ɔrocessing technique.

Figure 1(a) shows a ross sectional image of the 'MN on SrTiO$_3$. The ɔrresponding selected area liffraction (SAD) pattern Fig. 1(b)] shows that the 'MN is epitaxially grown on he SrTiO$_3$. The epitaxial ɔrientation of the PMN ilms with respect to the SrTiO$_3$ substrate can be ıummarized by the

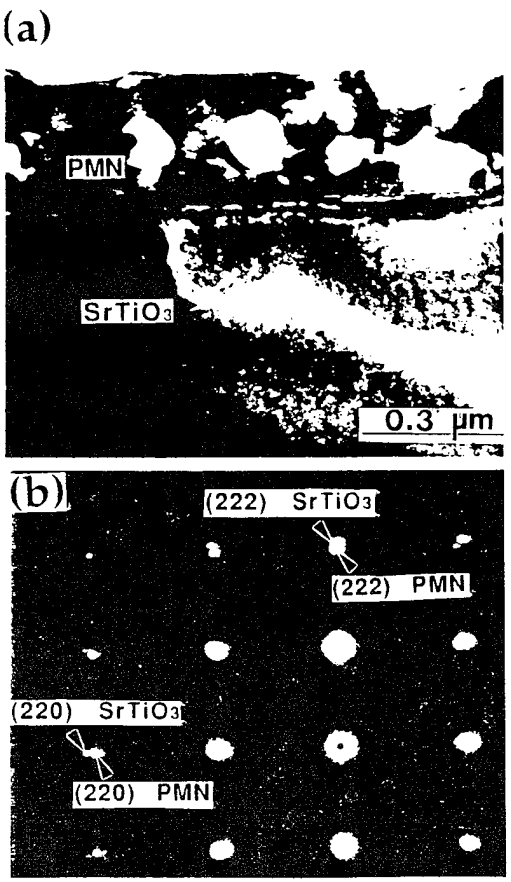

Figure 1 (a) A cross sectional image of (111) PMN on (111) $KNbO_3$. (b) A SAD pattern showing the epitaxial growth of PMN on $KNbO_3$.

relationships (111) PMN // (111) $SrTiO_3$ and [1$\bar{1}$0] PMN // [1$\bar{1}$0] $SrTiO_3$. These results raise questions of how and why the perovskite phase grows epitaxially on the $SrTiO_3$ substrate. In order to properly interpret this microstructure, it is necessary to understand the requirements for epitaxial growth and the microstructural evolution of sol-gel processed films.

Epitaxial films can simply be described as thin films which maintain a unique crystallographic orientation with respect to the substrate. The essential requirements for epitaxial growth are 1) a single crystal substrate, 2) nucleation and growth initiated on the substrate surface, and 3) a single energetically favorable nucleation orientation (usually, but not necessarily, determined by the minimum lattice mismatch between film and substrate). These are simplified requirements; specific requirements for different material systems need to be considered individually. An enormous amount of literature about epitaxial growth has been accumulated since 1839 [10].

An excellent review of the sol-gel process has been published by Yi and Sayer [11]. Briefly, the metalorganic stock solution is spin-coated on a suitable host substrate. A low temperature bake process is conducted to drive off excessive solvents in the metalorganic films. The films are then subjected to a high temperature anneal to crystallize the desired phase. The microstructural evolution after each processing step can be summarized as follows:

Metalorganic film ---> amorphous or microcrystalline film ---> crystalline film
(Spin-on coating) (low temp anneal) (High temp anneal)

Epitaxial growth of the sol-gel processed films can occur during the crystallization of the films. The films are either amorphous or microcrystalline before the high temperature anneal. A high temperature anneal can convert an amorphous film to an epitaxial one, if the annealing processes are controlled properly. This is essentially a **solid phase epitaxy (SPE)** process. In contrast, a high temperature anneal of a microcrystalline film can only achieve either a randomly or preferentially oriented film, because the growth and coalescence of the microcrystallites result in polycrystalline grains with various orientations.

Figure 2 illustrates the ideal growth evolution of the SPE process. Briefly, nucleation of the crystalline phase must initiate at the amorphous/crystalline interface. These nuclei grow and eventually coalesce to form a continuous film. The

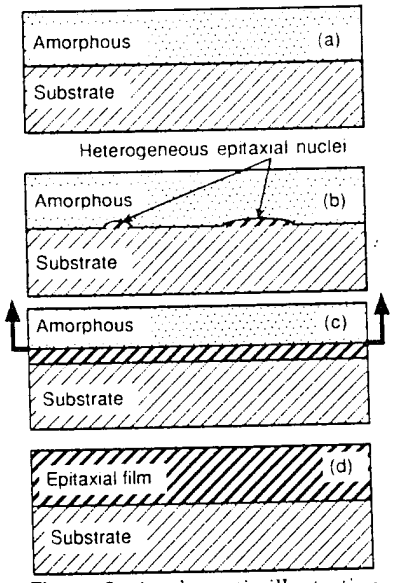

Figure 2 A schematic illustration of an ideal solid phase epitaxial growth. The anneal time increases from (a-d), with (a) at zero time, and (d) at completion.

stalline/amorphous interface then proceeds to the surface and completes the E growth. This ideal process requires epitaxial nucleation on the substrate face, but no random nucleation in the amorphous film. Although erogeneous nucleation is thermodynamically favored over homogeneous over entire process temperature range, this two nucleation processes compete ietically. Thus conditions are sought which minimize the probability of some mogeneous nucleation occuring. This can be achieved by raising the stallization temperature, which increases the relative stability of heterogeneous clei over the homogeneous nuclei. The approach to optimize the processing rameters for preparation of epitaxial films by the sol-gel process can be mmarized as follows:

An amorphous film with atomic scale compositional homogeneity on a single crystal substrate is required.

A high annealing temperature is preferred to minimize the probability of some homogeneous nucleation occuring.

In accordance with the previous point, rapid ramping rate to the annealing temperature is preferred.

e successful growth of the epitaxial PMN on $SrTiO_3$ occured because the ocessing parameters are in-line with the above requirements [12].

.2. Epitaxial Pt bottom electrodes and highly oriented MgO buffer layers

We have successfully grown epitaxial ferroelectric $KNbO_3$ and PZT films on ngle crystal (100) MgO, (0001) Al_2O_3, and $SrTiO_3$ substrates [13-14] for optical and ectrooptic applications. However, the use of oxide substrates is not very cost fective, and not compatible with the leading semiconductor technology. rther, severe interdiffusion [15] and the formation of a thick SiO_2 layer [13] at e film-substrate interface inhibited the epitaxial growth of ferroelectric $KNbO_3$ d PZT films on bare silicon substrates. Therefore, a buffer layer is required for e integration of epitaxial ferroelectric thin films with silicon. Thin films of gO on silicon and sapphire were investigated and the detailed processing issues ill be presented elsewhere [16]. The microstructures of MgO on silicon are aracterized in the following section.

The non-volatile memory device is one of the primary applications for rroelectric films. A maximum amount of polarization can be utilized if the evice is configured with a top-bottom electrode structure. Platinum has a small ttice mismatch with respect to (100) MgO and (0001) sapphire, and therefore a od candidate as an epitaxial bottom electrode. Epitaxial Pt films were ion beam utter-deposited on (100) MgO and (0001) sapphire at 400 °C. These epitaxial Pt ottom electrodes are the host for subsequent deposition of epitaxial ferroelectric lms. Properties of the epitaxial ferroelectric films can then be measured. licrostructures of epitaxial Pt on (100) MgO and (0001) Al_2O_3 are discussed in ction III.2.b.

I.2.a. Epitaxial and highly oriented MgO buffer layers on sapphire and Si

Figure 3(a) shows an SAD pattern of a plan view MgO/Si sample, taken ng the silicon [100] zone axis. It consists of one set of (100) silicon and one set of ghly oriented (100) MgO diffraction patterns. The corresponding microstructure ig. 3(b)] reveals that the MgO film is polycrystalline with a fine grain structure (< 200A grain size). One of the reasons to account for the small grain size is low deposition temperatures (400 °C or 500 °C). These results indicate that some of the MgO grains have either a twist or tilt orientational deviation from the perfect epitaxial relationship with respect to the silicon substrate. Figure 3(c) shows a cross sectional high resolution electron micrograph of the MgO/Si interface. A thin

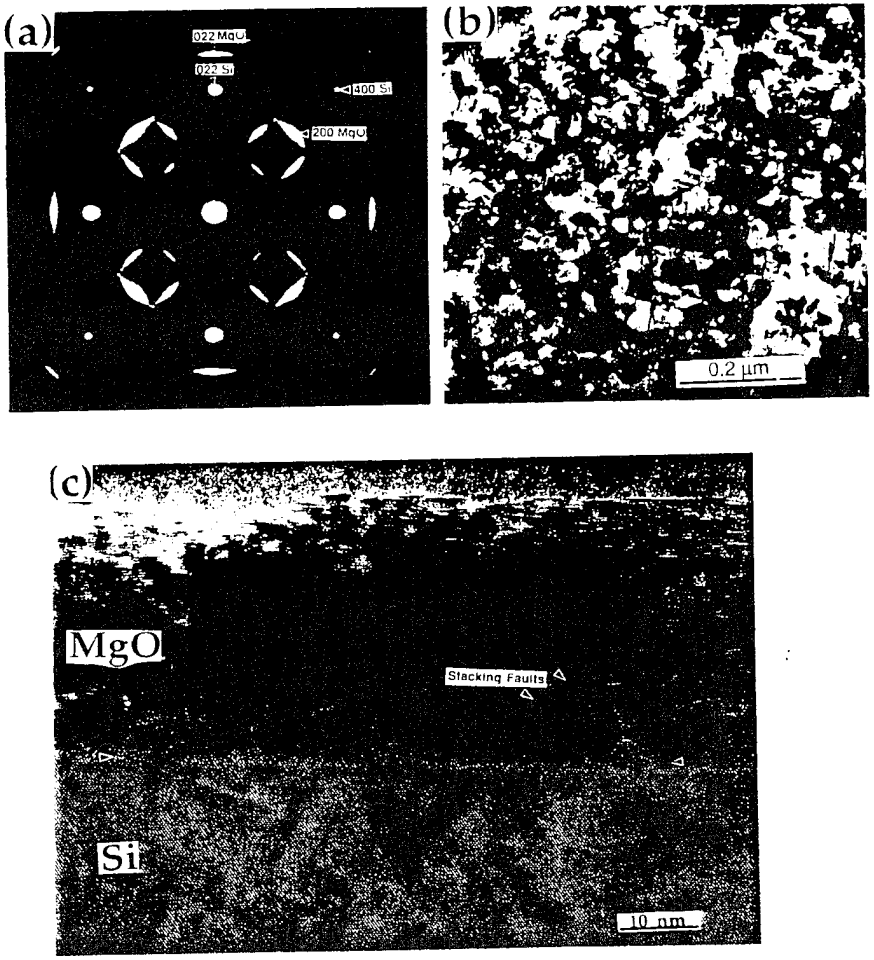

Figure 3 (a) A SAD pattern reveals the MgO is highly oriented on (100) Si. (b) the corresponding microstructure showing the fine grain polycrystalline MgO. (c) A cross sectional high resolution electron micrograph of the MgO/Si interface. A thin amorphous layer and stacking faults are shown as indicated by arrows.

morphous layer and a region with a high density of stacking faults (as indicated y arrows) near the interface can be observed. These are two of the probable iechanisms causing the tilt and twist of the MgO grains. We are currently ttempting to optimize the processing parameters to minimize the amount of tilt nd twist among MgO grains. Epitaxial MgO films have been deposited onto c-cut)001) and r-cut (10$\bar{1}$2) sapphire. The results and analyses will be published lsewhere [16].

The orientation of the MgO films with respect to the silicon substrate can be rinciply described by the relationships (100) MgO // (100) Si and [010] MgO // [010] i, if we ignore the twist and tilt of the MgO grains with respect to Si. This rientation relationship leads to a 22.4 % lattice mismatch between [100] MgO and 00] Si. This large lattice mismatch could be one of the causes for the small MgO rain size. It is apparent that the minimum lattice mismatch is not the most nportant criterion that determines the orientation of MgO on (100) Si, because a iinimum lattice mismatch between MgO and Si (less than 10 %) can be obtained 'ith the following orientation arrangements: (100) MgO // (100) Si and [010] MgO / [011] Si.

I.2.b. Epitaxial bottom electrodes (Pt/MgO and Pt/Al_2O_3)

Figure 4(a) shows a typical microstructure of an epitaxial Pt film grown on 00) MgO. The corresponding SAD pattern [Fig. 4(b)] confirms the epitaxial rowth of Pt films on (100) MgO. The epitaxial orientation of the Pt films with spect to the MgO substrate can be summarized by the relationships (100) Pt // 00) MgO and [010] Pt // [010] MgO. It is interesting to note that the Pt films ontain a very high density of defects, mainly dislocation loops shown as black ots in the micrograph. However, no grain boundaries can be observed. The Pt iicrostructure is different from what we have observed in the epitaxial rroelectric thin films directly deposited on MgO substrates. Low angle tilt and vist grain boundaries were the dominant defects in the epitaxial oxide films [17]. his could indicate that the strain accommodation mechanisms are different for ietallic and oxide thin films. In the case of Pt on MgO, the stress is relaxed by lastic deformation (formation of dislocations). In the case of oxide on MgO, low ngle grain boundaries are present to releave the strain. Some elongated ectangular features can be observed in these (100) oriented epitaxial Pt films. We ave identified them as Pt grains with {221} orientations.

The SAD pattern in Figure 4(c) shows that Pt films were also epitaxially rown on (0001) sapphire. The epitaxial orientation of the Pt films with respect to ie sapphire substrate can be summarized by the relationships (111) Pt // (0001) l_2O_3 and [110] Pt // [10$\bar{1}$0] Al_2O_3. Note that the Pt diffraction spots are slightly longated circumferentially. This implies that some Pt grains deviate slightly om the epitaxial relationships with respect to (0001) Al_2O_3. Furthermore, this idicates that the quality of (100) Pt on (100) MgO is better than that of (111) Pt on)001) sapphire. This result is somewhat mysterious because the lattice mismatch etween [100] Pt and [100] MgO is ≈6.9%, while that of [110] Pt and [10$\bar{1}$0] Al_2O_3 is ss than 3%. Further work is needed to understand how the different substrate irfaces affect the epitaxial growth of the Pt films.

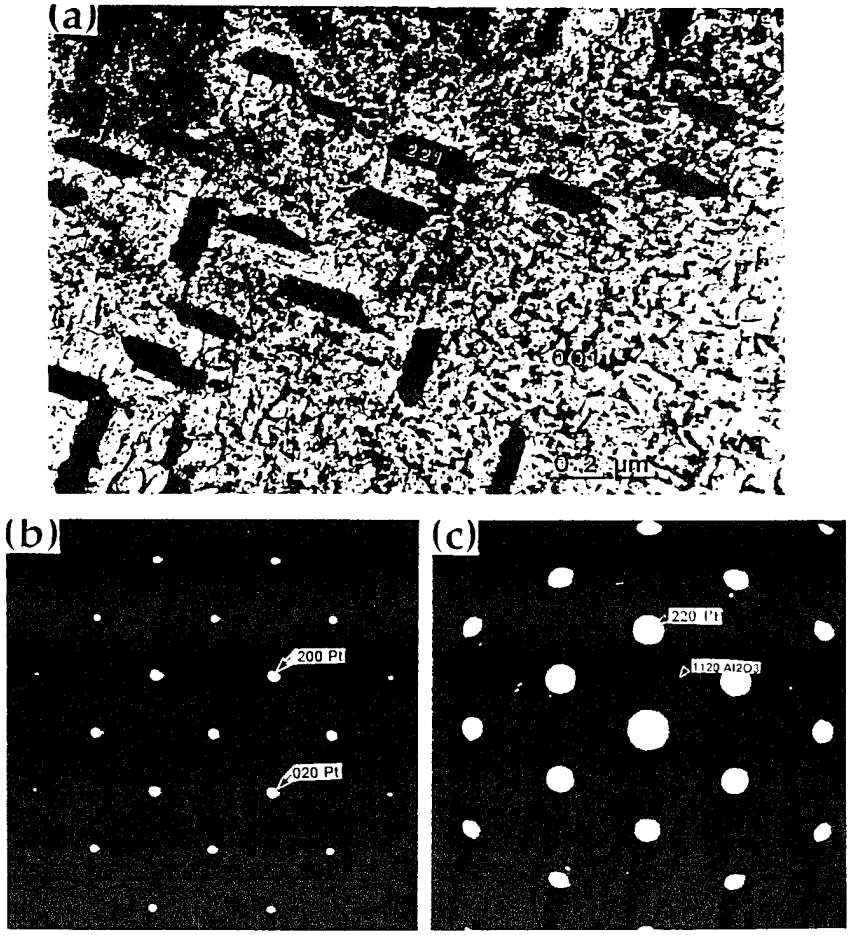

Figure 4 (a) A typical microstructure of the epitaxial Pt with both (100) and (221) oriented grains. (b) The corresponding SAD pattern confirming the epitaxial growth of Pt films on (100) MgO. (c) The SAD pattern of epitaxial Pt on (0001) sapphire.

III.3. Microstructural characterization of epitaxial multilayered films

Integration of epitaxial ferroelectric films on various multilayer structures has been investigated. Two multilayer films, $YBa_2Cu_3O_{7-\delta}$ on $KNbO_3$/MgO and $KNbO_3$ on MgO/Si, are reported in this section.

.a. (001) YBCO on (100) $KNbO_3$/(100) MgO

Superconducting YBCO films [18] were deposited onto (100) $KNbO_3$ films vn on (100) MgO substrates. The two main reasons to choose (100) $KNbO_3$ as a er layer are 1) to reduce the lattice mismatch (from about 9 % between [100] :O and [100] MgO to less than 5 % between [100] YBCO and [100] $KNbO_3$) and 2) eposit YBCO on a host with a similar perovskite structure.

Figure 5(a) shows the cross sectional micrograph of YBCO on $KNbO_3$/MgO. ; micrograph shows that both $KNbO_3$ and YBCO films have a columnar rostructure. It is interesting to note that the average grain size of YBCO is htly larger than that of $KNbO_3$. We surmise that the smaller lattice mismatch veen YBCO and $KNbO_3$ (less than 4%) compared to that between $KNbO_3$ and) (less than 5%), and a higher YBCO deposition temperature (700°C) compared hat of $KNbO_3$ (600 °C) result in a larger YBCO grain size. The YBCO grains w a highly preferred c-axis orientation and are slightly misoriented with ect to each other. The orientations of the YBCO grains are strongly influenced he surface roughness of the $KNbO_3$ film. The YBCO surface is considerably gher than that of the $KNbO_3$.

Figure 5(b) shows a high resolution image at the YBCO/$KNbO_3$ interface. interdiffusion layer is observed at the interface. We are not able to identify the se of this interfacial layer at present. This interdiffusion layer maintains an axial relationship with respect to YBCO and $KNbO_3$. Further, this rostructure suggests that the YBCO lattices are destroyed in a layer-by-layer ion along c-axis, the YBCO/$KNbO_3$ interface as marked by the solid line. The kness of the interdiffusion layer is not uniform and seems to be determined by orientation of the contact interface between YBCO and $KNbO_3$. The thickness he interdiffusion layer decreases with the increased deviation of the contact rface away from the $KNbO_3$ 100 plane.

.b. $KNbO_3$ on MgO/Si

Highly oriented (100) $KNbO_3$ films were deposited on MgO/Si employed our omated ion beam sputter-deposition technique [4]. The microstructure of the)/Si has been briefly discussed in section III.2.a. The plan view SAD pattern . 6(a)] confirms that the $KNbO_3$ on MgO/Si is highly oriented. Circum-ntially elongated $KNbO_3$ reflections in Figure 6(a) suggest that tilt and twist tionships are present among $KNbO_3$ grains. We conclude that the quality of) films affects that of $KNbO_3$ films, because epitaxial $KNbO_3$ films with a very ll amount of twist and tilt (less than 1°) can be deposited on single crystal MgO. misorientation of the $KNbO_3$ grains is smaller than that of the MgO grains, use the degree of spread of the 200 reflections of MgO is larger than that of bO_3. We surmise that the larger misorientation of the MgO is due to its ller grain size compared to that of the $KNbO_3$. The cross sectional image and orresponding SAD pattern of the multilayer structure [Fig. 6(b)] show that the rage grain size of $KNbO_3$ is larger than that of MgO. It is believed that the tively small lattice mismatch (5 %) between [100] MgO and [100] $KNbO_3$, and higher ratio of deposition temperature to melting temperature result in a er $KNbO_3$ grain size.

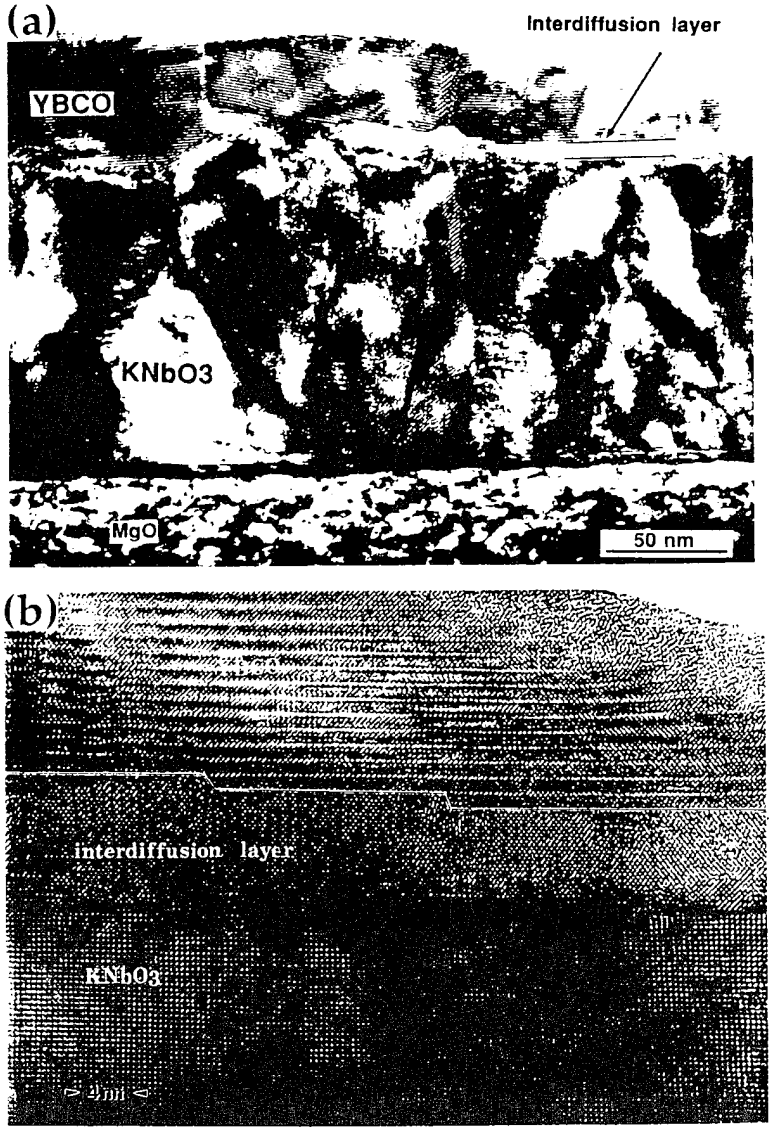

Figure 5 (a) A low magnification image of (001) YBCO on (100) $KNbO_3$/(100) MgO. (b) A high resolution image of the YBCO/$KNbO_3$ interface.

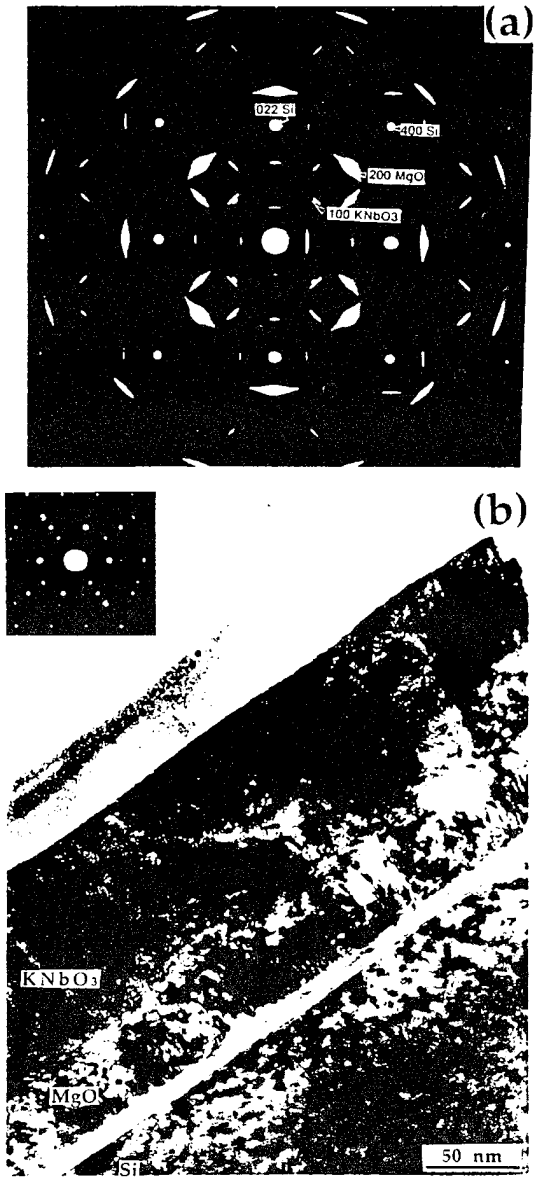

igure 6 (a) A plan view SAD pattern confirming the highly oriented $KNbO_3$ on fgO/Si. (b) The cross sectional image and its corresponding SAD pattern of the ıultilayer structure.

IV. CONCLUSIONS

Microstructural characterization provides us with the means to improve processes for fabricating better materials and to explore the causes of material behavior. Integration of epitaxial ferroelectric films with a variety of substrates is the primary thrust of this research. We have shown that a variety of epitaxial films can be produced, including (111) PMN on (111) $SrTiO_3$, (100) Pt on (100) MgO, (111) Pt on (0001) Al_2O_3, (100) MgO on (100) Si, (100) $KNbO_3$ on (100) Pt/(100) MgO, (001) YBCO on (100) $KNbO_3$/(100) MgO, and (100) $KNbO_3$ on (100) MgO/(100) Si.

ACKNOWLEDGEMENTS

This research is supported by the Office of Naval Research under contract N00014-88-K-0526, the National Science Foundation under contract DMR 88-07367, and the Defense Advance Research Project Agency under contract N00014-88-K-0525. The authors would like to extend gratitude to Dr. S. Swartz for providing the PMN films for microstructural characterization and would like to thank Dr. K. Christensen, H. N. Al-Shareef, K. D. Gifford and Dr. P. D. Hren for technical assistance.

REFERENCES

1. T.M. Graettinger, S.H. Rou, M.S. Ameen, O. Auciello, and A.I. Kingon, Appl. Phys. Lett. 58(18), p 1964, (1991).
2. H. Adachi and K. Wasa, Mat. Res. Soc. Symp. Proc. Vol 200, p. 103, (1990).
3. L.H. Parker, A.F. Tasch, IEEE Circuits and Devices Mag., p. 17, Jan 1990.
4. A.I. Kingon, O. Auciello, M.S. Auciello, M.S. Ameen, S.H. Rou, and A.R. Krauss, Appl. Phys. Lett., 55, p. 301, (1989).
5. V.E. Wood, J.R. Busch, S.D. Ramamurthi, and S.L. Swartz, J. Appl. Phys., in press, May 1, 1992.
6. M.S. Abrahams and C.J. Buiocchi, J. Appl. Phys., 45, p 3315, (1947).
7. S.H. Rou, P.D. Hren, and A.I. Kingon, Mat. Res. Soc. Symp. Proc., Vol. 199, p. 225, (1990).
8. Private communication with Dr. Kim Christensen.
9. C.C. Hsueh, M.L. Mecartney, Mat. Res. Soc. Symp. Proc., Vol. 200, p. 219, (1990).
10. J.W. Mattews, "Epitaxial Growth", Academic Press, (1975).
11. G. Yi and M. Sayer, Ceramic Bulletin, Vol. 70(9), p. 1173, (1991).
12. S.H. Rou, A.I. Kingon, and S. Schwartz, J. of Mat. Res., to be submitted.
13. A.I. Kingon, S.H. Rou, M.S. Ameen, T.M. Graettinger, K.D. Gifford, and O. Auciello, Ceramic Transaction, Vol. 14, p. 179, (1990).
14. S.H. Rou, Ph.D. dissertation, (1990).
15. P.D. Hren, S.H. Rou, O. Auciello, and A.I. Kingon, Ferroelectrics, in press.
16. A.F. Chow, S.H. Rou, D.J. Lichtenwalner, O. Auciello, and A.I. Kingon, to be presented at MRS spring 1992, "Mechanisms of Heteroepitaxial Growth".
17. A.I. Kingon, M.S. Ameen, O.H. Auciello, K.D. Gifford, H. Al-Shreef, T.M. Graettinger, S.H. Rou, P.D. Hren, Ferroelectrics, Vol. 116, p. 35, (1991).
18. D.J. Lichtenwalner, R.R. Woolcott, C.N. Soble, O. Auciello, and A.I. Kingon, J. Appl. Phys., 70, 1 (1991).

Appendix 10

"Ion-Beam Reactive Sputter Deposition of MgO Thin Films on Silicon and Sapphire Substrates," Alice F. Chow, Shang Hsieh Rou, Daniel J. Lichtenwalner, Orlando Auciello, and Angus I. Kingon, MRS Symposium Proceedings **268** (Materials Modification by Energetic Atoms and Ions), 253-258, 1992.

ION-BEAM REACTIVE SPUTTER DEPOSITION OF MgO THIN FILMS ON SILICON AND SAPPHIRE SUBSTRATES

ALICE F. CHOW, SHANG HSIEH ROU, DANIEL J. LICHTENWALNER, ORLANDO AUCIELLO*, and ANGUS I. KINGON, NORTH CAROLINA STATE UNIVERSITY, RALEIGH, NC; *also MICROELECTRONICS CENTER OF NORTH CAROLINA, RESEARCH TRIANGLE PARK, NC

ABSTRACT

MgO thin films were deposited on silicon and sapphire substrates using ion-beam reactive sputtering. Films have been analyzed using x-ray diffraction, transmission electron microscopy, and atomic force microscopy. Highly oriented (100) MgO films have been obtained on Si (100) substrates. The in-plane orientation is predominantly [100]MgO//[100]Si, although a twist of up to $\pm 10°$ between grains is observed. Epitaxial films of MgO were deposited on four different orientations of sapphire. The MgO film orientation was (111) on c-cut (0001) Al_2O_3 and exhibited double positioning boundaries in TEM analysis. On r-cut $(1\bar{1}02)$ Al_2O_3 , the MgO appeared to be oriented (730) with tilt and twist of $\pm 2°$ between the grains. Epitaxial MgO films oriented (110) and (111) were obtained on m-cut $(10\bar{1}0)$ and a-cut $(11\bar{2}0)$ sapphire orientations, respectively. In-plane directions were extracted from TEM analysis on all the samples. Atomic force microscopy revealed fairly smooth MgO films on sapphire, varying from 0.35 nm average roughness for the MgO film on the m-cut substrate to 0.80 nm on the r-cut substrate.

I. INTRODUCTION

The integration of novel superconducting, electro-optic, and ferroelectric thin film devices with existing semiconductor processing technology requires the deposition of thin films of $YBa_2Cu_3O_{7-x}$ (YBCO), $Pb(Zr_xTi_{1-x})O_3$ (PZT), or $KNbO_3$ on substrates such as silicon and sapphire. Silicon is ubiquitously used and its processing technology is well understood. Sapphire exhibits many desired attributes for microwave applications, such as low loss and low dielectric constant, large substrate availability at low cost, and good mechanical strength [1].

While the scientific importance of YBCO, PZT, and $KNbO_3$ on silicon or sapphire is evident, processing difficulties have hindered progress in this area. Buffer layers must be introduced to prevent interfacial reactions and diffusion between layers. For many applications, potential buffer layers must be epitaxially deposited on the substrate and be a good host lattice for the overlayer, as well as be chemically inert with respect to the substrate and overlayers. A few candidates for buffer layers are YSZ and CeO_2 [2]. Here we have chosen MgO because it has a low dielectric constant, good thermodynamic stability, chemical compatiblity with many materials, and provides an acceptable lattice match for the multicomponent oxide films mentioned above.

The properties of YBCO, $KNbO_3$, and PZT are known to be dependent on crystal orientation. For instance, c-axis YBCO results in the optimal J_c and T_c values, and thus a (100) oriented epitaxial MgO underlayer is desired for deposition of c-axis YBCO films. The electro-optic properties of $KNbO_3$ thin films and the ferroelectric properties of PZT thin films as a function of crystal orientation have not been thoroughly studied. Our goals in this work are two-fold: 1) to obtain epitaxial MgO films on silicon and sapphire substrates; and 2) to achieve various orientations of MgO films to enable further study of $KNbO_3$ and PZT properties as a function of film orientation.

II. EXPERIMENT

Ion-beam reactive sputtering was used to deposit the MgO films examined in this study. The deposition system has been described in detail elsewhere [3]. Briefly, the system is pumped using a 330 l/s turbomolecular pump, attaining a background pressure in the mid 10^{-7} Torr range. A 3-cm diameter Kaufman-type ion source is used to sputter a 12.5 cm diameter magnesium metal target. A 500eV, 20mA Xe^+ ion beam was used, with O_2 gas added to the chamber

Mat. Res. Soc. Symp. Proc. Vol. 268. ©1992 Materials Research Society

serving as the reactive species. Substrates were mounted to a radiatively heated substrate block using silver paste. Substrate thermocouple temperatures were calibrated using an optical pyrometer to measure a Si substrate, and comparing it to the melting point of an Al bead mounted nearby.

Acetone, methanol, and deionized water were used for cleaning both silicon and sapphire substrates. Because silicon readily oxidizes and the amorphous silicon oxide may disrupt the epitaxial correlation of silicon with the arriving film atoms, passivation of the surface is required. A buffered hydrogen flouride (BOE) dip etch was used to achieve a hydrogen terminated silicon surface [4].

After the substrates were mounted, heated to the desired temperature at approximately 10°C/minute, and chamber pressure minimized, the magnesium target was presputtered while the substrates were shuttered. While the sapphire substrates are insensitive to an oxygen environment, silicon must be especially guarded from an oxygen background to prevent silicon oxide formation. Therefore, for deposition on silicon, the magnesium was presputtered with no oxygen added. After opening the shutter and depositing ~10Å of material, 0.5 sccm of oxygen flow (1.2×10^{-4} Torr) was initiated, resulting in reactive sputtering of MgO. A substrate temperature of 500°C was used. For sapphire, a steady oxygen pressure was established before the run. An oxygen flow of 0.5 sccm was also used, and substrate temperatures ranged from 500-700°C. The establishment of 0.5 sccm oxygen flow resulted from an earlier oxygen flow/deposition rate calibration to determine minimum oxygen flow required to have a magnesium oxide (reacted) target surface. Minimum oxygen flow was demanded due to the possibility of obstruction of oriented growth by the presence of too much oxygen [5].

X-ray diffraction (XRD), transmission electron microscopy (TEM), and atomic force microscopy (AFM) were performed to characterize our samples. This provides a complete analysis of film orientation, microstructure, and surface morphology.

III. RESULTS and DISCUSSION

X-ray diffraction was performed on all samples. The XRD results show oriented MgO(100) on Si(100), MgO(111) on Al_2O_3(0001), MgO(110) on $Al_2O_3(10\bar{1}0)$, and MgO(111) on $Al_2O_3(11\bar{2}0)$. These XRD patterns are shown in Fig. 1. The XRD results, although indicating oriented film growth, are not sufficient to confirm epitaxy. No MgO peaks were observed for films deposited on $(1\bar{1}02)$ Al_2O_3.

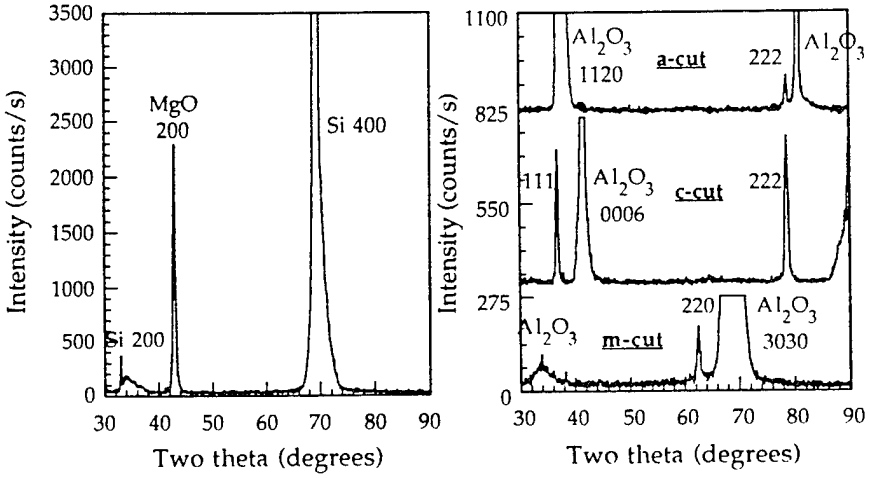

Fig. 1. X-ray diffraction patterns of MgO on silicon, and on a-cut, c-cut, and m-cut sapphire.

The MgO films on Si were further examined using both plan-view and cross-sectional TEM. A plan view micrograph and electron diffraction pattern are shown in Fig. 2. A large selected area aperture size was used to obtain the electron diffraction patterns from a reasonably large area. The diffraction pattern indicates that the (001) MgO in-plane orientation lies parallel to the (001)Si, although twisted up to ±10° about the substrate normal. The twist is large enough to produce distinct grain boundaries in the MgO film. The grain size is about 300Å, as seen in the TEM micrograph (Fig. 2). These highly oriented MgO films would serve as suitable buffer layers for PZT films used as nonvolatile memories. Cross-sectional TEM has revealed that a thin (<15Å) amorphous layer is present at the MgO/Si interface. It has not been determined whether this layer forms before, during, or after deposition. Because of the non-UHV conditions of the deposition chamber, it is possible that an oxide formed prior to deposition. The presence of a thin amorphous region on the substrate initially could explain the lack of complete epitaxy for the MgO film. Improving the Si passivation procedure may remedy this occurrence [6].

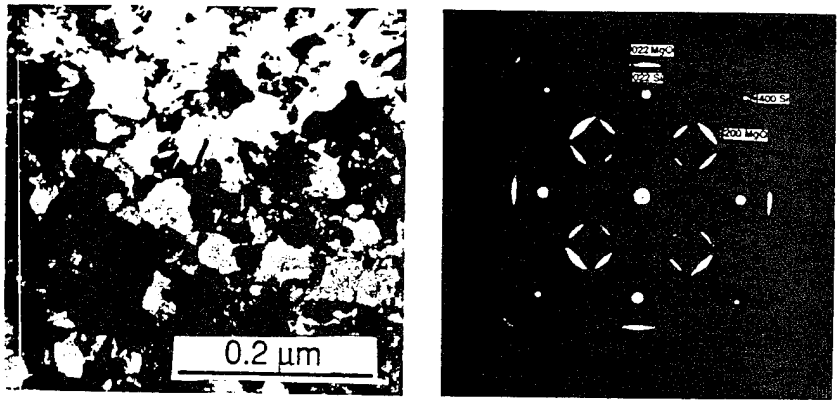

Fig. 2. Plan view micrograph and electron diffraction pattern of MgO film on (100) silicon.

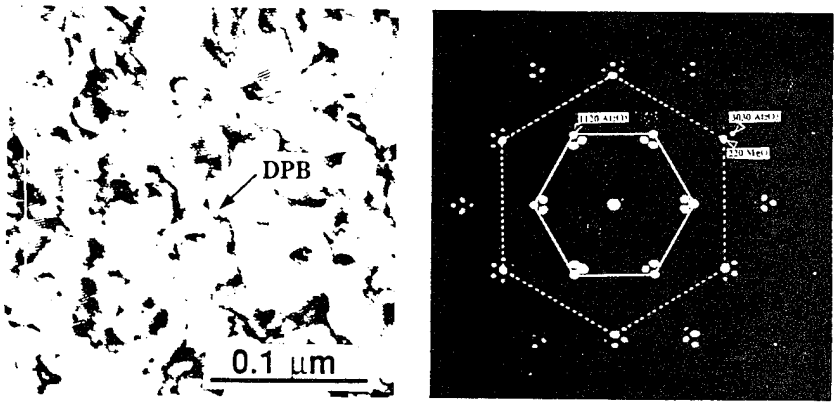

Fig. 3. Plan view micrograph and electron diffraction pattern of MgO on c-cut sapphire. The bou ndaries observed in the micrograph are double positioning boundaries.

All MgO films on sapphire exhibited epitaxial growth as revealed by the plan-view electron diffraction patterns. The MgO on c-cut $(0001)Al_2O_3$ contained double positioning boundaries as shown by the micrograph in Fig. 3. Two energetically equivalent sets of nucleation sites are present, thus the arriving atoms have a choice of adsorption sites resulting in grains separated by partial dislocation-like boundaries, or double positioning boundaries ($^1/_6[\bar{2}11]$ lattice shifts). The electron diffraction pattern shows the in-plane epitaxial alignment $[01\bar{1}]MgO//[10\bar{1}0]Al_2O_3$ and $[\bar{2}11]MgO//[\bar{1}2\bar{1}0]Al_2O_3$.

The r-cut $(1\bar{1}02)Al_2O_3$ sample revealed tilt and twists of $\pm 2°$ between the grains shown in Fig. 4. Low angle boundaries and dislocations were also identified. The electron diffraction pattern showed (100)MgO plane matching with $(2\bar{2}01)Al_2O_3$. (The diffraction pattern shown was obtained by tilting the sample 23° from the r-plane, resulting in an epitaxial (100)MgO pattern.) When the sample was not tilted, only one direction of the MgO diffraction spots was detected aligning with the $[11\bar{2}0]Al_2O_3$ while the diffraction spots in the other in-plane direction were not visible, therefore a crystal orientation could not be deterined. It was deduced from the electron diffraction pattern that a high index (730)MgO plane matched with r-cut $(1\bar{1}02)Al_2O_3$. The in-plane orientations were $[\bar{3}70]MgO//[\bar{1}101]Al_2O_3$ and $[001]MgO//[11\bar{2}0]Al_2O_3$.

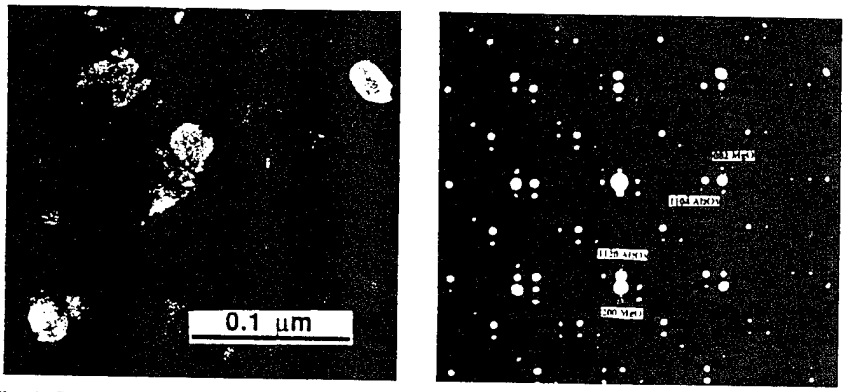

Fig. 4. Plan view micrograph and electron diffraction pattern of MgO on r-cut sapphire. The MgO is epitaxial with tilt and twists of ±2° between the grains.

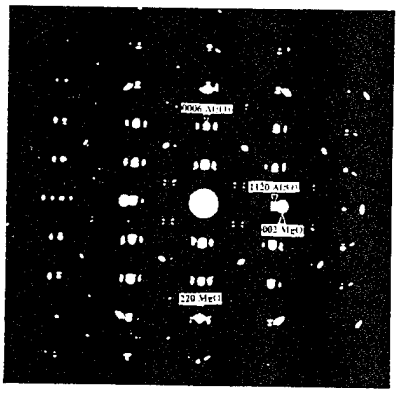

Fig. 5. Electron diffraction pattern of MgO on m-cut sapphire.

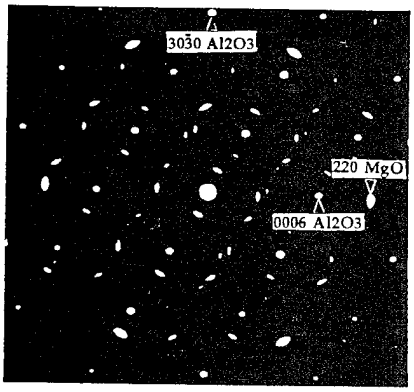

Fig. 6. Electron diffraction pattern of MgO on a-cut sapphire.

The microstructure of the MgO(110) on m-cut $(10\bar{1}0)Al_2O_3$ consists of low angle grain boundaries, tilt and twists of $\pm 3°$ between the grains, and dislocations due to the lattice mismatch. The electron diffraction pattern in Fig. 5 reveals in-plane orientations of $[001]MgO//[1\bar{2}10]Al_2O_3$ and $[\bar{1}10]MgO//[0001]Al_2O_3$.

TEM analysis of the MgO(111) on a-cut $(11\bar{2}0)Al_2O_3$ revealed a microstructure also of low angle grain boundaries with tilt and twists of $\pm 3°$ between the grains. The in-plane orientations are $[01\bar{1}]MgO//[000\bar{1}]Al_2O_3$ and $[\bar{2}11]MgO//[\bar{1}100]Al_2O_3$ as determined by the electron diffraction pattern in Fig. 6.

The orientations of our MgO on sapphire match those reported by Talvacchio et al. [7], except for the MgO orientation on r-cut sapphire; they achieved MgO(100) on r-cut sapphire as determined by XRD and RHEED analysis. However, their film processing included post deposition annealing, while our films were deposited in situ, and they did not perform microstructural characterization on their MgO films.

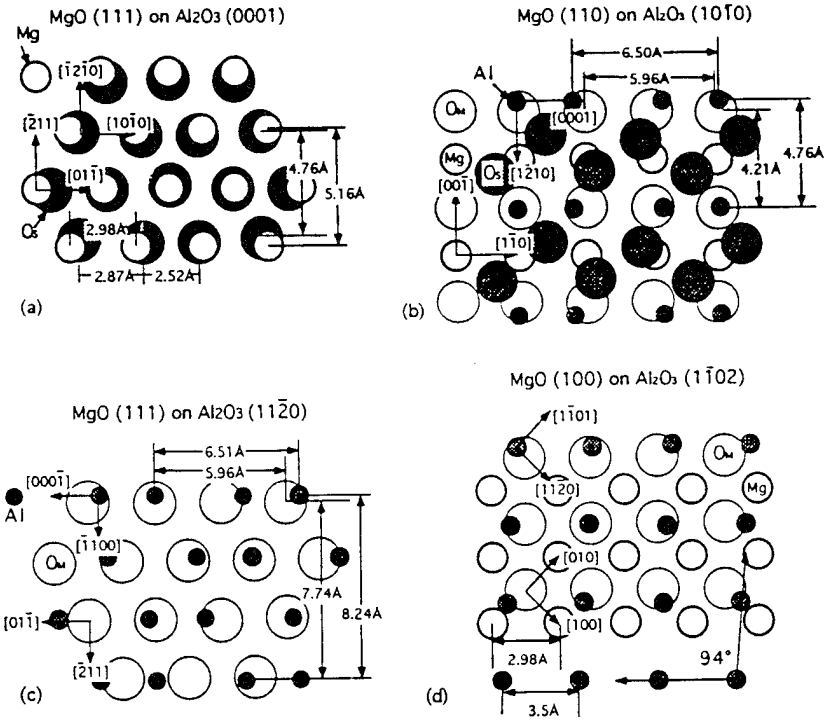

Fig. 7. Planar views of atomic orientations of MgO on various orientations of Al_2O_3 as suggested from TEM electron diffraction patterns. These are shown for the purpose of visualizing lattice match and symmetry, not to imply the actual atomic positions of the Mg and O atoms bonded to sapphire; O_S=Oxygen atom of sapphire, O_M=Oxygen atom of MgO.

Lattice matching diagrams were constructed to reveal the epitaxial relationships between the MgO and sapphire. The lattice mismatch between first neighbor atom-atom lengths was between 6-12%. Although this is an appreciable amount of mismatch, the epitaxial growth of the MgO and the symmetry correlation of the MgO with Al_2O_3 suggest that structural symmetry is a more important factor here in determining orientation than simply lattice mismatch. For the c-cut and a-cut sapphire, the surface comprised planes of either all aluminum or all oxygen as depicted in Figs. 7(a) and 7(c) which would explain the matching of the close-packed (111)MgO plane which also contains all oxygen or magnesium atoms. Whereas, in the case of m-cut and r-cut, the surface consisted of a mixture of aluminum and oxygen atoms seen in Fig.7(b) and 7(d). For the MgO on r-cut sapphire schematic, although the oxygen atoms of the MgO match symmetrically reasonably well with the array of the Al atoms in the r-plane (although with 15% mismatch), the Al atoms are arranged in a distorted array, having a 94° angle between atoms. This distorted Al array, plus the large lattice mismatch, is expected to be the cause of the MgO being tilted away from the (100) orientation in our films, as well as for those reported by Berezin et al. [5].

Atomic force microscopy (AFM) revealed smooth texture for the MgO films on sapphire. The MgO film deposited at 700°C on m-cut $(10\bar{1}0)Al_2O_3$ measured over 1000 nm distance displayed an average surface roughness, R_a, of 0.35 nm. Also deposited at 700°C, the film on c-cut $(0001)Al_2O_3$ displayed an R_a of 0.53 nm. For the MgO on r-cut $(1\bar{1}02)Al_2O_3$, the film was a bit rougher with the R_a= 0.80 nm. That particular sample was deposited at 500°C which may have contributed to producing a rougher surface, along with the film growth orientation.

V. CONCLUSIONS

Highly oriented MgO(100) films on Si(100) and epitaxial MgO films on Al_2O_3 were deposited using ion-beam reactive sputtering. The orientation and microstructure of the MgO films on Al_2O_3 are controlled by the Al_2O_3 orientation. Analysis of the surface smoothness using AFM revealed that the MgO films on Al_2O_3 have average roughness of ~5Å, which is extremely smooth.

Consequently, results on silicon may be improved by producing better surface passivation. Effects of temperature and oxygen pressure variations on the orientation of MgO should be explored. Growth conditions and sapphire orientations resulting in (100)MgO on Al_2O_3 need to be addressed further. Large area substrate deposition and overlayer deposition of YBCO, PZT, and $KNbO_3$, along with studies of orientation-dependent properties will be attempted as well.

V. ACKNOWLEDGEMENTS

We acknowledge support from the Office of Naval Research under contract N00014-91-J-1307 and from the National Science Foundation under grant DMR-88-07367.

VI. REFERENCES

1. X.D. Wu, R.E. Muenchausen, N.S. Nogar, A. Pique, R. Edwards, B. Wilkens, T.S. Ravi, D.M. Hwang, and C.Y. Chen, Appl. Phys. Lett 58, 304 1991).
2. T. Inoue, T. Ohsuna, L. Luo, X.D. Wu, C.J. Maggiore, Y. Yamamoto, Y. Sakurai, and J.H. Chang, Appl. Phys. Lett. 59, 3604 (1991).
3. D.J. Lichtenwalner, O. Auciello, R.R. Woolcott Jr., C.N. Soble II, to be published in J. Vac. Sci. Tech. A 10, July/Aug. (1992).
4. G.S. Higashi, R.S. Becker, Y.J. Chabal, and A.J. Becker, Appl. Phys. Lett. 58, 15 (1991).
5. A.B. Berezin, C.W. Yuan, A.L. de Lozanne, S.M. Garrison, and R.W. Barton, IEEE Trans. Magnetics 27, 970 (1991).
6. D.B. Fenner, D.K. Biegelsen, and R.D. Bringans, J. Appl. Phys. 66, 419 (1989).
7. J. Talvacchio, G.R. Wagner, and H.C. Pohl, Physica C 162-164, 659-60 (1989).

Appendix 11

"Optical Characterization of Potassium Niobate Thin Film Planar Waveguides," Thomas M. Graettinger and Angus I. Kingon, MRS Symposium Proceedings **243** (Ferroelectric Thin Films II), 557-563, 1992.

OPTICAL CHARACTERIZATION OF POTASSIUM NIOBATE THIN FILM PLANAR WAVEGUIDES

THOMAS M. GRAETTINGER AND A. I. KINGON
North Carolina State University
Dept. of Materials Science and Engineering
Raleigh, NC 27695-7919

ABSTRACT

Initial results of the waveguiding properties of $KNbO_3$ thin films are presented. The refractive indices of epitaxial films deposited on single crystal magnesium oxide substrates have been measured. Additionally, these films have been used as the basis for modelling a potassium niobate thin film phase modulator. Results of the model are compared with existing technology.

INTRODUCTION

Ferroelectric materials possess great potential for use in integrated optics due to their strong electro-optic and non-linear optical effects. Thin film fabrication methods for these materials are currently the subject of much study. High quality, transparent, low loss films must be grown for application into device structures. An important parameter in determining the quality of ferroelectric thin films is the refractive index which can be measured using several techniques including the prism coupling method. Lower than bulk values of refractive index often indicate porous, off-stoichiometry, or poor quality thin films unsuitable for devices.

Of the materials being considered for use in integrated optic switching devices, potassium niobate ranks very highly due to its very strong electro-optic effect and moderate dielectric susceptibilities. This ferroelectric has been difficult to grow in bulk crystalline form, but thin films have recently been deposited making it attractive for the integrated optic applications.

EXPERIMENTAL PROCEDURE

Potassium niobate thin films were prepared by an ion beam sputtering technique described previously.[1] Sequential deposition of very thin layers of potassium oxide and niobium oxide from potassium superoxide pressed powder and niobium metal targets resulted in the formation of the desired perovskite phase. Film composition and thickness were determined from Rutherford Backscattering (RBS) spectra. The single phase nature of the films was determined from X-ray Diffractometer (XRD) scans of the films and Selected Area Diffraction (SAD) patterns from transmission electron microscope (TEM) specimens.

Optical guided waves were launched into the thin films using a symmetrical rutile prism coupler [2] with a base angle of 60° and refractive index of 2.8659. The prism and film were clamped together to achieve a good coupling spot and the clamped assembly was mounted on a goniometer. A helium-neon laser (λ = 632.8 nm) was focused on the coupling spot at the prism-film interface. The light was polarized in order to launch only TE modes in the films. A schematic of the system is shown in figure 1. The reflected beam from the prism coupler was detected with a silicon photodiode and its signal monitored with a chart recorder. The prism coupling assembly was rotated until a sharp decrease in the reflected beam intensity was detected signaling the launching of a guided mode. The coupling angle relative to normal incidence of the input beam on the entrance face of the prism was measured. A computer was used to perform the iterative calculation necessary to determine the refractive index of the film from the coupling angle and the film thickness.[3]

Mat. Res. Soc. Symp. Proc. Vol. 243. © 1992 Materials Research Society

$KNbO_3$ Phase Modulator Model

To demonstrate the utility of the ion beam sputter-deposited potassium niobate thin films, a waveguide electro-optic modulator based on the thin films was modeled. High quality films of $KNbO_3$ have been deposited on single crystal magnesium oxide (001). These films have been grown heteroepitaxially on the MgO surface with $\mathbf{P_S}$ of the orthorhombic $KNbO_3$ oriented in the plane of the film. These films will serve as the basis for the electro-optic phase modulator model. There are four equivalent directions for $\mathbf{P_S}$ in the plane of the film, but, for the purposes of this model, a film whose polarization vectors all point in a single direction will be considered. The results of the model will then be compared to existing technology.

The optical indicatrix for $KNbO_3$, a biaxial material, can be written as[4]

$$B_1x_1^2 + B_2x_2^2 + B_3x_3^2 + 2B_4x_2x_3 + 2B_5x_1x_3 + 2B_6x_1x_2 = 1 \qquad (1)$$

where $B_i = 1/n_i^2$, and the subscripts use contracted indices. Deformation of the optical indicatrix occurs as a result of the electro-optic effect when an electric field is applied to the crystal. Potassium niobate belongs to the crystal class mm2, so the deformation of the indicatrix obeys the relation

$$(B_1 + r_{13}E_3)x_1^2 + (B_2 + r_{23}E_3)x_2^2 + (B_3 + r_{33}E_3)x_3^2 + 2r_{42}E_2x_2x_3 + 2r_{51}E_1x_1x_3 = 1 \qquad (2)$$

For the use of the $KNbO_3$ films discussed above in guided-wave devices, light must propagate in the 1-3 plane. The guided wave may be polarized either TE (in the 1-3 plane) or TM (normal to the 1-3 plane) in a single mode waveguide. Thus, for these thin films the fourth term in Eq. (2) is of no consequence since light can not be polarized in the 4 direction.

For a field applied along x_3, Eq. (2) reduces to

$$(B_1 + r_{13}E_3)x_1^2 + (B_2 + r_{23}E_3)x_2^2 + (B_3 + r_{33}E_3)x_3^2 = 1 \qquad (3a)$$

while for a field applied along x_1, Eq. (2) becomes

$$B_1x_1^2 + B_2x_2^2 + B_3x_3^2 + 2r_{51}E_1x_1x_3 = 1. \qquad (3b)$$

Of the linear electro-optic coefficients appearing in Eqs. (3a) and (3b), r_{51} is the largest for $KNbO_3$, 105 x10^{-12} m/V.[5] Utilization of this strong effect requires that a TE guided mode propagating in the 5 direction (the shear direction between the x_1 and x_3 axes) in the crystal be used. The geometry of the proposed device is shown in Fig. 5.

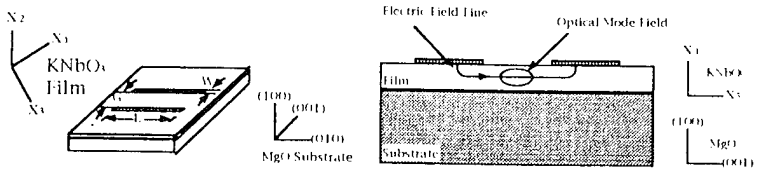

Fig. 5. Geometry of the proposed $KNbO_3$ electro-optic modulator.

The total phase shift for a TE mode propagating a distance L along the 5 direction in the film is $\Delta\beta L = 2\pi L(\Delta n_5)/\lambda$. From Eq. (3b), Δn_5 can be found to be

$$\Delta n_5 = -\tfrac{1}{2}n_5^3 r_{51}E_1 \qquad (4)$$

To determine the applied electric field, E must be determined for the electrode geometry shown in Fig. 7-1(b). The electrode geometry shown, where the horizontal field is used for modulation, has been studied in depth by several researchers[6,7,8,9], with the result that E_1 in Eq.(4) can be replaced by $\Gamma V/\sqrt{2}\,G$ where V is the applied voltage, G is the gap between the strip electrodes and Γ represents the overlap integral between the electrical and optical fields. The expression is modified by $1/\sqrt{2}$ to determine the component of the total field in the x_1 direction. The overlap integral can be calculated from

$$\Gamma = \left(\frac{G}{V}\right)\iint E|E'|^2\,\partial A \qquad (5)$$

where E is the applied electric field and E' is the normalized optical field distribution. Using Eqs. (4) and (5), the total phase shift can be written as

$$\Delta\beta L = -\frac{\pi}{\sqrt{2}}n_5^3 r_{51}\Gamma(V/G)(L/\lambda) \qquad (6)$$

Device length and modulation voltage are two critical parameters in device design. For device optimization the product VL should be minimized. Equation (6) can be rewritten to identify the relationship between the other device parameters and the VL product. The result, using π as the desired phase shift for the modulator, is

$$VL = \frac{\sqrt{2}\lambda G}{n_5^3 r_{51}\Gamma} \qquad (7)$$

For minimization of VL, (G/ Γ) must be minimized. However, Γ is a function of G and the optical mode size. Alferness[6] and Marcuse[7] have graphically presented this relationship for use in device design.

Before choosing actual device dimensions, modulation bandwidth must be considered. The modulation bandwidth when determined from the lumped electrode parameters is dependent on the electrode design and the dielectric constant of the thin film. The bandwidth is determined from $\Delta f = 1/\pi RC$ where R is the impedance of the device, typically 50 Ω (matched to the driving circuit), and C is the capacitance of the strip electrodes. For symmetric strip electrodes as shown in Fig. 5, the capacitance per unit length is[6,10]

$$\frac{C}{L} = \varepsilon_{eff}\frac{K'(r_s)}{K(r_s)} \qquad (8)$$

where $r_S = (2W/G+1)^{-1}$ and $\varepsilon_{eff} = (\varepsilon_0/2)(1+\varepsilon_S)$ is the RF dielectric constant. For $KNbO_3$ in the geometry considered here, $\varepsilon_S = \varepsilon_5 = 74$. K is the complete elliptic integral of the first kind and $K'(r_S) = K[(1-r_S^2)^{1/2}]$. Alferness[6] has graphically determined C/L and $\Delta f \cdot L$ vs. G/W for $LiNbO_3$ and the results can be scaled appropriately for $KNbO_3$.

Modulation bandwidth can also be limited by the inverse of the optical or electrical transit times. Normally, the bandwidth is limited by the electrodes and is determined as above. The bandwidth is therefore dependent on G/W, increasing as the ratio of G/W increases. However, from Eq. (7) it can be seen that a small electrode gap is required to minimize the VL product.

Therefore, to maximize the modulation bandwidth requires a small electrode width. The electrical transit time cutoff frequency places a practical limit on the electrode gap to width ratio. Calculated as

$$f_t = \frac{c}{\pi\left(\varepsilon_{eff} L\right)^{1/2}} \tag{9}$$

the cutoff frequency for $KNbO_3$ is 1.5 GHz•cm and 2.2 GHz•cm for $LiNbO_3$. There is thus no advantage for G/W > 3 for a $KNbO_3$ device.

The ratio of drive voltage to modulation bandwidth can be used as a figure of merit in evaluating device design. Using Eqs. (7) and (8) presented above, the ratio is

$$V/\Delta f = \sqrt{2}\pi R\lambda\left(1/n_5^3 r_{51}\right)\left(G/\Gamma\right)\left(G/L\right) \tag{10}$$

Table 1 summarizes the device geometry and operation parameters for optimized modulators based on potassium niobate thin films and X-cut, Y-propagating titanium-diffused lithium niobate waveguides. Based upon the drive voltage to modulation bandwidth ratio and the VL product, the potassium niobate based modulator compares favorably with the lithium niobate modulator. The potassium niobate modulator uses a much larger electro-optic coefficient than the lithium niobate modulator, but the advantage gained is partially offset by the larger dielectric constant of $KNbO_3$ for the geometry considered. Based on the drive voltage to modulation bandwidth ratio, the theoretical potassium niobate modulator represents an 80% improvement over the lithium niobate modulator.

Table 1. Comparison of optimized phase modulators.

	$KNbO_3$ Thin Film	Ti-diffused $LiNbO_3$
Electro-optic Coefficient	$r_{51} = 105\times10^{-12}$ m/V	$r_{33} = 30.8\times10^{-12}$ m/V
RF Dielectric Constant, ε_S	74	35
Electrode Gap, G, (mm)	2	1
Electrode Width, W, (mm)	1	2
Wavelength, λ, (nm)	633	633
Overlap Integral, Γ	0.7	0.3
V•L Product, (V•mm)	2.2	6.4
Electrical Cutoff Freq., f_t, (GHz•cm)	1.5	2.2
RC Bandwidth•Length, Δf_{RC}•L, (GHz•cm)	1.4	2.1
$(V/\Delta f)_{min}$, (V/GHz)	0.2	0.5

Very high quality lithium niobate devices are currently being produced. However, a large market for these devices has yet to develop. One of the principle reasons for the small market is the difficulty in integrating these devices with thin film optoelectronic technology. It is in this area that thin films such as potassium niobate can excel. Several very important materials issues need to be addressed before the thin films can take the place of the bulk single crystal devices, however. High optical losses continue to plague thin film waveguides. These losses, primarily due to scattering, must be decreased to acceptable levels based upon the device being considered. In addition, for best use of the thin film materials, they must be grown on silicon or gallium arsenide. Due to the high indices of refraction of Si and GaAs, low index (<2) buffer layers must first be grown on the substrates before the electro-optic material. These buffer layers must possess a lattice suitable to match both the substrate and the electro-optic material. Work is currently in progress at North Carolina State University to grow such materials.

SUMMARY

The refractive indices of epitaxial potassium niobate (001) thin films deposited on single crystal magnesium oxide (001) have been measured using a prism coupler. The films were fabricated using an ion beam sputter-deposition system and their compositions determined from Rutherford Backscattering spectra. The thickness of the films was in the range of 2000 to 2500Å so the films supported only one TE mode. Smooth, transparent films that were slightly potassium deficient had a refractive index of 2.28. This result falls within the expected range of 2.279 to 2.329 for bulk single crystal $KNbO_3$ with the same orientation as the films.

A model of an electro-optic phase modulator was developed which optimizes the drive voltage and modulation bandwidth of the device. The model was based on the epitaxial $KNbO_3$ films grown on MgO (001) using the ion beam sputter-deposition technique. The characteristics of the optimized device demonstrate the potential of $KNbO_3$ films to surpass bulk single crystal $LiNbO_3$, which is currently the material of choice for guided-wave integrated optics devices.

ACKNOWLEDGEMENTS

The authors would like to acknowledge the support of the Office of Naval Research for its support of this research program, Dr. O. Auciello, Dr. K. J. Bachmann, and Dr. S. H. Rou for useful discussions contributing to this work, and the National Defense Science and Engineering Graduate Fellowship program for their support of T. M. Graettinger.

[1] A. I. Kingon, S. H. Rou, M. S. Ameen, T. M. Graettinger, K. Gifford, O. Auciello, and A. R. Krauss, in *Ceramic Transactions*, vol. 14: Electrooptics and Non-Linear Optic Materials, edited by A. S. Bhalla, E. M. Vogel, and K. M. Nair (American Ceramic Society, Westerville, Ohio, 1990), pp. 179-196.

[2] P. K. Tien and R. Ulrich, J. Opt. Soc. Am. 60(10), 1325-1337 (1970).

[3] R. Ulrich and R. Torge, Applied Optics 12(12), 2901-2908 (1973).

[4] I. P. Kaminow, An Introduction to Electrooptic Devices, (Academic Press, New York, 1974), p. 25.

[5] Landolt-Bornstein, New Series, Group III (Springer, New York, 1981), Vol. 16, pt. A.

[6] R. C. Alferness, IEEE Trans. Microwave Theory Tech., MTT-23, 1121-1137 (1982).

[7] D. Marcuse, IEEE J. Quantum Electron., QE-18, 393-398 (1982).

[8] D. Marcuse, (corrections to ref. 4),IEEE J. Quantum Electron., QE-18, 807 (1982).

[9] O. G. Ramer, IEEE J. Quantum Electron., QE-18, 386-392 (1982).

[10] J. S. Wei, IEEE J. Quantum Electron., QE-13, 152-158 (1977).

Final Report Distribution List

"The Deposition of Electro-Optic Films on Semiconductors"

ONR Contract No. N0014-91-J-1307

January 1, 1991 - December 31, 1994

Addressee	Unclassified Unliimited
Wallace A. Smith Scientific Officer Code: 1131 Office of Naval Research 800 North Quincy Street Arlington, Virginia 22217-5000	3
Administrative Grants Officer Office of Naval Research Resident Representative N66005 Administrative Contracting Officer The Ohio State Univ. Research Ctr 1314 Kinnear Road Columbus, OH 43212-1194	1
Director, Naval Research Laboratory Attn: Code 2627 Washington, DC 20375	1
Defense Technical Information Center Building 5, Cameron Station Alexandria, Virginia 22304-6145	2
Angus I Kingon, Principal Investigator	1
Orlando Auciello, Principal Investigator	1
Klaus K Bachmann, Principal Investigator North Carolina State University Box 7919 Raleigh, NC 27695-7919	1
Engineering Research Programs, NCSU Attn: Connie Clark 238 Page Hall Raleigh, NC 27695	2